Universidade do Minho
Escola de Engenharia

Vera Lúcia Matos Macedo

Materials and processes for 3D printed electronics

Julho de 2021

Materials and processes for 3D printed electronics
Vera Lúcia Matos Macedo
UMinho | 2021

Universidade do Minho
Escola de Engenharia

Vera Lúcia Matos Macedo

Materials and processes for 3D printed electronics

Dissertação de Mestrado
Mestrado Integrado em Engenharia de Materiais

Trabalho realizado sob orientação de:
Pedro Libânio Abreu Martins
Investigador Auxiliar do Departamento de Física da Universidade do Minho

Carlos Miguel da Silva Costa
Investigador Júnior do Departamento de Física da Universidade do Minho

Julho de 2021

Acknowledgments

This work was carried out from September 2019 to July 2021 at University of Minho.

First of all, I would like to thank University of Minho, my institution during all my Integrated Master's degree. To the Electroactive Smart Materials group, for welcoming me, helping me, and making me feel comfortable into their midst.

I would like to express my thanks to my colleague and friend Bruno Hermenegildo for all the help and availability he had and for his motivation and friendship. My thanks to MSc Nelson Pereira for helping me with the electronic issues, the materials applications and to solve any problem even when calling me annoying. My thanks also to MSc Liliana Fernandes for helping me doing the gold deposition sputtering by plasma, and to MSc João Serra and MSc Rafael Pinto for helping me with the bioprinter.

Into laboratory work I would like to thanks to Ricardo Lima, for help and teaching me how to work with the equipment's. My also thanks to all colleges of laboratory for helping me always I ask for help.

My thanks to my supervisor PhD Pedro Martins, who made this master thesis possible and supported me through it and at any time I required it, and to my co-supervisor, PhD Carlos Silva, for his support and advice.

To Professor Senentxu Lanceros-Mendez, PhD, to whom I owe an eternal debt of gratitude, for welcoming me into his research group, always having an open door and a friendly smile, being always available to listen my worries and concerns, and giving me precious advice.

A special thanks to my friend Anabel Campos, who had always supported me, even in my worst moments, always taking care of mem and pushing me to be better. My thanks to Diana Carvalho and my boyfriend for all the encouragement. To my family for all the support and concert, specially to my brother Rui Macedo who always "smacked my head" about it, so I could finish it in a better way. To my cousin Elisabete Abreu for helping me with my English.
Finally, a quote I find inspiring, related to this work and about the source of knowledge:

"Nature is the source of all true knowledge. She has her own logic, her own laws, she has no effect without cause nor invention without necessity." (Leonardo da Vinci)

STATEMENT OF INTEGRITY

I hereby declare having conducted this academic work with integrity. I confirm that I have not used plagiarism or any form of undue use of information or falsification of results along the process leading to its elaboration.

I further declare that I have fully acknowledged the Code of Ethical Conduct of the University of Minho.

Abstract

The traditional manufacturing of electronic components consists of complex and with high environmental impact methods. Those materials are potentially dangerous for both environmental and public health, during the manufacturing process and at the end of the product lifetime when not correctly handled. Thus, the goal consists of producing in a simpler/cheaper way and with lower environmental impact, materials to be used into electronic components. In this work inks based of a natural polymer (carrageenan) and ultrapure water (a "green" solvent) were used to produce more environmentally friendly printable electronic components.

To achieve magnetic, conductive and dielectric properties $CoFe_2O_4$ (CFO), multiwalled carbon nanotubes (MWCNTs) and $BaTiO_3$ (BTO) nanoparticles were added, respectively. To promote a better dispersion and, therefore, to improve the properties of the final product, Triton X-100 was used as a surfactant. Trition X-100 was selected among other surfactants, since it has shown better results on initial selection tests. For the printing process, the most suitable parameters were selected according to the ink viscosity to improve the process as well as to optimize the method to introduce the ink into the syringe. Morphological, thermal, and mechanical tests were performed in order to evaluate the effects of fillers addition and concentration. Dielectric tests were carried out to the samples with BTO. The higher dielectric constant has been obtained for the sample with 20 wt.% BTO content, reaching 1.3×10^4 at 10 kHz. The electrical conductivity evaluation in the samples with MWCNTs shows that a DC conductivity of 0.026 $S.m^{-1}$ is achieved for the sample with 5 wt.% MWCTNs content. Vibrating sample magnetometer (VSM) test was performed to analyse the magnetic behaviour of the composite samples with CFO, a saturation magnetization of 11 $emu.g^{-1}$ being obtained for the samples with 20 wt.% CFO content. The inks developed on this work highlights the relevance of the implementation of natural materials as a base for the development of functional and multifunctional materials. Adding to that, this work can also act as an incentive to the study of materials and manufacturing procedures with lower environmental risks with the capacity of still answering society's needs.

Resumo

A manufatura tradicional de componentes eletrónicos consiste em métodos complexos, com elevado impacto ambiental, quer por gasto energético quer pelos materiais usados que são potencialmente nocivos para o ambiente e para a saúde pública, durante o processo de fabrico e no final de vida do produto, quando não corretamente processados. Visto isto, o objetivo deste projeto consiste em produzir de um modo simples, com baixo custo e com menor impacto ambiental materiais que possam ser usados em componentes eletrónicos. Assim, neste trabalho foram desenvolvidas tintas à base de um polímero natural (carragenina) e água ultrapura (usada como solvente "verde") para produzir componentes eletrónicos impressos mais amigos do ambiente.

De modo a fornecer propriedades magnéticas, condutivas e dielétricas foram adicionadas nanopartículas de $CoFe_2O_4$ (CFO), Multicamadas de Nanotubos de Carbono (MWCNTs) e $BaTiO_3$ (BTO), respetivamente. Para promover uma melhor dispersão foi usado Triton X-100 como surfactante. No processo de impressão foram estudados os parâmetros mais adequados de acordo com a viscosidade da tinta para tornar o processo mais rentável assim como tentar encontrar o melhor método para introduzir a tinta dentro da seringa com a menor formação de bolhas possível. Os testes morfológicos, térmicos e mecânicos foram feitos para todas as amostras para comparar as propriedades fornecidas pela adição das partículas, avaliando a sua interferência com o aumento da concentração de filler. Os testes dielétricos foram realizados para as amostras de BTO. A constante dielétrica com valor mais elevado foi obtido para a amostra com concentração de 20 wt.% BTO, atingindo 1.3×10^4 a 10 kHz. A avaliação dos testes de condutividade elétrica nas amostras de MWCNTs, mostraram uma condutividade DC de 0.026 $S.m^{-1}$ foi obtida para a mostra com concentração de 5 wt.% MWCTNs. O teste de mapeamento de fluxo de valor (VSM) foi realizado para analisar o comportamento magnético do compósito com partículas de CFO, a magnetização de saturação de 11 $emu.g^{-1}$ foi obtida para a amostra com concentração de 20 wt.% CFO . As tintas desenvolvidas neste trabalho veem dar relevância à implementação de materiais naturais como base para o desenvolvimento de materiais funcionais e multifuncionais. Vem também promover o estudo de materiais e métodos de produção com menos impacto ambiental e que consigam manter a resposta às necessidades da sociedade.

List of contents

List of Figures

List of tables

List of symbols and abbreviations

- 0D – zero-dimensional
- 1D – one-dimensional
- 2D – Two-dimensional
- 3D – Three-dimensional
- 3SP – Scan, Spin and selectively photo cure
- ABS - acrylonitrile butadiene styrene
- BSA – Bovine Serum Albumin
- AC – Alternating Current
- ADC – Analogue to Digital Converter
- AgNW – silver nanowire
- AM – Additive Manufacturing
- ASTM - American Society for Testing and Materials
- ATR – Attenuated Total Reflection
- AZO – aluminium-doped zinc oxide
- BTO – Barium Titanate
- BBP – Benzyl butyl phthalate
- BFRs – Brominated Flame Retardant
- BMIMI – 1-butyl-3-methylimidazolium iodide
- CAD – computer aided design (technology for design and technical documentation)
- CFO – Cobalt ferrite
- CMC – Critical micelle concentration
- CMOS – complementary metal oxide semiconductor or Complementary MOS

- CNTs – carbon nanotubes
- CTAB – Hexadecyl Ammonium Bromide
- DC- Direct Current
- DEA – Dielectric Analysis
- DEMP – Diethyl methyl phosphonate
- DIBP – Diisobutyl phthalate
- DHPC – O-(2,3-dihydroxypropyl) cellulose
- DMD – Direct metal deposition
- DMLS – Directive Deposition Lamination
- DOD – Drop on Demand
- DPP – Diketopyrrolopyrrole
- DSC – Differential Scanning Calorimetry
- DSSC – Dye-sensitized solar cell
- DTGS – Deuterated Triglycine Sulphate
- DVS – Digital Versatile Disc
- EBF3 – Electron Beam Free-form Fabrication
- EBM – Electron Beam Heating
- EDLC – electrical double layer capacitor
- EDX – Energy-Dispersive X-ray Analysis
- EEE – Electric and electronic equipment
- EPA – The Environmental Protection Agency
- ERP – European Recycling Platform
- ESH – Environmentally safely and health
- ESM – Environmentally Sound Managements

- EoL- End of Life
- FDM – Fused Deposition Modelling
- FFF – Fused Filament Fabrication
- FRI – Embedding radio frequency identification
- FTIR – Fourier Transform Infrared
- G'' – Loss Modulus
- G' – Elastic Modulus
- ICs – Integrated Circuits
- IOT - Internet of Things
- ISO - International Organization for Standardization
- IT – Information Technology
- IZO – Indium-doped zinc oxide
- LIGA – Litrographie Garvanoformung Adformung in German for Lithography Electroplating and Moulding
- LED – Light Emitting Diode
- LENS – laser Engineered net shaping
- LMD – Laser metal deposition
- LOM – Laminated object manufacturing
- LPCUD – Low - Pressure Chemical Vapor Deposition
- ME – Magnetoelectric
- MEMs – Microelectronic systems
- MJM – Multi Jet Modelling
- MLCCs – Multilayers Ceramic Capacitors
- MRI – Magnetic Resonance Imaging
- MWCNTs – Multi Walled Carbon Nanotubes

- NEPSI – National Electronic Product Stewardship Initiative
- NPs – Nanoparticles
- OFET – Organic field-effect transistor
- OLED – Organic Light-Emitting Diode
- PACE - Partnership for Action on Computing Equipment
- PAH – Polycyclic Aromatic Hydrocarb's
- PBBs – Polybrominated Biphenyls
- PBDEs – Polybrominated Diphenyl ethers
- PC – Personal Computer
- PDMS – Polydimethylsiloxane
- PE -Printed Electronics
- PEEK – Polyether ketone
- PECVD – Plasma-enhanced chemical vapor deposition
- PEG – poly (ethylene glycol)
- PEN – Polyethylene naphthalene
- PET – terephthalate
- PI – Polyimide
- PL – Polycarbonate
- PLA – Polylactic acid
- PLC – Phospholipase C
- PLGA – Poly (lactic-co-glycolic acid)
- PSBs – Polychlorinated Biphenyls
- PSC - Perovskite solar cells
- PVA – polyvinyl alcohol

- PVC – Polyvinyl Chloride
- PVDF – Polyvinylidene Fluoride
- PWBS – Printed wired boards
- PZT - lead zirconate titanate
- REACH – Registration, Evaluation, Authorisation and Restriction of Chemicals
- RFID - Radio-Frequency Identification
- RIE – Reactive-ion etching
- RoHs – Restrictions of Hazardous substances directive
- SDL – Selective Deposition Lamination
- SDS – Sodium Dodecyl Sulphate
- SEM – Scanning Electron Microscopy
- SHS – Selective Het Sintering
- SLA – Stereolithography
- SLM – Selective Laser Sintering
- SoC – System-on-chip solution
- STEP – Solving the E-waste Problem Initiative (multi-stakeholder platform for designing strategies)
- STL - "Standard Triangle Language" File format
- STM – Surface mount technology
- SVTC – Silicon Valley Toxic Coalition
- SWCNTs – Single Walled Carbon Nanotubes
- Tc – Crystallization Temperature
- TCLP – Toxic Characteristic Leading Procedure
- TCNs – cellulose nanocrystals

- TFTs - thin-film transistors
- TG – Glass Transition Temperature
- TGA – Dynamic Thermogravimetric Analysis
- Tm – Melting Temperature
- TVs – Televisions
- UAM – Ultrasonic Additive Manufacturing
- ULTEM – Polyetherimide
- US – United States
- USB- Universal Serial Bus
- UV – Ultraviolet
- VSM – Vibrating Sample Magnetometer
- WEE – Waste electrical and electronic equipment directive
- ε^*- Complex Dielectric permittivity
- ε' – Real part of the Complex Dielectric permittivity
- ε'' - Imaginary part of the Complex Dielectric permittivity
- ε_r – Complex Relative Permittivity
- μ_r - complex relative permeability
- k-Carrageenan – Kappa-Carrageenan
- ι-Carrageenan – iota-carrageenan
- ω – Angular Frequency

Chapter 1- Introduction

1. Introduction

1.1. Background and motivations

Technological development has allowed the growth of the *Internet of Things* (IOT) concept, which involves the connection of every device through a network, in the context of industry 4.0 [1, 2]. This has become the trigger to innovation, the pursuit from the "new" to accomplish the human need or wishes [1]. IOT has taken place in many places used in daily-life, on transportation, communication [3], medicine and science itself [4]. IOT consists of the interrelation and connection of network of smart devices with store and converting information capability. Some of these examples had already been named such as sensors, actuators, the embedded computers, among others. It has been useful on human vital infrastructures since the construction and execution of the concept of smart cities into industries sectors, like health and food production [3, 4], has allowed to turn industries more efficient and speed up manufacturing processes [1].

Smart materials combined with IOT concepts are promoting the enhancement on electronic devices, to improve the wireless, sustainable and interconnected self-sufficient smart devices as well as systems and smart cities [1]. Thus, smart materials have potential for the evolution of electronics and consequently an important role on the IOT concept. Due to their performance, smart materials have been being widely introduced into many new developing technologies. Smart material consists of a material that when a physical stimulus is applied, such as electrical fields, magnetic fields, heat or light, it responds by modifying its geometry, capacity or electrical resistance. What makes it a smart material is the fact that it is possible to control their response facing the stimulus being able to take the best advantage from it [5]. This materials are being applied into smart devices in order to reach their full potential, to better respond to human needs, in lifestyle and health, by their intrinsic properties like self-healing, self-cleaning, shape-memory, photomechanical, electroactive, and magnetic abilities[6]. One of the most important optimization steps is related with the development of sensors with lower energy consumption or even capable of harvesting its own energy [2].

Piezoelectric materials are an example of active smart materials, which can convert mechanical energy to electrical energy, and vice-versa. A successful development of such smart materials requires knowledge on materials science, electrical and mechanical

engineering, physics, nanotechnologies and biochemistry [6]. In addition to piezoelectric materials, there are also piezoresistive, magnetorheological, magnetostrictive, magnetoelectric, electrorheological, and chromic materials [1].

Smart materials are currently the material focus in Addictive Manufacturing (AM), often referred as 3-dimensional (3D) printing [7]. The 3D printing technologies determines the requirements for printability of a material, and not all 3D printing techniques are suitable for bioprinting. The printed material on 3D bioprinting is referred to as a "bioink," which can be described as an ink formulation that allows the printing of living cells. The ideal "bioink" formulation should satisfy some material and biological requirements. Material properties required are printability, mechanics, degradation, and functionality. Biological conditions mainly include biocompatibility, cytocompatibility, and bioactivity. Direct Ink Writing (DIW) belongs to the techniques compatible with bioprinters, as seen in Figure 1.1-a [8]. DIW belongs to the group of AM techniques, it is an extrusion-based printing, derived from Fused Deposition Modelling processes (FDM), and has become widely popular and interesting from research comparing to the 3D techniques. Its popularity comes from the capacity of constructing and retaining the shape and structure of objects, once the ink exits the nozzle by rheology properties, instead of drying or solidifying [7]. DIW on bioprinting allows extrusion of high viscosity solutions, hydrogels, and colloidal suspensions. The high viscosity polymer solutions are less likely to flow easily which may allow the printed structure to hold its shape longer after printing. However, the ink requires higher pressures to flow, limiting the gage size and smallest achievable print size [8]. The greatest advantages of DIW are lower costs and the ability of constructing complex shapes and structures, without the necessity of using additional masks or dies [7]. The junction of DIW with bioprinting allows the use of "bioinks" and construction of a 3D structure. The fact of it being able to produce a sensor with a 3D geometry may make it possible to acquire further information due to the increase of material surface, allowing the reception of stimuli from different directions.

DIW has some applications on batteries manufacturing [7, 9], on ICs using a hybrid 3D printing, which combines the DIW with pick-and-place of functional electrical components. DIW allows, too, the implementation of graphene-based composites as supercapacitors with tailored microstructure and high performance [7]. It has a bright future on the production of soft electronic components and devices with good potential to be applied into soft robotics, wearable devices, and biomedical devices [7]. DIW might be the most popular 3D printing

technique for hydrogel actuators [10]. The production of multilayer sensors including insulation, sensing and cover layers still being explored using the DIW technology [11].

DIW is largely automated and assembly free, making it possible to avoid laborious manufacture and a bust turnaround time from 3D computer-aided-design (CAD) creating a draw to the prototypes in few hours instead of a day, as it occurs in the case of PDMS [12, 13]. It can be used with practically all kinds of materials. The most used are ceramics, metal alloys and polymers, and others more unusual for applications in biomaterials, food, colloidal gelds, hydrogels or even electronically functionally materials.

Despite avoiding the waste of material, DIW can also avoid some problems associated to both traditional methodologies and materials related to electronic manufacturing. Electronic components have a high environmental impact, since some materials of its constitution are hazardous substances [7] being signalled by the RoHS (the Restriction of Hazardous Substances Directive) and WEEE (Waste Electrical and Electronic Equipment Directive) [14]. For some time, these two directives worked in partnership, until they diverged about equipment categories. The RoHS aimed to eliminate hazardous substances from newly produced electrical and electronic equipment (EEE). The WEEE Directive aimed to decrease the amount of EEE waste designed for landfill by establishing collection categories where consumers returned their WEEE for free. [14]. The most common materials on e-waste are metals and polymers, as shown in Figure 1.1-b. In metal fractions found in WEE, the presence of iron and steel is most common. The third major e-wastes are screens and the minores are metal-plastic mixtures, pollutant cables, PCBs and others, respectively [15].

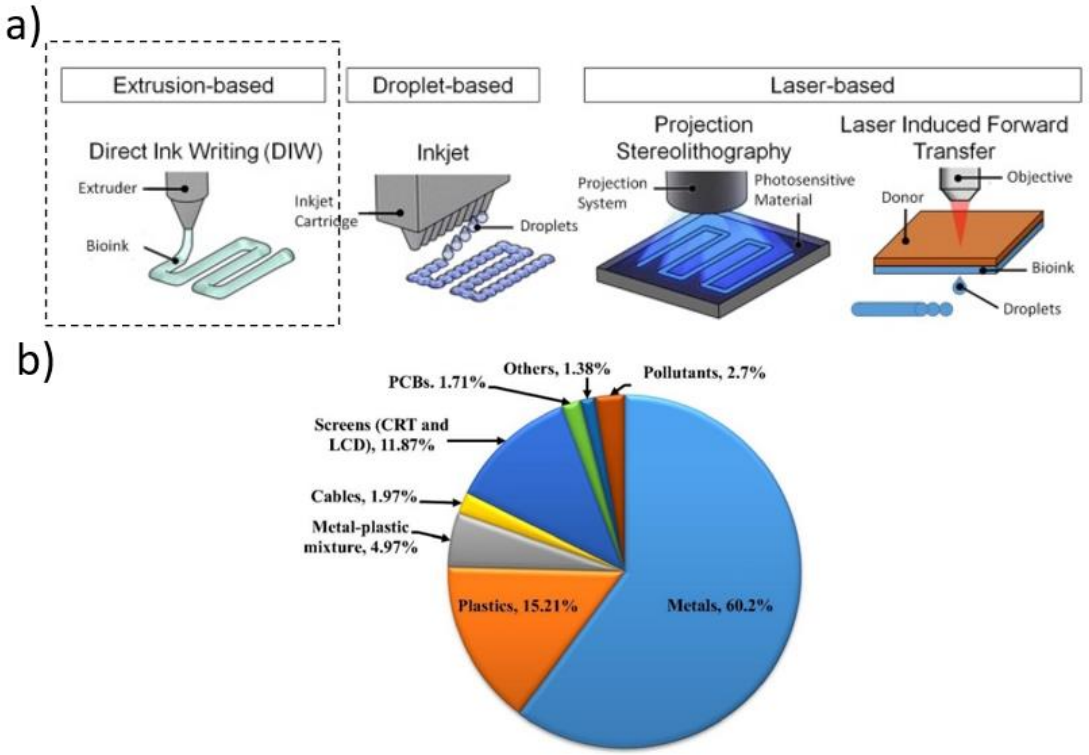

Figure 1.1. a) 3D bioprinting techniques for bioprinting taken from [8] b)Generalised material composition in e-waste taken from [15]

Given the environmental problems associated with electronics manufacturing, biodegradable, biocompatible and natural materials, such as natural polymers are quickly becoming a new standard [16]. In the last decade studies have been conducted on hydrogels based on natural polymers due their biodegradability, biocompatibility, and for their environmentally friendly flexible behaviour being identical to natural tissue [17]. Within protein-based polymers it is possible to find albumin, gelatine, soy, and collagen. In the case of polysaccharides, the examples are chitosan, agarose, gum Arabic, dextran, hyaluronic acid, alginate, carrageenan and cyclodextrin. Adding to these natural polymers, there are other promising biodegradable polymers, such as Pullulan, Zein and Pectin, Lignin, Gliadin and Legumin, Cyclodextrins. The more known are alginate and chitosan, but despite the promising properties of alginate to form gel, some natural polymers as soy, gum Arabic and carrageen also seem to be encouraging [18]. The advantage of these materials to this work is the promising behaviour of their rheology and elasticity, to be used in printing techniques [18, 19].

The main disadvantages of natural polymers on electronic fields are the lower electrical, conductive, and magnetic proprieties as well as the degradability which can shorten

the life time of the product [20]. The challenge, despite the enhancement of the electronic aimed properties, is the after-cure behaviour [18, 19]. Although degradability can act as a disadvantage, it can also be an advantage, since it can ease the recycling process making components less toxic, more eco-friendly and biocompatible, such as wearable sensors [21]. However, when natural materials are used, usually some other kind of synthetic materials or solvent with some toxicity are employed too, in order to obtain certain properties that only with natural based materials would be hard to be acquired [22].

Among all the natural polymers, Carrageenan has shown to be interesting due to its excellent rheology and jellification proprieties for a good printing behaviour [23-26]. It was chosen due to the advantages into printing techniques, and not specifically for its application on electronics. It is a polymer extracted from red algae, and it is a water-soluble sulphated polysaccharides [24]. Due to its physicochemical properties, carrageenan is used as a thickener, stabilizer, and emulsifier. Carrageenan was also used to successfully produce a 3D product, the rheology may not only allow the addition of filler, as well as also support the weight of the nest layers, without over changing the aimed geometry and avoid ink line rupture [26-28]. To be used with eco-friendly solvents there are alcohols (1-butanol and 2-butanol) some esters (t-butyl acetate, isopropyl acetate, propyl acetate, and dimethyl carbonate, ethyl acetate and methyl acetate are most problematic). The groups as ketones, aromatic hydrocarbons, ethers, dipolar aprotic have some issues evaluated to ranking their risk by healthy score, environmental score and safety score [29-31]. Even so, being carrageenan water soluble, it seems a good attempt to make the ink the most eco-friendly as possible. However, using water can bring some problems in the dissolution and dispersion on the fillers, which can be solved by adding some surfactants. The use of surfactants can lead to particle activation, followed by its dispersion and homogenization.

Since Carrageenan does not possess the required electrical, conductive and magnetic properties for the desired applications, it is necessary to add particles, homogeneously dispersed into the ink solution, to promote a final isotropic material. The particles' size varies between nanometres to micrometres, depending on the material's nature. The recycling process more likely possible and preferred in these cases is through reusing. Since Carrageenan will be used, which dissolves in water, it is easy to remove it by dissolution and through separation methods (ex: through a magnet to attract magnetic charges) and obtain the materials at its basic forms, separately, and reuse the filler into another device.

To acquire some dielectric response, barium titanate ($BaTiO_3$/BTO) will be used, which can also be used as a piezoelectric [2]. To get electrically conductive properties carbon nanotubes (CNTs) will be used, more specifically Multi Walled Carbon Nanotubes (MWCNTs) and it can be applied in piezoresistive sensor. To get magnetic properties the employment of some ferrite materials is greatly used. Ferrites, being in a great number of ferromagnetic ceramics, are promising materials known by its magnetic properties and its large application potential on optoelectronic devices and electronic field. From these group of ferrites the more common is iron oxide (Fe_3O_4) an ? inverse spinel with less than 30nm [32]- also known as magnetite, which is a super magnetic material, with a not permanent magnetic field usually used in magnetic storage media, catalysis, targeted drug delivery, magnetic field assisted separations and analyses, and contrast agents in magnetic resonance imaging (MRI) [32, 33]. Nevertheless cobalt ferrite (CoFe2O4/CFO), a ferrites which is also an inverse spinel with 4nm to 40nm [34] is very interesting due its proprieties [35]. Cobalt ferrite is a ferromagnetic material, which can be permanently magnetized, i.e. even without applying an external magnetic field the material can remain with a permanent magnetic field, as in the case of data storage devices [34]. Cobalt ferrite can be applied in magnetic actuators.

In this scenario carrageenan-based materials produced by DIW will be tested for electronic applications. Fillers such as MWCNTs (conductivity), BTO (dielectric) and CFO (magnetic) will be used to induce tailored smart behaviour on carrageenin.

There are no related works about ι-carrageenan and bioprinting by DIW technique with addition of CFO, MWCNTs or BTO fillers as well. The scheme from Figure 1.2 clearly shows the motivations and how the thought is constructed to implement into this work.

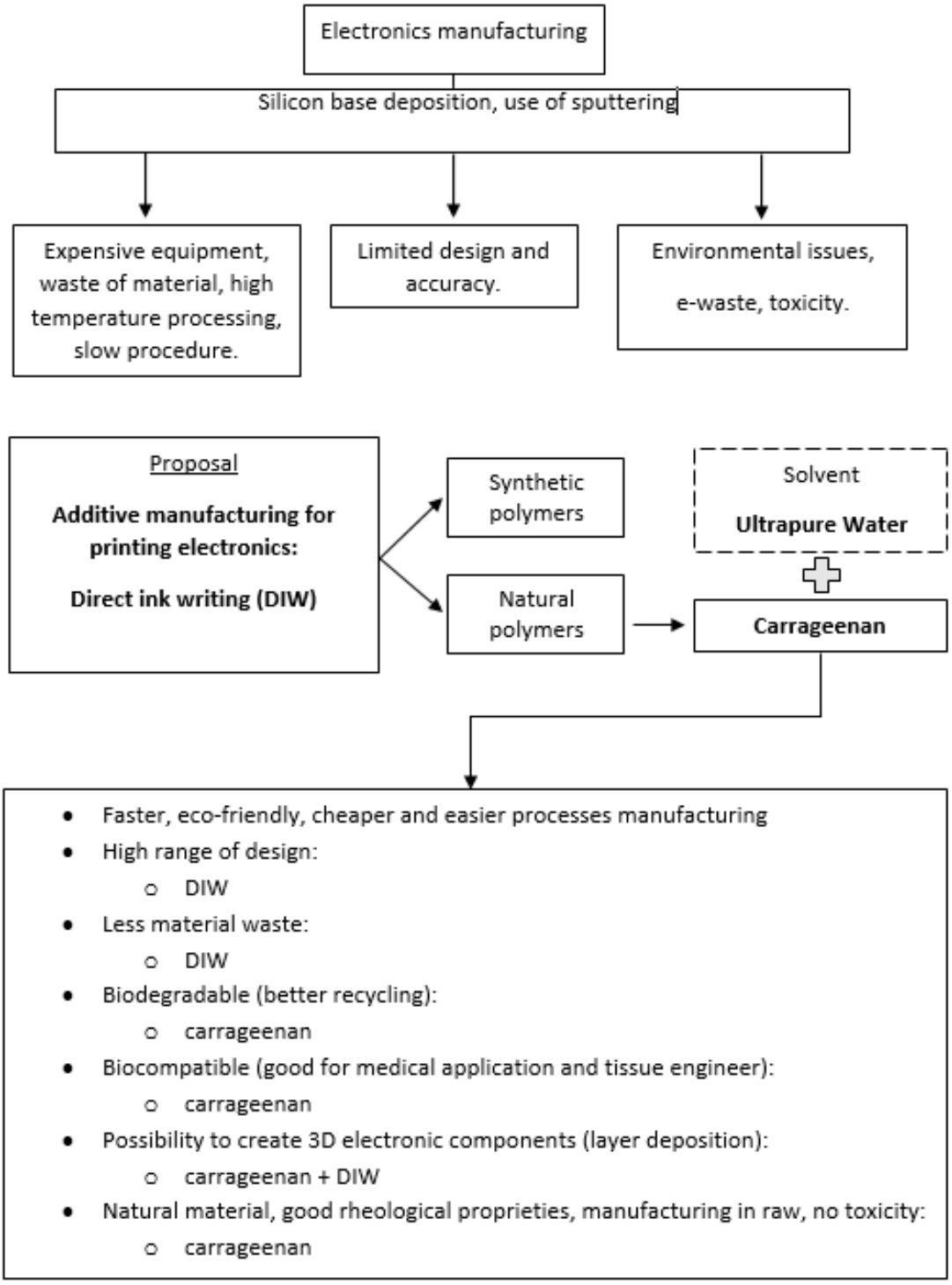

Figure 1.2. Scheme about motivations and proposal solution to study.

1.2. Thesis objectives

This thesis will focus on solving some issues mentioned on literature. The alternative methodology that will be used to solve those problems is based on the printing of electronic components through environmentally friendly materials. These will facilitate compounds manufacturing and bring new materials to this task, also adjusting to environment issues, as are the natural polymers.

The main objective is the use of DIW for printing electronic devices through the development of dielectric, magnetic and conductive inks, based on ι-carrageenan as polymer and ultrapure water as solvent. The electrical, magnetic, and conductive properties will be evaluated as a function of the filler (BTO for the dielectric, CFO for the magnetic and Multi Walled Carbon Nanotubes for the conductive ink) content on the polymeric matrix.

It will be studied how the printing parameters and chemical composition of inks influence the rheological behaviour during DIW processes to optimize the process. After getting 2D structures of the natural polymer by DIW and testing new 2D geometries, a larger number of layers will be added to produce 3D geometries and analyse the material behaviour during the curing process.

At the end, the recycling and reuse procedures for these compounds will be studied, boosting a circular economy approach.

1.3. Thesis structure

This thesis is divided in five chapters, the introduction, the state of the art, the materials and methods, the results & analysis and the conclusion.

In the first chapter the background beyond this work is presented, in which the motivation is described, and the proposed objectives are announced. It is explained how this work is divided accompanied with a brief description of each chapter.

The second chapter consist of the state of the art in which the bibliographic research about the explored thematic of this thesis is presented. Some concepts of electronic components, from materials to manufacturing techniques and the way that they evolved are also addressed, focusing on the Direct Ink Writing (DIW) technique and on the environmental problems related with printed electronics.

On the third chapter all materials used during the experimental part are announced, as well as the respective techniques and the conditions for the characterization procedure. The theoretical concepts will be also discussed.

In the fourth chapter all results, and the respective discussion are presented.

Finally, on the fifth chapter a conclusion is made about the general results, how they impact future works and the aimed applications.

Chapter 2 – State of the art

2. State of the art

2.1. Electronic industry

Technological development has been focussing on minimization, producing smaller components (transistors, sensors, and capacitors) and reducing devices sizes, making them almost invisible, easier to use and with lower energy consumption, with smart capabilities [36]. This has allowed an easier transportation and incorporation into other systems turning it into a more complex and functional one. Thus, there are necessary proper mechanical, geometric and optical functionalities [7]. The electronic industry is based on passive components as resistors, inductors and capacitors, by semiconductor components as integrated circuits, by printed circuit boards as single and multilayer boards, and by printed wiring assemblies [37]. In Table 2.1 these electronic concepts are distinguished, having a summarized explanation of production mechanisms and steps.

Table 2.1.Electronics manufacturing sectors adapted from [37].

Semiconductors and passive components	❖ **Manufacturing stages:** crystal growth; acid etch and epitaxy formation; doping and oxidation; diffusion and ion implantation; metallization; chemical vapor deposition; die separation; die attachment; post-solder, cleaning; wire bonding, encapsulation; packaging; and final testing, marking and packaging. ❖ Production includes carcinogenic and mutagenic substances and so the production should be carried out in closed systems.
Printed circuit board (PCB)	❖ **Three types of boards:** single sided boards (circuits on one side only); double sided boards (circuits on both sides); and multilayer boards (three or more circuit layers). ❖ The production of templates of conductive material on a nonconductive substrate through additive or subtractive processes (conductor usually copper; base can be pressed epoxy, Teflon, or glass).

	❖ **Production processes:** cleaning and surface preparation of the base; electroless copper plating; pattern printing and masking; electroplating; and etching.
Printed wiring assemblies	❖ Components attached to one or both sides of the printed circuit board "through hole" or by "surface mount". ❖ **"Through hole technology ":** the "legs" of the components are introduced through holes in the board and soldered (usually by tin-lead alloy) in place from underneath. ❖ **"Surface mount" technology (SMT):** components are linked to the surface by solder or conductive adhesive.

The manufacturing of small electronics is based on microelectronic systems (MEMS) which technological devices have mechanical and electrical components with micrometre dimensions. Merging MEMS into a single circuit turns out to make it possible to execute several tasks [38].

The integrated circuits (IC) consist of an electronic device group as diodes and resistors, that are produced and interconnected onto a small flat chip of semiconductor material. ICs base materials includes silicon (Si), germanium (Ge) and in rare cases gallium arsenide (GaAs) [39].

The circuits in which MEMS are integrated with are mostly IC. IC acts as the “brain” of the system and the MEMS the “limbs”, i.e. the “arms” or “legs” that perform the information or the orders received from the “brain” [40]. So, microsensors of MEMS get data information through sensing environment external factors, whether they are mechanical, chemical, thermal, optical, magnetic and/or biological stimuli, and then it is processed by IC which sends back the signal or response via micro actuators [38]. Microsensors and micro actuators perform as devices that convert energy, from one form to another, being classified as “transducers” [41]. The data processing goes through an analogue-to-digital conversion, temperature compensation, amplification, filtering, or storage, and also makes the system

testing of logic and communication functions [42]. Both, MEMS and ICs, can be combined based on two different methods, as in Figure 2.1- a and b.

In the case represented in Figure 2.1-a, MEMS and IC components are produced in separated substrates mostly by MEMS and IC techniques, being hybridized in the final system. These systems are usually referred as side-by-side integrated or as a two-dimensional system. In the case of the chip being attached to the package in a vertical way, it is called a system-on-chip (SoC) or a multi-chip module, represented in Figure 2.1-b). For SoC solution the scientist community and industry are still looking for new production methods and integrated schemes for MEMES and IC combinations. These can lead to some distinct advantage and disadvantage, being the ideal solution strongly dependent on the application device, the field of application and the product requests [42].

The scheme below, on Table 2.2, summarizes the information about the processes and materials used in each of them.

Table 2.2. Materials and manufacturing processes of MEMS and ICs adapted from [38, 39, 43-45].

IC's	**Materials:** ❖ **Si, SiO_2, Si_3N_4, Al.**
	Processes: ❖ Photolithography, thermal oxidation, dopant diffusion, Ion implantation, LPCVD, PECVD, evaporation, sputtering, wet etching, plasma etching, reactive ion etching (RIE), ion milling.
	Restrictions ❖ High costs in manufacturing; leaks due to the reduction of the lateral dimensions of the transistor; thermodynamic limit on the introduction of impurities; statistical variation of impurity concentration.
MEMS	**Materials:** ❖ Piezoelectric films (PZT), magnetic films (e.g., Fe, Ni, Co) high temperature materials (SiC and ceramics), mechanically robust Aluminium alloys, stainless steel, Pt; Au, sheet glass, plastics (PVC and PDMS).
	Processes (derived from CMOS standard technologies)

	Same as IC's processes, with additional highly specialized micromachining processes: ❖ Micromachining (photolithography, etching, LIGA, mechanical micromachining); Bulk micromachining (wet and dry etching of silicon); surface micromachining (LPCVD); wafer bonding (anodic or field-assisted bonding, intermediate-layers bonding assisted bonding and direct or fusion bonding); deep RIE; LIGA "Lithography Galvanoformung Adformung" (X-ray lithography and mask technology; Electroforming, Plastic Moulding); batch micro assembly; electroplating, spin casting.
	Restrictions ❖ Microfluidics and optical applications.

Silicon is still the most used material in electronic manufacturing [38]. The manufacturing of electronic integrated circuits consists of different steps, in an order that depends on the type of layer that is required. The steps can vary from deposition and/or elimination, to the growth of an isolation layer onto the silicon substrate, and impurity diffusion in silicon regions and ionic implantation of dopants to give them electrical properties [37, 39, 43]. These steps are incorporated in the methodology of some processes referred in Table 2.2.

2.1.1.1. Additive manufacturing and printed electronics

Nowadays AM has emerged as a disruptive concept and consists in technologies that allow the design and fast processing of complex geometries and microstructures, based on layer-by-layer production [7, 46]. In AM are techniques that melt or soften materials and others that cure liquid materials as a tactic to construct layers [46, 47]. Usually, the techniques which use these concepts also uses a computer, with a 3D modelling software, a layering material, and a manufacturing machine. The layering material can be ceramics, composites, metals, and polymers which can be in liquid, powder or solid state. Polymers are mostly used in both solid and liquid form because they have generally been used in their available forms, formability, and end-use properties [48, 49].

AM has benefits on Embedding Radio Frequency Identification (RFID), devices embedded inside solid materials, on short lead time electronic products, for polymer based, three-dimensional micro-electromechanical systems and even to microwave circuits fabricated on paper substrates [48]. AM involves lower energy consumption, fast and simpler fabrication steps, lower temperature processes, less waste of material, lower costs on printing

equipment, new designs and geometries, part consolidation (fewer parts with more complex design), customization of parts, easy scale-up, eco-friendly approach, multi-subtract allowance, large area high yield [1, 48, 49].

The classification by ASTM F42 and ISO/ASTM 52900 standard defines seven major AM processes, Photopolymerization, Material Jetting, Binder Jetting, Material Extrusion, Powder Bed Fusion, Sheet Lamination, and Direct Energy Deposition, as shown and described in Table 2.3 [48, 49]. Some of the recurrent technologies involve fused deposition modelling (FDM), stereolithography (SLA), laminated object manufacturing (LOM), selective laser melting (SLM) and selective laser sintering (SLS) [49]. The usual thermoplastics used in AM are Polycarbonate (PC), acrylonitrile butadiene styrene (ABS), poly ether ester ketone (PEEK), polyetherimide (ULTEM) and Nylon [50].

Table 2.3. The seven major AM processes by ASTMF42 adapted from [48].

Process	Description	Technology
Photopolymerization	A vat of liquid photopolymer resin is cured through selective exposure to light (by a laser or projector). After polymerization begins and transforms the exposed areas into a solid part.	❖ Stereolithography (SLA) ❖ Digital Light Processing (DLP) ❖ Continuous Liquid Interphase Production (CLIP) ❖ Scan, Spin, and Selectively photo cure (3SP)
Material Jetting	Droplets of material are deposited layer by layer to create parts. Generally, consist of jetting a photo-curable resin and curing it with UV light, as well as jetting thermally molten materials which solidify at ambient temperature. This process was the origin for the term “3D Printing”.	❖ 3D Printing (3DP) ❖ Multi-Jet Modelling (MJM) ❖ Drop on Demand (DOD)
Binder Jetting	Liquid bonding agents are selectively applied onto thin layers of powdered material layer by layer to produce parts.	❖ Drop on Powder (DOP) ❖ Powder Bed printing

	The binders include organic and inorganic materials. Metal or ceramic powdered parts are typically fired up in a furnace after they are printed.	
Material Extrusion	Material is extruded through a nozzle or orifice in tracks or beads, and then combined into multi-layer models. They usually involve heated thermoplastic extrusion (like a hot glue gun) and syringe dispensing.	❖ Fused Deposition Modelling (FDM) ❖ Fused Filament Fabrication (FFF)
Powder Bed Fusion	Powdered materials are selectively consolidated by melting them together using a heat source (a laser or electron beam). The powder near the consolidated part acts as support material for overhanging features.	❖ Selective Heat Sintering (SHS) ❖ Direct Metal Laser Sintering (DMLS) ❖ Electron Beam Melting (EBM) ❖ Selective Laser Melting (SLM) ❖ Selective Laser Sintering (SLS).
Sheet Lamination	Sheets of material are loaded and laminated together to form an object. The lamination method can be adhesives, ultrasonic welding, or brazing (metals). Unnecessary areas are cut out, layer by layer, and removed after the object is built.	❖ Selective Deposition Lamination (SDL) ❖ Laminated Object Manufacturing (LOM) ❖ Ultrasonic Additive Manufacturing (UAM)
Direct Energy Deposition	Metal powder or wire is fed into a melt pool which has been created on the surface of the part where it adheres to the underlying part or layer. The energy source is mostly a laser or electron beam. This process is essentially a form of automated build-up welding.	❖ Laser Metal Deposition (LMD) ❖ Electron Beam Free-Form Fabrication (EBF3) ❖ Direct metal deposition (DMD) ❖ Laser Engineered Net Shaping (LENS)

Despite the great benefits of these techniques, they are still in progress and consequently some drawbacks are associated to them. Some limitations on superficial finishing and

precision, associated to the thermal and mechanical characteristics can occur. If the material cools rapidly it can lead to distortions and stresses, which can cause problems in the areas of the piece that are cyclically loaded or under stress by an external force. The development of AM techniques are just at the beginning, so it is necessary to reach many parameters. There is the need to search for faster, more efficient and precise methods, simultaneously with materials progressing to range the full potential of 3D printing platforms [14]. To avoid some of these problems there are hybrid mechanisms which combine AM and conventional techniques [49].

The combination between AM techniques and electronics lead specially to printed electronics (PE). PE is another technique that can replace some of the MEMS manufacturing processes, and still grows [51]. This is reinforced by the graph of Figure 2.1-c that shows the crescent growth of published works about PE and printed flexible electronics.

PE made the beginning of flexible electronic possible due to the possibility to processing the components at temperatures identical to the flexible polymer substrates. This is not allowed in the case of traditional methods, since they use rigid materials as printed circuit boards, usually made of glass reformed epoxy laminated FR4, or even as wafer materials.

However, PE permits a low-cost, high-volume fabrication, a manufacture of a big amount of micro and nanoscale devices in a much easier, faster and cost-effective way [19], as showed in Figure 2.1-d. It also demonstrates that PE saves a lot of energy and labour comparing to the traditional electronics manufacturing. As showed in Figure 2.1-d, conventional methods involve masking and etching of sacrificial materials (subtractive process) which is avoided in PE and in a simpler way [52].

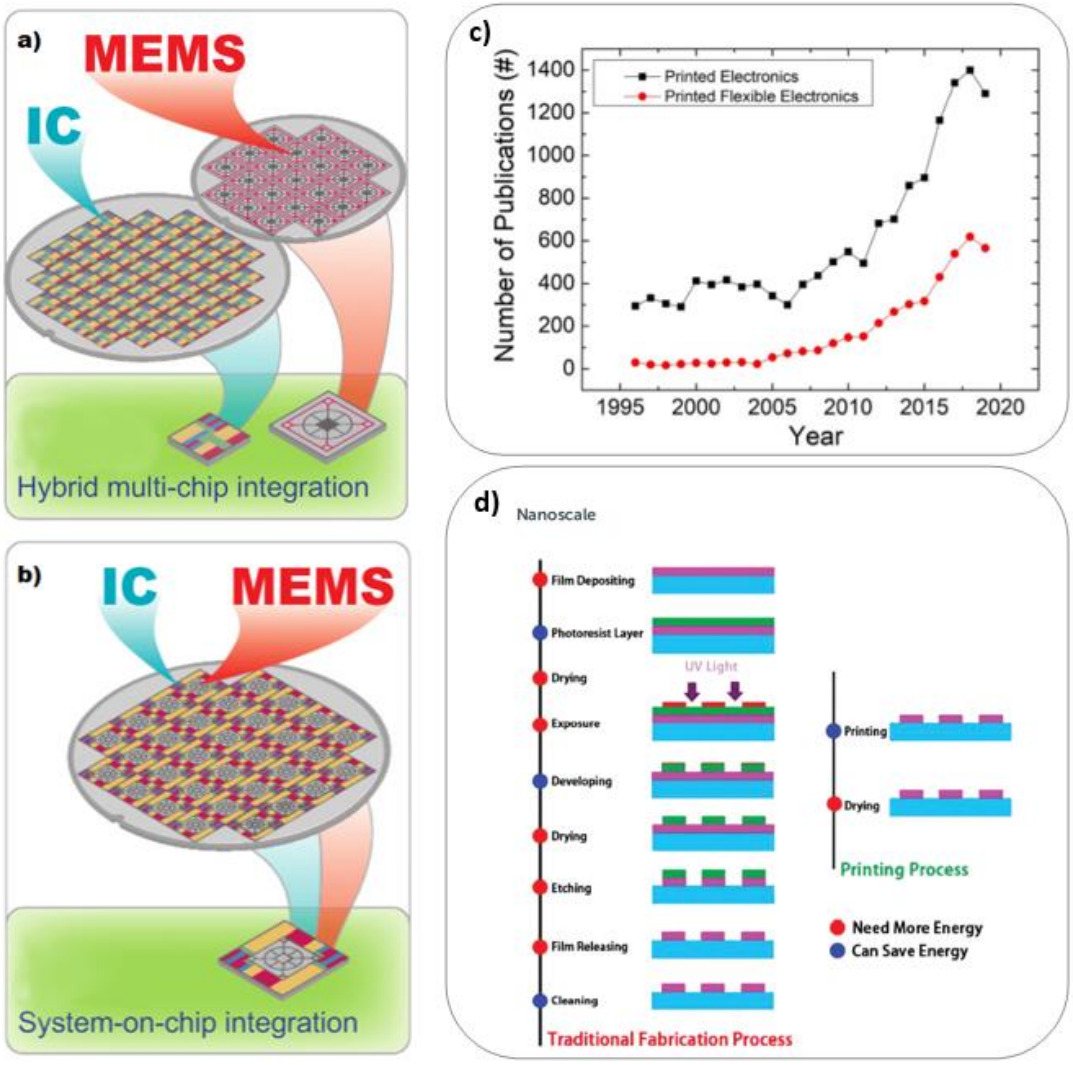

Figure 2.1.MEMS and IC integrations methodologies by a) Hybrid multi-chip solution and b) System-on-chip solution(SoC) taken from [42], year-wise number of published works in printed electronics as key word taken from [53] and d) Comparison of traditional manufactural procedures and printing technique (production of RFID antennas) taken from [19].

As represented in Figure 2.1-d, the functional material (the conductive, semiconductive or dielectric ink) is just simply added onto the substrate. One kind of ink is printed at a time on a patterned layer, then a patterned layer of another kind of ink is printed, and at the end all these layers form an electrical structure, that can be an interconnection which can also possess passive or active components [16, 52].

PE is a promising manufacturing technique to produce thin, lightweight, flexible, and low-cost electronic products since it allows the quick manufacturing of large areas. Depending on the printing technique used it has its own advantage, although the common factor of them all is that they are all additive processes. This methodology can be processed through its

application onto many kinds of substrates and makes it possible to execute a 3-dimensional printing. These facts are going to change the way that electronic devices are produced, from design and manufacturing phases to material selection, device structure and architectures. PE provides better economics to electronics producers, comparing to traditional electronic that are only cheap on the mass production scale. Moreover, printing methodologies allow new business models, for example with inkjet technology it is possible to do "desktop manufacturing", being related to small-scale micro-factories with small, fixed costs [16, 52].

PE materials are based on inks or pastes and substrate. It is formed by a set of techniques from micro-/nanoscale electronic to large-area electronics to produce a large range of products. To acquire a good performance in PE, consideration should be given to the combinations of printable materials, printing methods, printability, sintering parameters, structures, and other process conditions during product manufacture. The ink's requirement strongly depends on the technologies used, which are directly connected to the product application, depending on the final product function, if it needs to be small, thin, flexible, lightweight, etc [16, 49, 51, 52].

Depending on all these, the ink must have the ideal rheology, and be able to be deposited onto various subtracts to improve wetting and have the ideal adhesion. Inks can be solvent free energy curable or solvent-based (organic or aqueous), and have a large range of viscosities and superficial tension. The key factor of PE is printing and consequently the inks and their physical properties. To find the optimal combination between inks and a suitable functional structure are very challenging, since the printability of the inks (rheology, surficial energy, charge properties, etc) and the cure process must be considered [16, 52].

PE functional inks are a mixture of pigments, polymers, solvents, and additives, and differ from the ordinary ones when the pigments are substituted by particles which give some additional proprieties to the ink [16, 51, 52].

PE techniques are divided into two types of techniques, the contact ones (analogue printing), where the printing plate is in contact with the substrate (example: screen printing, flexography, gravure, nano—printing, dry-transfer, micro-contact, offset and soft lithography techniques) and the non-contact techniques (digital printing), where the only thing that touches the substrate is the ink (example: slot-die, spray printing, aerosol printing, inkjet printing, laser direct writing) [1, 16, 51, 52]. In Figure 2.2, there are represented some of the

main PE manufacturing techniques: inkjet printing, gravure printing, flexographic printing, and screen printing [51].

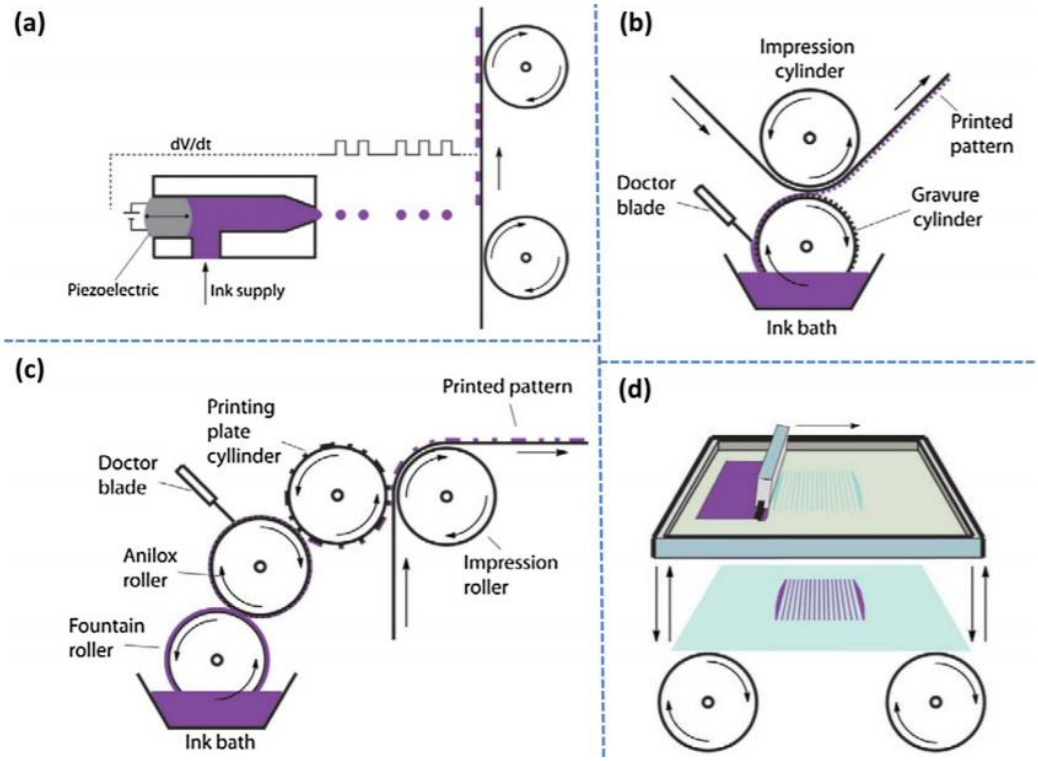

Figure 2.2. PE main manufacturing techniques a) Inkjet printing b) gravure printing c) flexographic printing *and d) screen printing taken from [51].*

Table 2.4 resumes the description and the material variety and proprieties of the main techniques mentioned in Figure 2.2. Most used by industry, allow a great bunch of patters.

Table 2.4- Description and limitations of PE principal techniques used by industry adapted from [1, 19, 21].

Technique	Description	Limitations
Inkjet printing	Drop-on-demand (DOD): printer ejects drops of inks when asked by a digital signal. Two methods (ink is jetted from the nozzle): ❖ Bubble-jet printing model - a heating unit inside the print head prepares the bubble of ink and forces a drop of ink out the nozzle.	❖ Viscosity: 0.01 - 0.03 Pa.s ❖ Coffee-ring effect. ❖ Swelling. ❖ Clogging, and satellite droplets, can lead to poor reproducibility.

	❖ Piezoelectric printing model – droplet is forced from the nozzle by a ceramic piezoelectric tile in the nozzle flexes into the ink reservoir in the print head. Simple, fast, and low temperature processes (Flash point > 45 [°C]), small and medium product volumes (waste reduction), usual resolution 0.01 mm. Printing parameters: ❖ Ink jetting frequency, ink jetting temperature, diameter of printing nozzles, number of printing nozzles, print height, and ink jetting waveform.	❖ Surface Tension: 25-36 [mN/m]. ❖ Max. particle diameter: 0.2 [µm].
Gravure printing	A metal cylinder which incorporates the image (engrave or etched) on its surface, rolls through an ink pan. Thus, the ink is directly transferred to the substrate. Allows for cost effective, high-quality patterns, good image reproduction, variable depth, and area printing, and printing on either regidor flexible and absorbent or non-absorbent substrates. Printing parameters: ❖ Properties of ink and ratio of microcell width/depth. The depth of microcell varies from 10 to 30 µm and the width of micro cell wall varies from 3 to 5 µm. ❖ Ink transfer depends on the ink solvent and viscosity, tracking property, transfer roll material and pressure applied on it.	❖ Viscosity: 0.1-1Pa.s ❖ Short cylinder life duration. ❖ Expensive cylinder. ❖ Rough printing. ❖ Bad edges definition. ❖ Pick out effect. ❖ Low reliability. ❖ Unprecise control of shapes and sizes.
Flexography printing	Plates with backward reading which reveal a correct reading impression. The depth of the cell in the anilox roller is constant, creating an ink of constant thickness which is transferred to the soft plate roller. Next the inks are transferred to substrates by printing pressures and forming printed patterns. The excess of ink is removed by doctor blade from de non-engraved surface of the anilox and released areas of image pass to the printing plate (flexoplate). High-speed and cost effect fabrication of 2D materials printing applications. Printing parameters: ❖ Successful printing needs a homogeneous and controlled ink transferring mechanism onto the substrates, defined by the solvent of inks, pressure and materials of transfer roll. The thin homogeneous layer between the anilox roller and the flexoplate (called web) should be soft and flexible to be able to wrap from one to another.	❖ Viscosity: 0.05-0.5Pa.s. ❖ Squeezing. ❖ High tensile stresses. ❖ Marbling effect. ❖ Pattern flaws. ❖ Non-uniform patterns. ❖ Expensive plates and die. ❖ Line width limitations.

Screen printing	The screen is filled with ink and taken into next to the substrate. A squeegee is then forced to the screen making it in contact with the substrate. The squeegee is moved linearly across the screen pushing coating solution through the open areas (made from thin sheet of material, fine porous mesh of fabric, synthetic fibres or silk, with closed areas made form photo-polymerized resin) onto the substrate, reproducing the pattern. <u>Printing parameters:</u> ❖ The volume of ink deposition depends on the thread count of the screen (number of threads per unit distance and thread diameter), the thread diameter (thickness of the screen and the depth of the ink column at each open hole in the mesh) and the pressure (the angle between squeegee and the screen that describes the area of contact, and blade speed during the contact with the screen through printing).	❖ Viscosity: 0.5-5Pa.s ❖ Needs small roughness substrates ❖ Needs a different structure for different patterns. ❖ Sizeable waste of material. ❖ Low maximum resolution. ❖ Quality of the printed materials is strongly influenced by the processing parameters.

Gravure, screen printing and flexography printing are a type of roll-on-roll printing (R2R) - classic printing technology with a printing master, in which the lines or patterns are created on printing plate, often loaded onto a roller [19].

In printing electronics, some of the materials used are metallic nanoparticles (Au, Ag, Pd, Cu, Sn, Ni, NPs and their alloys or composites, transparent conducting oxide(ZnO doped with aluminium (AZO), gallium (GZO), and indium (IZO), SnO2 doped with fluorine (FTO), CdO, Ga_2O_3, and In_2O_3 Inks), carbon nanomaterials, inorganic oxide nanomaterials (ZnO, TiO_2, MoS_2, perovskite, and kesterite) [19]. Popular substrates to printed electronics include foils made of polyimide (PI), polyethylene naphthalene (PEN) or polyethylene terephthalate (PET). For substrates of rigid materials silicon or glass are usually used.

The applications of printed electronics can vary between flexible displays and lightning, sensors, printed TFT's, energy store and harvesters like capacitors and solar cells, conduct lines and electrodes as transparent electrodes and RFID tags [19, 54].

Now PE involves a bunch of application from micro-nanoscale electronic devices to large area electronics beyond many products. Innovation in printing technologies has yielded the high-volume production of electronic devices possible at low cost on soft plastic, paper or textile substrates [19].

A disadvantage of PE is that its electrical performance is not at the same level comparing to silicon-based electronics applications. Although, as these technologies are evolving and becoming more mature, their performance are expected to improve as well. Thus, the reliability of structures not always seems to be high, which can lead to a short lifetime of the product [16, 52].

2.1.1.2. Direct ink writing

Direct ink writing (DIW) is an extrusion-based AM methodology strongly applied in meso- and micro-scale. In this technique the liquid-phase "ink" is deposited using a XYZ positioning system under controlled flow rates from a small nozzle and dumped along a digitally defined path in order to create a 3D structure layer-by-layer [55, 56]. The image from Figure 2.3-a shows the basic method of DIW. 3D printing technologies most commonly considered for bioprinting, are DIW and inkjet printing [8].

This technique can be divided into two basic types, continuous filament writing and ink droplet jetting [7]. In the first one, ink is continuously extruding from a nozzle and the filament is moulded into a fixed platform to form the object. For instance, in the ink-jetting printing the process is made by deposit drop-by-drop of the ink, and not through a continuous filament. These two different methodologies are demonstrated in Figure 2.3 -b and b [7].

The viscosity of bioinks for extrusion-based DIW bioprinting ranges from 30 to 6 x mPa.s [8].

It is necessary to consider two things: first the ink rheology that must be controlled to avoid the nozzle obstruction during injection, caused by the absence of shear thinning, and second, the mechanical stiffness and strength of the inks must be suitable to the feature, so the structure does not collapse.

Despite that, DIW must have high shear-thinning behaviour and viscoelasticity. As the ink viscosity is under driven force, it can be extruded easily from the machine in the form of a continuous rod-like filament, and then exhibits rapid "curing" to keep a stable shape without collapsing due to its sufficiently high yield stress and storage modulus. The high solid content of the ink can prevent, as far as possible, the fluctuations of volume and shape of the printed object during the subsequent treatment. With the control of these factors, the ink can form a

stable dispersion, promoting the transition from fluid to gel. It ensures the blending with the previously deposited layer and retention of the printed shapes at the same time.

In this technique the properties of the inks control the properties and stability of the final product [7].

One of the biggest requirements to the efficiency of DIW, apart from a high viscosity, is the need of an ability to rapidly self-healing after extrusion. It means that, during the injection a lower viscosity is needed (loss modulus G''> elastic modulus G'), caused by the shear force, and then the polymer recovers its mechanical properties (G''<G'). An ink that exceeds the 10^3 $Pa.s^{-1}$ has a high-profile, which is a great candidate to be able to hold more than one vertical layer [28]. The shear-thinning characteristic is desired to compensate for the high shear stress related with high viscosity. The global mechanics, i.e., achievable stiffness, is important to create self-supporting constructs [8].

In a simple way to explain how to process in practice, a digital drawing is needed, in a CAD programme (STL code) (SolidWorks), to define the product geometry. Next step is to translate it to another program language, to a Gcode, to ensure that the printer can "read" what it is supposed to draw and where. It is where all the aimed parameters to the printing process are defined, such as extrusion rate flow, speed of the needle from the designed path, distance between syringe and substrate plate, the infill of the scratch, and the kind of the line inside the structure. This process is showed by steps on Figure 2.3-c.

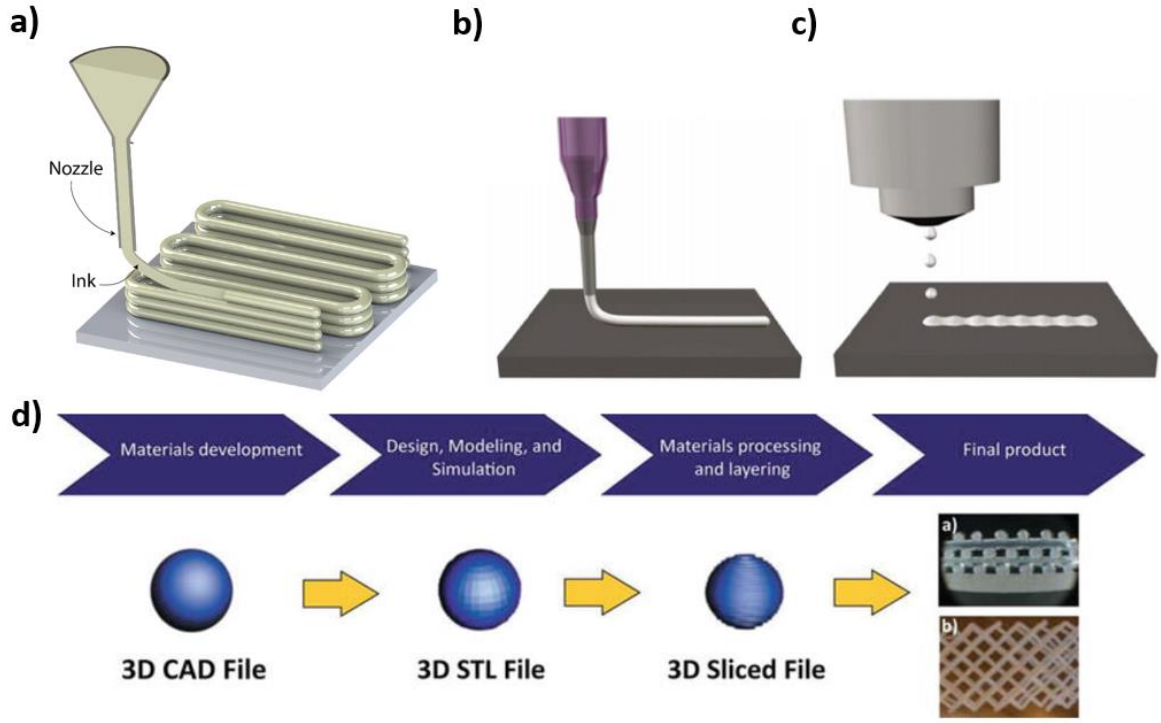

Figure 2.3. a)Direct ink writing basic process taken from [55] and DIW by b) continuous filament writing and c) ink-jetting printing taken from [7] and c) general steps for AM procedure and applied on DIW taken from [46]

2.2. Environmental problems: electronic waste

In the last twenty years there has been a large increment of the use of electronic devices and consequently a rapid change of the economic and social landscape, which leads to the formation of tons of electrical and electronic waste (e-waste) every year [57]. E-waste is electrical or electronical equipment (EEE) from all types which has been disposed of with no intent to be reused by the owner [58]. The EEE are items which possess a battery or a power cord, and the e-waste from it is divided into 3 main groups: large household appliances as refrigerators and washing machines, information technology (IT) and telecom (personal computers, laptops, monitors) and consumer equipment (DVD players, TVs, mobile phones, leisure, and sporting equipment's and mp3 players). Batteries, circuit boards, lead capacitors, activated glass, plastic casings and cathode-ray tubes can also be called e-waste equipment parts [59].

This waste has been a global challenge to manage, even the developing countries have not been able to significantly change their path on this. Consequently, the e-waste contamination is still being a great part of hazardous e-waste, with a huge impact on both

ecological environment and public health. China, for example, has been one of the countries whose e-waste became the large proportion of the waste stream, in both quantity and toxic terms [57]. The firsts alarms of e-waste products been transferred from rich countries as Europe, US, and Canada to poor countries, (which are now in infamous sites in Asia and Africa) to be processed in dangerous conditions for both workers and environment, were sounded in reports from BaselAction Network (BAN 2002), Toxics Link India (2003) and Greenpeace International (2005) [60]. It Figure 2.4-a, are the first international conferences that has been made in order to establish some rules and agreements to alleviate or solve some of the e-waste environmental problematics is represented.

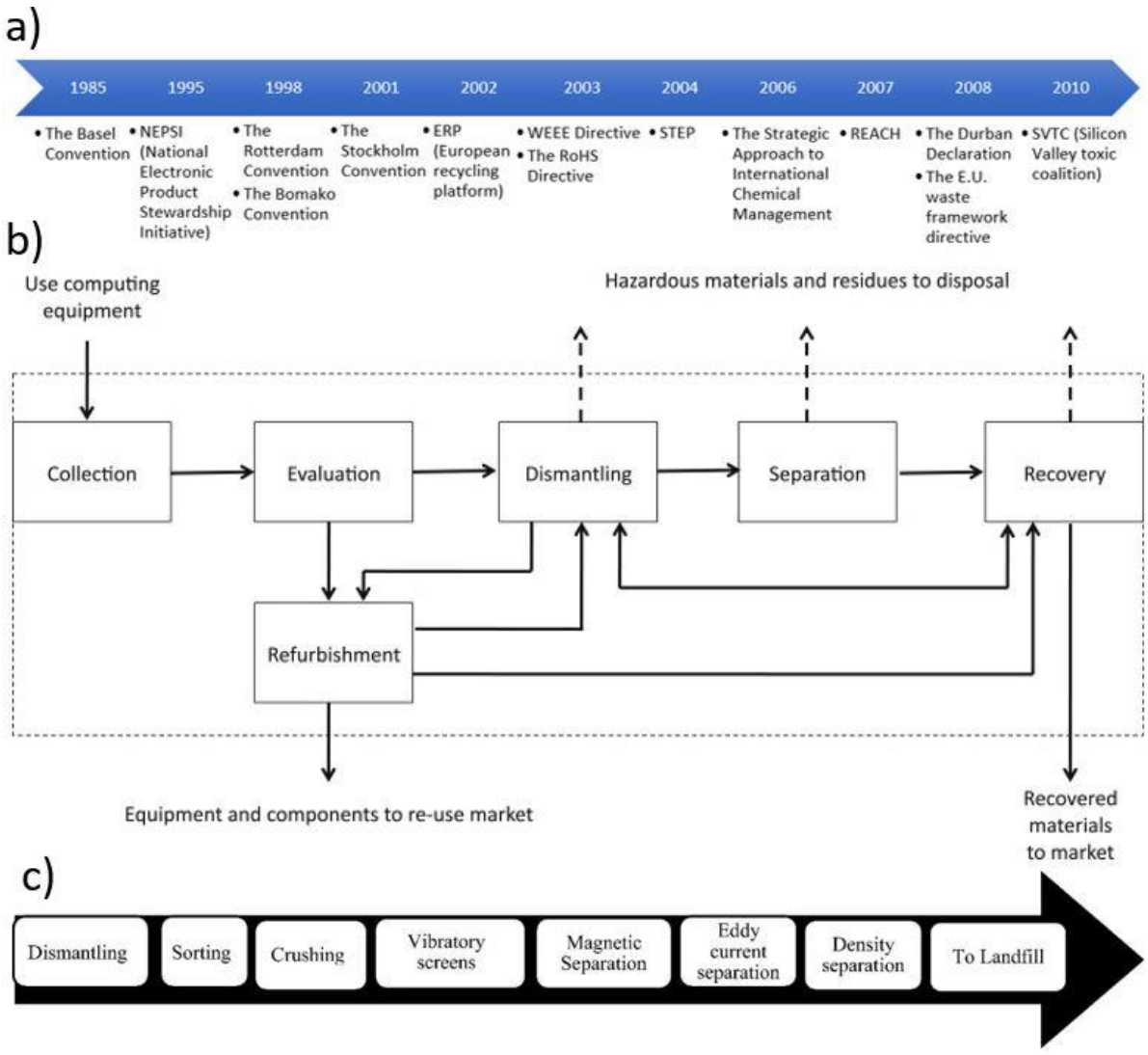

Figure 2.4. a) . First International conferences about e-waste environmental issues adapted from [61], b) aimed flux diagram of ESM for e-waste in a recycling facility taken from [59], c) Correct deposition of landfill of e-waste material non-recyclable steps taken from [61].

Globally, a highly efficient recycling technology is required, which has been blocked due to distinct variations in reginal legislation, consumer participation and technical capacities. These problems start to be happening also in small countries, which become even more problematic due to 3 factors: extremely limited land area and severe high population density which make it very difficult to spend space to create a field plant to process e -waste; in these areas the collection and treatment of e-waste have no station to be transferred to and thus it has to be performed with no assistance; at last since e-waste is one of the hazardous wastes it is prohibited by the Basel Convention from transboundary movements [58]. They also must establish their own facilities (or plants) to solve e-waste issues. Due to all these restrictions, it is critical for these places to fight to mitigate the negative ecological impacts and recycle some useful resources from e-waste. Although Basel Convention (the Parties to the Basel Convention on the Control of Transboundary Movements of Hazardous Wastes and Their Disposal) had introduced the Partnership for Action on Computing Equipment (PACE) in order to simplify an environmentally sound management (ESM) of used and end-of-life computing equipment. PACE defend that a charitable donation consist on a "transfer of computing equipment or its components, that are not waste, for their intended direct reuse for purposes of charity without any monetary rewards or benefits, or for barter" [59] . Figure 2.4-b represents the ideal flux diagram for ESM for e-waste recycling facilities.

Until now, e-waste has been treated or disposed of by landfill (in some developed countries) or by informal incineration (in some developing countries) [57]. The "informal" sector of e-waste recycling is where modern industrial methods are not used and where worker protection is frequently inadequate [59]. Although, there are some electronic components in which the recycling is not available, so the landfill deposition is needed, but it must be done in a sequential of steps that make it more secure, as in Figure 2.4-c. At first, it must be dismantled down to the component level and then categorized according to their physio-chemical properties [61].

Recently, technological innovations and recycling processes for both regional and global e-waste recycling have been developed. The most common method is based on physical processes. There have also been established some operational plants for e-waste recycling in various countries, for example in China over 100 licence field recycling plants have been

stabilised which process e-waste by sophisticated and combined strategies as dismantling, crushing and separation. A portable demonstration plant in a container lorry has been added and employed for processing e-waste residues by a hydrometallurgical procedure [57].

E-waste has a potential to recover valuable materials as iron, aluminium, copper, gold, solver, and rare earth metals, that is why it is globally recognized as a resource for these elements/materials [58, 59]. The recycling of metals from electronic devices may reduce the need for mining virgin materials. Although since there is a low e-waste collection rate and poor recycling or inefficient end processing for EEE, many of these valuable resources are lost [58].

Yet, these products have not been aimed to efficiently recover the materials or for their safe disposal. In various low and middle-incoming countries the handling and disposal of e-waste is commonly unregulated. Concerns about the health and environmental risks associated to e-waste raised due to contained hazardous components on e-waste as lead, mercury and chromium, some chemicals in polymers and flame retardants. There has been an increment of documentation about health effects associated to air, soil and water contamination to who lives and/or works at or near informal e-waste processing places. The protection of human health and the environmental with the increment of evidence of harmful effects on health and the growth of the amount of e-waste spots is a growing challenge [58].

The common basis labour procedures include the use of acid baths (to extract precious metals as gold, an absence of protective clothing leads to high risks of chemical injuries), burning cables (processing cables to recover copper – burning the plastic coating from wires, releases harmful polyvinyl chloride, furans, dioxins, brominated flame retardants and polycyclic aromatic hydrocarbons (PAH) into the environment in which people live and/or work turn out to be immersed in thick black toxic smoke), breaking apart toxic solders and dumping consequent waste material. The burning of e-waste is a harmful combustion and increases the risk of respiratory and skin diseases, eye infection and even cancer for people nearby, who have been chronically exposed to many chemical pollutants either directly by contact or inhalation, or then indirectly by contamination of the water and food supplies [58]. The three main e-waste recycling methods are shown at Figure 2.5.

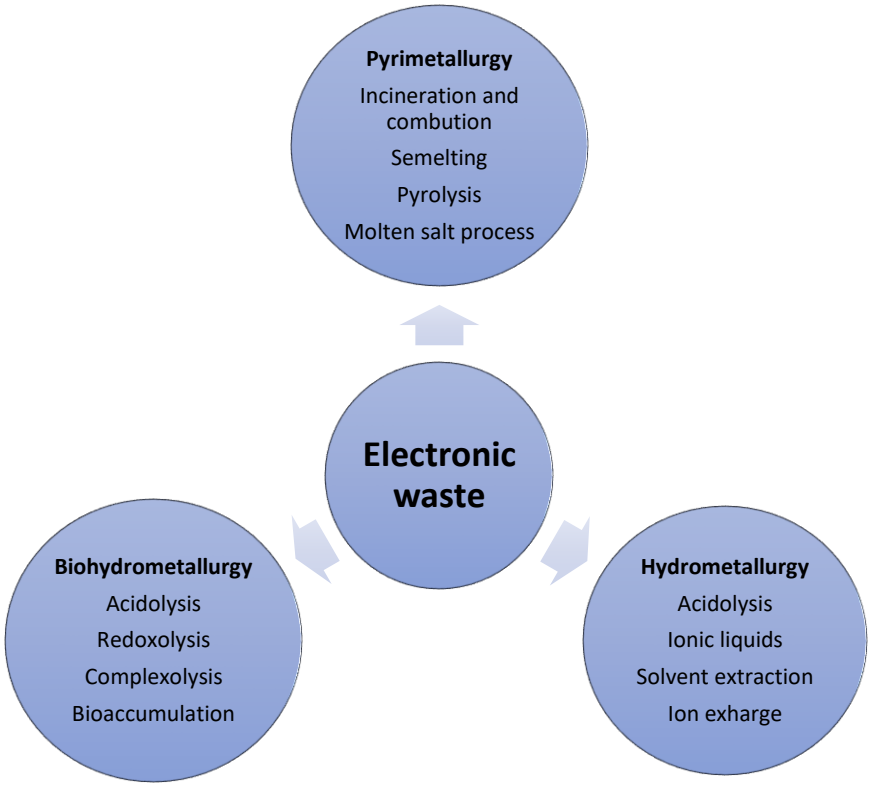

Figure 2.5. The three main approaches to e-waste recycling adapted from [62].

All these methodologies have their advantages and some disadvantages as the further toxic gases' treatment, high energy consumption or even low efficiency in recovering some valuable elements, required to develop these and new techniques in order to make the e-waste recycling more efficient and appealing [62].

To workers who dismantle e-waste they could dangerously get into direct contact with polychlorinated biphenyls (PCBs) and other persistent organic pollutants in fluids, lubricants, and coolants [58].

2.2.1. Environmental impact of printing electronic

The solid waste from printed circuit boards consists of scrap board materials, plating and hydroxide sludges and inks. The Printed writing assemblies consists of solder dross, scrap boards, components, organic solvents, and metals. These boards may cause some environmental risks if disposed into landfills, since they are treated with brominated flame retardants [37]. From all electronic components, the printed wired boards (PWBs) are those who contains the most toxic waste in both quantity and variety, which are heavy metal lead

(Pb)and the brominated flame retardant (BFRs). EPA toxicity characteristic leading procedure (TCLP) has announced Lead (Pb) as the most significant toxicant of PWBs in PCs, since lead concentration in the TCLP gets of the vast majority of PWBs ranged from 150 to 500 mg/L, which should be at a regulatory level of 5mg/L for classifying a waste hazard, so it is 30 to 100 times the regulatory value. The ideal solution to PWBs waste would be recycling and/ or reuse, although that is currently not economically viable. The necessary metallurgical processes for the recovery of noble metals are very sophisticated, and the generated secondary pollutants from processing and dealing are most expensive then the market value of the materials which could be recovered from PWBs. Currently, the dispose of landfill is still being the predominant way for the e-waste disposal including PWBs. As it realises lead leaches at greater level tant the characteristic limit, the concern about the disposal of it at landfills is still growing [63].

Some ideas to pollution prevention and control of PWBs manufacturing is shown in Table 2.5 [37].

Table 2.5.Prevention and control methodologies for PWBs manufacturing adapted from [37]..

Pollution prevention and control of PWBs manufacturing	
Board manufacturing	❖ Preference of 'surface mount' technology (SMT) than plated by hole technology, injection moulded substrate, additive plating.
Cleaning and surface preparation	❖ Utilization of non-chelating cleaners, extend bath life, improve rinse efficiency, counter current cleaning, recycle/reuse cleaners and rinses.
Pattern printing and masking	❖ Aqueous processable resist; screen printing to substitute photolithography; dry photoresist; recycle/reuse photoresist strippers; separate streams; recover metals.
Etching	❖ Apply differential plating; non-chelated etchants and non-chrome etchant; pattern against panel plating; additive against subtractive process; recycle/reuse etchants.
Virgin metal extraction	❖ Metal recovery trough regenerative electrowinning results in a near zero effluent discharge for segregated metal bearing streams. Heavy metals are recovered to metal sheets which eliminates 95% of sludge disposal. Metal carrying sludges that are not treated for recovery of metals should be disposed in secure landfills.

In relation to the recent printed electronics previously mentioned the biggest question marks are the evaluation of the environmental, safety and health (ESH) problematics due to the use of nanoparticles. ESH problems of nanoparticles is challenging since it is very hard if not impossible to generalize the results achieved from studies on one type of nanoparticles due to the large variety and non-homogeneity of nanoparticles. Besides, there is a lack of methodology, metrology among other basics as it is the way to monitored nanoparticles. Ats last, it is still unclear regarding the characteristics of the nanoparticles as size, shape, surface area, surface properties -charge, reactivity, etc - and agglomeration, which of these could cause the possible toxic effects. Despite these, it is also possible that some environmental factors as pH, salinity, etc, or the solvent used and/or the presence of any coating could have some effect on potential toxicity [52].

The reason why the ESH issues have raised some concerns are connected to the fact that nanoparticles can cross cell membranes due to their small size (at the same scale as cellular components and large proteins). It has also led to the suggestion that nanoparticles may invade natural defences of humans as well as other species and damage cells. In each life cycle phase the risk of exposition is low but is still more significant in the manufacturing phase if not all the appropriated protective measures are used as well as in the end of life (EoL) phase if the nanoparticles used are released to the nature. Even so, nanoparticles are considered as a possible risk in each life cycle. Since EoL challenges are different to every application, there are still ongoing studies on other technologies and materials. Giving to the report of Finland's Environmental Administration, exposure to nanoparticles is improbable in the use phase but some environmental problems may occur at the end of life of the product. When applied nanoparticles in printed electronics are already sintered, which consists of heating the nanoparticles until they adhere to each other, so the final product would not have free/wild nanoparticles. But it is not completely certain that all nanoparticles are really sintered, or how strong the cohesion is [52].

There is still a lot of insecurity since now most of the applications already created are demonstration models and are not yet in the market, there is no knowledge about the real risk when produced in masses. Consequently, to study the risks intrinsic at printed electronics all cycle-life must be considered, since the material extraction to the end-life of the product. Among this, at an economic point of view, the cost to build the production line with the required equipment and energy cost are not known [16]. Thus, as referred before, the waste

associated to electronic devices has lightly grown. Compiling this to the fact of the lifetime of printed electronics being usually rather short than other electronic devices and the cost of reparation does not reimburse the price of a new one, it can aggravate the environmental problematic and the disposal in landfill as well [16]. If the lifetime of the material is short, it leads to a higher consumption of the product, and as printed electronics promote the large number of possible applications it can also increase the electronic waste. At the end of life of the printed electronic there are many options. The best option from the environmental point of view, is for the product or its parts to be reused as it is, it can also be recycled or can even be used as valorised as energy source by incineration. Not excluding the most probable end which is the deposing in landfill, mainly if it is part of the package or some other product [52].

Before it hits the market there are three major directives concerning about environmental issues of electronics, the Restriction of Hazardous Substances (RoHS), WEEE and EcoDesign Directives. RoHS Directive, by now restricts the use of lead, mercury, cadmium, hexavalent, chromium, polybrominated biphenyls (PBB) and polybrominated diphenyl ethers (PBDE), which to the printed electronics is not hard to avoid in contrast to the electronic traditional manufacturing. Despite that, another advantage of printing manufacturing is that the materials used are more easily traceable and consequently easier to split. While in the traditional electronics the product are often built from hundreds of distinct components, and each containing different materials and manufactured in different locations, with printed electronics it is only needed to know which are the different kind of inks within the product [52].

Through the Registration, Evaluation, Authorisation and restriction of Chemicals) (REACH) Directive it is possible that some of the substances used at printed electronics will be restricted, and that some chemicals or substances not very common and not worth to register will be banished from the market [52].

Despite more studies being required, printed electronics allow the minimization of the amount of essive chemicals involved in the manufacturing compared to the conventional electronic production, and depending on the technique and processing conditions have less energy consumption, it is required lower amount of material to manufacture, and it is possible to implement environmentally friendly materials [16].

One of the main trends in order to solve these problems consists of the development of new biodegradable electronics through natural and/or biodegradable materials and their improvement. Currently, there are already some biodegradable materials used as substrates as leather, silk and hot-pressed cotton-fibre paper, so the next step would include the development of new inks to this end. This is not only interesting from the environmental point of view but also to the economical perspective since biodegradable materials have lower costs. Biomaterials already studied include sugar, gelatine, indigo, food colours (indanthrenes) and cosmetic colours (perylene diamide) and small molecular nucleobases which family can work as dielectrics as adenine, guanine cytosine and thymine [52].

2.2.1.1. Direct ink writing: environmental impact

Comparing to the other AM techniques DIW are the methodology which require less quantity of material for the manufacturing process [56, 64]. It only needs to fill the syringe with the amount of needed ink and all the material inside the syringe is used to print the product and thus it generates low waste. Therefore, according to the circular economy models this is a good process to be adapted since it requires low quantity of material, and the productivity greatly depends on the capacity to provide the maximum added value to the extracted material [56].

Despite that, it is necessary to evaluate the product quality to assure if the technology is suitable. Comparing to DIW the best candidate is SLM. SLM another technique that can manufacture more or less the same quality product. Comparing both, SLM has more geometry options with less design limits. Both have in common the possibility of adjusting the desired infill and changing the geometry until it is optimized. DIW has a worse surface finish, but both require post processing so at the end, this fact is not determinant [56].

2.3. Natural polymers

Natural polymers are macromolecules, that can be found in natural substances, for example in proteins, like collagen, gelatine, hyaluronic acid, zein silk, in polysaccharides, such as starch, cellulose, alginate, chitosan, in terpenes as natural rubber and in lipids. The

advantage of its use is the biocompatibility, degradability and the capability of simulating the chemical environment nature. [23].

In Table 2.6 is represented some natural and bio-based polymers, with the respective sources and properties.

Table 2.6-Natural and bio-based polymers adapted from [23].

Polymer type	Polymer	Source	Main material's properties
Natural	Alginate	Brown seaweed	Hydrogel-forming.
	Cellulose	Plant fibbers and wood	Film-forming (high tensile strength) The high rate of water absorption.
	Chitosan	Shells of crustaceans	Film and hydrogel-forming -antimicrobial properties.
	Gelatine	Hydrolysis of collagen from skin, bone, and connective tissues of animals	Hydrogel and film-forming. Highly soluble in water (affinity for cells and other biomolecules).
	Pullulan	Fungal exopolysaccharide (*Aureobasidium pullulans*)	Film-forming.
	Zein	Corn	Film-forming. hydrophobic and non-water soluble (unlike most natural polymers) no need of crosslinking steps in a final material.
	Carrageenan	Anionic sulphated polysaccharide obtained from red algae	Gel-forming polysaccharide fractions at low concentrations of a few ion's salts, such as KCl and $CaCl_2$
Bio-based	Polyamide-6 (PA-6)	Ring-opening polymerization of caprolactam	Excellent mechanical properties. Can be processed through different methods. Chemically like collagen.
	Polycaprolactone (PCL)	Ring-opening polymerization of ε-	Film-forming. Large range of processability. Unusual mechanical

		caprolactone or condensation of 6-hydroxy caproic acid	properties which confer high tensile strength and viscoelasticity to materials.
	Polylactic acid (PLA)	Ring-opening polymerization of lactide or direct condensation of lactic acid monomers	Film-forming. Mechanical properties can diverge from soft and elastic to stiff and high strength materials, depending on the polymer Molecular weight. Can be processed through different technologies. Degradation through hydrolysis (can take from months to years).
	Poly (lactic-*co*-glycolic acid) (PLGA)	Polycondensation of glycolic acid and lactic acid or ring-opening polymerization of lactide and glycoside	Physical properties depend on the Mw of monomers, exposure to water, and storage temperature. Degradation through hydrolysis (can take from days to months).
	Polyvinyl alcohol (PVA)	Polymerization of vinyl acetate followed by transformation to polyvinyl alcohol	Film and hydrogel-forming. Water soluble, what requires crosslinking the final material.

These materials are specially used in medicine, on tissue engineering and drug delivery [18] because of the biocompatibility and also degradability, which in some cases can be useful, as implants [20, 65]. On electronic technologies these materials can give advantages on recycling due to the degradability. They can also make components less toxic and more eco-friendly, and biocompatible sash as wearable sensors [21]. Within these field applications one natural material with good results is silk, a natural fibre [22]. When these kinds of materials are used, other kinds of synthetic or toxic materials are also used, to obtain certain properties that only with the use of natural polymer are hard to acquire [22].

As it seems from the previous examples, despite the attempt in the use of biopolymers, to have the biodegradability behaviour, it does not always imply the use of natural based polymers.

Natural polymers have lower conductivity levels, when compared to the synthetic ones. So, despite this fact, they must be studied/optimized in order to improve their

application, due to their great environment friendly behaviour and the natural basis structure they offer to the component, such as hydrogels rheology during solution. The challenge, despite the enhancement of the electronic aimed properties, is the after-cure behaviour [18, 19]. Among all natural polymers from Table 2.6, carrageenan seems a promising material since it is a natural based and biodegradable polymer, so it is environmentally friendly, with excellent printing rheological behaviour, soluble in water, and strong gel properties after cooling [66].

2.3.1. Carrageenan

Carrageenan is a natural sulphated and anionic polysaccharide (carbohydrate), extracted from the multicellular wall of certain species of red algae seaweeds of the *Rhodophyceae* family [25, 67], such as Chondrus crispus, Gigartina, Euchuema and Hypnea. There is a great low-cost abundance in nature, and it is water-soluble, non-toxic and biodegradable [18, 67-71].

The molecules of this biopolymer have two fundamental characteristics: its structure is made by a monomer, a galactan, it contains in its structure's galactose, 3,6-anhydrogalactose units (3, 6-AG) joined by α-1, 3 and β-1, 4-glycosidic linkage, carboxy and hydroxy groups and ester sulphates [18, 26, 71, 72] and is rich of sulphates (OSO^-) radical, which is the negative charge [69]. Usually, natural polysaccharides are hybrid and contain repetitive disaccharide units of several carrageenan types attached in a single polymer chain [24].

Depending on the the number and position of sulphate groups on the disaccharide repeating unit as well as through the presence or absence of 3,6-anhydrogalactose in a 1,4-linked residue, three main types of carrageenan can be found: kappa (κ), iota (ι), and lambda (λ), where their sulfate content is 20 w/w%, 33 w/w% and 41 w/w%, respectively [24-26, 72, 73]. The hydration, strength, texture, and temperature properties are influenced by these structural variations of gel formation [72]. Carrageenans with higher levels of sulphation tend to decrease the gel strength and solubility temperature [25].

Carrageenan's structure and polymerisation degree are related to the nature of the algae used as well to the extraction conditions [68]. Its structure is rich of hydroxyl groups (sulphated or methylated, substituted by pyruvic acid residues or D-xylose [24]) which can

form cross-linking networks with other elements and oxygen atom important to form coordinated bonds with cations [70, 73]. The cleavage of the glycosidic linkages of carrageenan's increases over time and temperatures and they are very sensitive to acid and oxidative breakdowns [74]. In Table 2.7 some properties from the three main types of carrageenan are identified.

Table 2.7. Properties and characteristics form the three main types of carrageenan adapted from [72].

Carrageenan types	k-	λ-	ι-
3,6-anydrogalactose ring (%)	34	n/a	30
Sulphate groups (%)	25	35	32
Gelling (°C)	30–60	n/a	40–70
Solubility (°C)	>70	25	>70
Melting (°C)	40–75	n/a	50–80
pH stability	4–10	4–10	4–10
Cation added to gel	K+ and Ca2+	No	Ca2+

Usually, carrageenan is commercialized available with addition of calcium, magnesium, potassium, and sodium salts, being more usual as a mix of these. It will affect the conformational transition and gelation behaviour of carrageenan [67].

When gelation occurs, an infinite network is formed by a coil to helix conformational transitions and then an aggregation of the ordered molecules, which increase its crystalline proprieties [67]. As such the helix of a single carrageenan molecule must get into a closer proximity to a second identical single carrageenan helix, to form a double helix. Then, the double helix must aggregate to form a three-dimensional network [75]. The cross-linkage of Carrageenan gels has been considered as a side-by-side aggregation of helical molecules [76].

k and ι-carrageenan are the main gel-forming polysaccharide fractions at low concentrations of a few ion's salts, such as KCl and $CaCl_2$, because of their helicoidal secondary structure [24]. All carrageenans are soluble in hot water and hydrate at high temperatures,

and particularly both ι- and k-carrageenan exhibit a low fluid viscosity. The cooling set of these carrageenan's are between 40-60 °C, depending on the cations within them. The potassium and calcium salts of both ι- and k- carrageenan do not dissolve in cold water but sodium salts do. The structure of the various types of carrageenan is exposed in Figure 2.6.

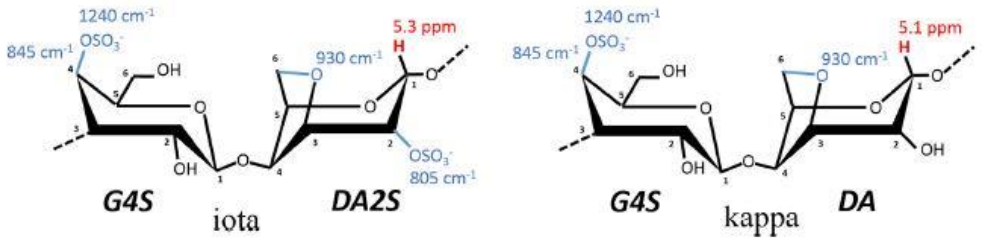

Figure 2.6.Chemical structure of ι and K-carrageenan [77].

ι-Carrageenan is the most alike to k-carrageenan, but it does possess a supplemental sulfuric ester substitute, at level 2 on 3,6 anhydrogalactose. Due to the presence of additional sulphate groups in the anhydrous galactose residue the hydrophobic behaviour of ι-carrageenan decreases, which improves its ability to inhibit syneresis. Although, as ι-carrageenan has lower aggregation capacity it forms a less rigid gel, a weaker gel [67, 72, 75].

In aqueous solution, it produces thermo-reversible gel below critical temperature on cooling process. During this the conformation shifts from random coil single chains to the structure of double helices of carrageenan chains, and therefore to a gel. This mechanism is promoted when added of cations as potassium, calcium and sodium [25, 75]. The charge density of carrageenan chains increases with decreasing temperature, due to the temperature-induced coil-to-helix transition and the aggregation of helices. The macroscopics properties of this gel are strongly influenced by cation species [76].

Carrageenan is extracted through dry and wash of the seaweed with cold water, being after broken and agitated in a hot alkaline solution and obtained in a powder form. This natural polymer has many benefits like gelling, thickening, emulsifying, stabilizing, anticancer, anticoagulant, antihyperlipidemic and immunomodulatory properties [18, 71]. Although it has an adhesiveness and positive surface charge and can be combined with many materials as polyvinyl alcohol hydrogels, Au-nanofillers, and chitosan [24]. Carrageenan is also used in

food, such as fat substitute specially in milk products, textile formulations, printing, pharmaceutical and cosmetic industries. The gel formed by ι-carrageenan is elastic with good freeze, thaw and rehealing properties [73].

It has a physical aspect of powder at pure and dry form, with no smell and no taste. Usually, it is translucid and when added into other solutions there is no change in the taste or original colour. In a solution the carrageenan polymer has a behaviour of anionic hydrophobic colloids. For the application in 3D printing, it has a great capability to create a water-retaining hydrogel [69]. The type of carrageenan in this study is ι-carrageenan because of its intermediate value of sulphate.

2.4. Fillers

Carrageenan is a promising green material to many applications, although it is still in studies due to the environmental issues that have been going on, so it is needed to develop and improve techniques and knowledge about these materials.

One of the limitations of these materials is the fact of it not having the required electric, conductive and magnetic properties for the desired applications. So, it is necessary to add different kinds of fillers to promote them [18, 19].

Yet, in most of the cases the help of a surfactant to make the filler dispersion into the solvent more efficient is needed. Nanoparticles, if in smaller size than the surface-to-volume area increases, which makes a given volume of them more reactive than a similar volume of the same material in micro or macroscopic form(major particles size) [78].

Since the purpose is to create the “greenest” materials, into a “green” solvent the filler dispersion can be even more difficult, so a surfactant can turn into a key factor.

2.4.1. Surfactants

The term surfactants comes from “surface active agent” [79]. They are amphiphilic molecules usually with both polar and apolar groups, which adsorb on the interface between immiscible bulk phases, for example the oil and water, air and water or even particles and solution, and act to decrease hydrophilic tension [80, 81]. So, they change the interfacial

properties of liquids in which they are introduced to [79]. Surfactants are unique due to their duality, the hydrophilic region which is the polar head, and the hydrophobic region which is the tail that usually contains one or few hydrocarbon chains. Depending on the nature of hydrophobic, which depends on the chemical structure of the head group, and on the kind of charge of the head group it can be classified as cationic, anionic, non-ionic or zwitterionic [80, 82].

Anionic surfactants have a negative charge on the head group. Example of this are the traditional long-chain carboxylate soaps and the early synthetic detergents, sulphates and sulphonates. Sulphates and sulphonates have advantage over the carboxylates since they have better tolerance of divalent metal ions in hard water. These kinds of surfactants are widely used on cleaning formulations [79, 80].

For cationic surfactants, the hydrophilic group contains a positive charge, and generally consists of imidazolium, ammonium or alkyl pyridinium compounds. Cationic surfactants have a strong affinity to negatively charged fibres as it is with cotton and hair [79, 80].

On the non-ionic surfactant's cases, they do not carry any charge on the head group, they are water soluble due to polar groups as alkyl ethoxylates. They also include some semi-polar compounds as amine oxide, phosphine oxides, sulfoxides, pyrrolidone's and alkanolamides and are widely used in low-temperature detergents and emulsifiers [79, 80]. Triton X-100 is one non-ionic surfactant and is commonly used in biochemical application to solubilize proteins, in the permeabilization of cells for immunofluorescence staining, in western blot analysis and for preparation of cell section in immunogold labelling for electronic microscope [83].

Zwitterionic or amphoteric [79] surfactants, due to the fact of having both positive and negative charge groups in their hydrophilic part, can act both as cationic or anionic, depending on the pH of the solution. Compounds with zwitterionic surfactants are softer on the skin and have low eye irritation, which leads to their use in toiletries and baby shampoos [79, 80].

In Figure 2.7 is showed the general structure of surfactants and the different classifications.

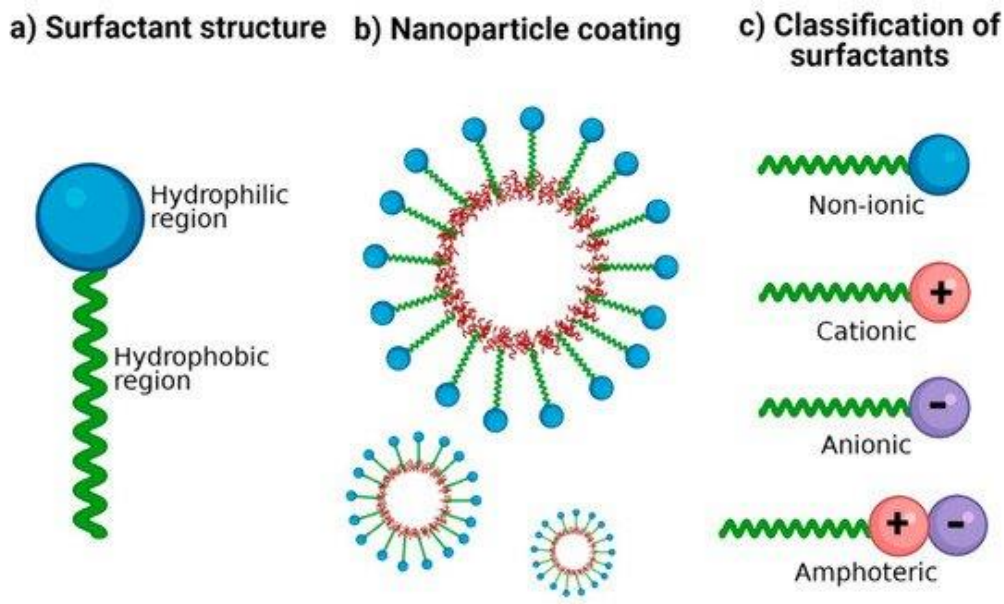

Figure 2.7. Structural representation of surfactants [84].

To process stable colloidal dispersion the adsorption on interface and self-assimilation into supramolecular structure are some advantageous characteristics of surfactants. The capacity of adsorption from surfactants onto organic or inorganic surfaces depends on the chemical characteristics of particles, surfactant molecules and solvent. The ionic adsorption on charged surfaces occurs due to the driving force called coulombic attractions and can be explained as the force formed between negatively charged solid surface and the surfactant's positively charged head group. In non-ionic surfactants' adsorption onto a hydrophobic surface, the mechanism is based on a strong hydrophobic attraction between the solid surface and the surfactant's hydrophobic tail group. When the adsorption interaction between the surfactant molecules and the solid surface is stabilised, the self-organization of the surfactant into micelles is expected to happen (aggregative structures of surfactants) above a critical micelle concentration (CMC) [81].

2.4.2. Cobalt ferrite

CFO nanoparticles have an inverse spiral crystallographic structure (AB_2O_4) which also can be described as a face-centred cubic (FCC) arrangement of atoms. The crystallographic site of CFO is an inverse spinel structure, where ½ of Fe (III) cations are on tetrahedral sites (A) and the other half are placed on octahedral sites (B) along with Co (II) cations [85-87] and it is

represented in Figure 2.8-a. In the case of ferrites, it can be rewritten as MB_2O_4, where M is iron metal.

CFO is a permanent magnetic material i.e., the material has the ability of remaining magnetized after the magnetic field drops to zero [88]. It has the behaviour of a hard magnetic material as well. The difference between soft and herd magnetic materials is represented in figure 2.8-c. Soft magnetic materials have high permeabilities (measure of the magnetic field within the material) and lower coercivities, which corresponds to a weak anisotropy and a large magnetization. Hard magnetic materials have large saturation magnetization, large coercivities, large energy products and are usually used in permanent magnet functions. The intermediate magnetic materials communally have coercivities values around 1kOe and in this group are Fe_2O_3, Co_80Cr_{20}, $Co_{77}Ni_{10}O_{13}$, as well as thin films. Soft magnetic materials are needed where the magnetization should completely align with even a small magnetic field for applications as sensors, motors and transformers [89]. Figure 2.8-b shows the how the Magnetization Saturation, Remanence Magnetization and Coercivity Magnetic Field are represented in a magnetic hysteresis curve.

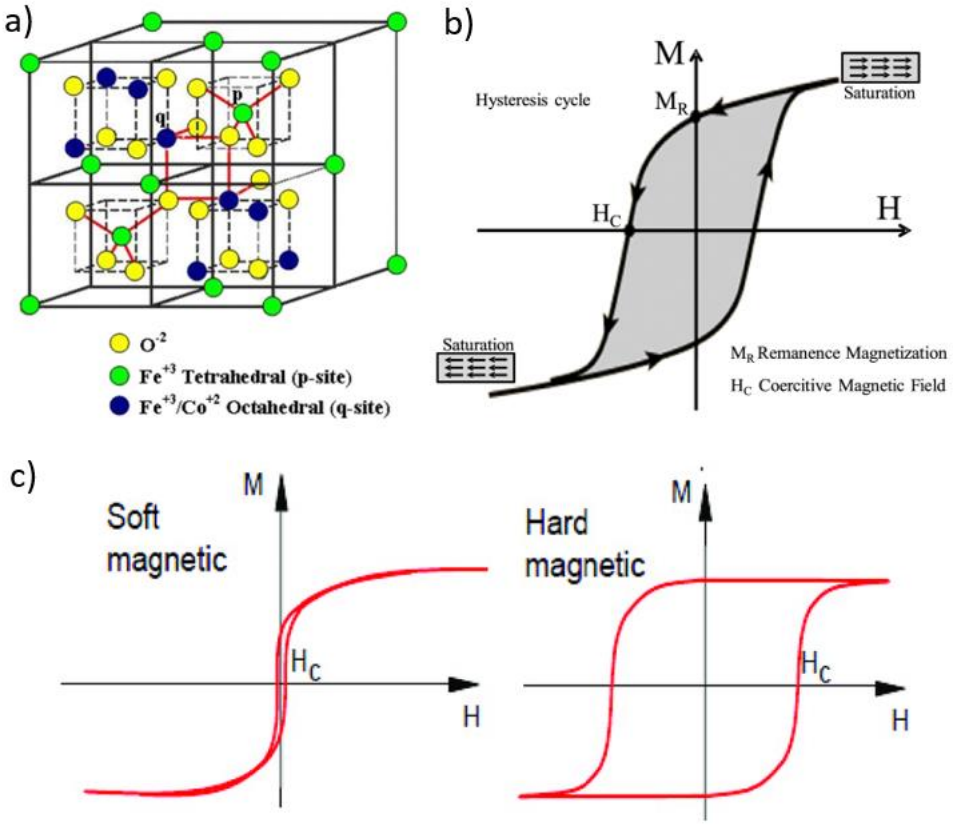

Figure 2.8. a) Representation of the inverse spinel crystallography of $CoFe_2O_4$ [90], b) schematic representation of Magnetization Saturation, Remanence Magnetization and Coercivity Magnetic Field [91], and c) difference of soft and hard magnetic hysteresis curves [92].

CFO nanoparticles can merge some useful and physical proprieties with low production cost and high chemical stability [93]. Among these, CFO nanoparticles also have good mechanical hardness [93], high coercivity strength [35, 88, 93], wear anisotropy [35, 86, 87, 93], high mechanical strength [35, 93], moderate saturation magnetization [35, 86, 87], and high-temperature magnetic order(520°C) [35, 93], large magneto crystalline anisotropy constant (1.8-3) x 10^5 $J^{-1}m^3$ [35, 94], high Curie temperature [86, 87]. Comparing to microparticles, CFO nanoparticles have been more interesting due to high-density magnetic [35, 93, 94], tuneable electrical conductivity [94], low eddy-current losses [35, 85, 93], considerable electrical resistance with low dielectric loss [35, 85].

Due to its specific proprieties, CFO has been widely considered to be integrated into some of the recent and evolving electronic and electromagnetic devices [94]. CFO can also be integrated in materials in order to acquire various applications such as in electronic [35, 94, 95] and photoelectric devices [93], photomagnetic [113], magnetoelectric materials [93, 95],

micromagnetic materials [93, 95], photoelectric devices, information storage [86, 94], supercapacitors [94], spintronics [88, 94], catalysis [86, 94], flexible and organic electronic (transistors, FWTs) [94], ultra-high-density magnetic recording media [88, 93], multiferroic hetero-structure composites [88], magneto-elastic devices [35, 88], optoelectrical devices [35], resistive switching [86], oil-water multiphase separation [86], on biomedical field there are applications on drug delivery [35, 86, 87, 94, 95], biosensors [93], as contrast enhancement agent in magnetic resonance imaging (MRI) [35, 86, 87, 94, 95], magneto-sensitive, tissue imaging [35, 95], cancer therapy [95], molecular imaging [94, 95], hyperthermia treatment as heat mediators [35, 86, 87, 94, 95]. Hence, CFO NPs has been emerging as an interesting material to be implemented into modern electronic devices, as capacitors, sensors or high-capacity batteries. CFO can also be a good approach in sustainable mobility such as solar vehicles, thus it has been a great interest to optimizing and synthesising this material [96].

Before its implementation, there are some precautions to be accounted with, since CFO particles are directly affected by its nanoparticles' size, strains/defects and most of those applications need a narrow particle size distribution [86, 94]. Consequently, these depend on the CFO manufacturing method.

2.4.3. Carbon nanotubes

Carbon nanotubes (CNTs) are one of the many allotropic of carbon forms. There is graphene, which is a 2D carbon form and they can wrap and form fullerenes (a 0D structure), or a 1D structure in order to originate nanotube. When piled up they form graphite. In Figure 2.9-a,b,c, and d these structures are demonstrated [97].

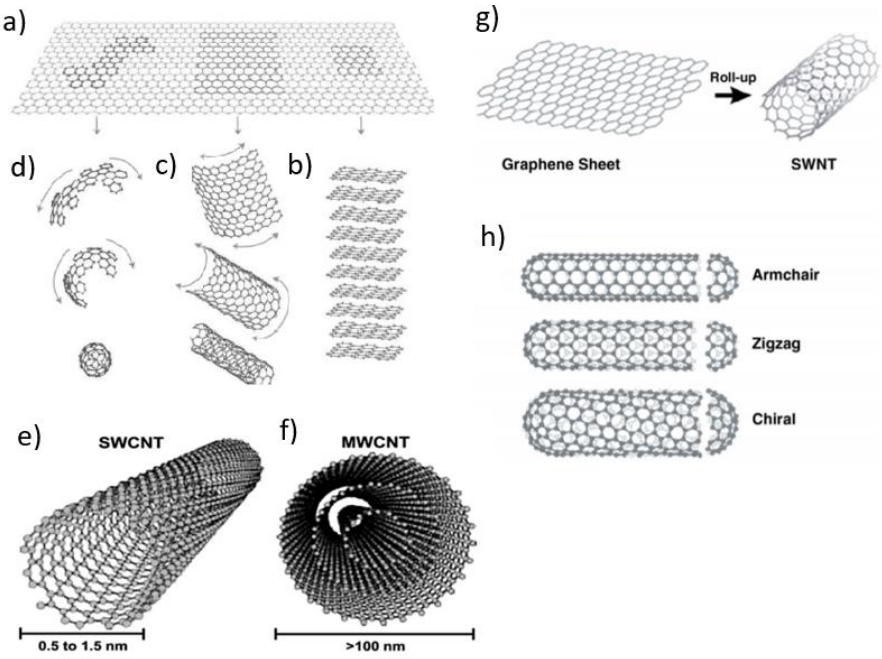

Figure 2.9. Allotropic forms of carbon as a) graphene b) pilled to create graphite c) rolled up to form nanotubes and wrapped to origin fullerenes taken from [97], Representation of e) SWCNTs and f)MWCTNs [98] and g) SNCNT formation and its h) different classifications [99].

Nanotubes are cylindrical molecules which roll themselves out on thin sheets of graphene. CNTs diameter are typically measured in nanometres and can be described as a long fullerene whose walls of the tubes are hexagonal carbon, which can be classified as single wall (SWCNTs) or multiwall (MWCNTs) depending on the number of concentrically interlinked nanotubes cylinder [98, 100, 101] and based on their size, structure and electromechanical properties [101]. Figure 2.9-e and f show the visual differences between both SWCTNs and MWCNTs.

Comparing to other fillers CNTs are the strongest and most conductive ones [98, 100], they have exceptional geometric structure, excellent properties [102, 103] and high surface area and large aspect ratio [101, 104]. The high aspect ratio of CNTs lead to a strong Van de Waals attraction forces between individual nanotubes, that is why they exist mostly in bundles/packs. In order to achieve their full potential in property improvement they must have a good adhesion to the polymer matrix from the composite which leads to a well-dispersion reinforcing agent. Their role as a reinforcement depends not only on the amount added to the hostage but also to the level of dispersion. These is still a challenge that will allow the achievement of composites with lower density, improved mechanical behaviour, electrical

or thermal conductivity. These might be more difficult since the usuals polymeric materials used are non-conductive [105].

Both SWCNTs and MWCNTs have remarkable mechanical proprieties [102, 104, 106, 107], with high tensile strength 63 GPa (50 higher than steel) and elastic modulus 1000 GPa (5 times higher than steel) [98, 103, 108, 109] , good electric properties [102-104, 106] and low electrical resistivity, high thermal stability (lower thermal expansion coefficient) [98, 101, 102, 104, 105] due to the high thermal conductivity on the plane of graphene [109], it has lightweight of $\approx 2 g^{-1} cm^3$ [98, 101, 102, 104, 108], unique optical properties [102], high waviness characteristics [102], high corrosion resistance [102], chemical stability [101, 103], thermal stability/flame retardation [110], strong hydrophobicity [108], immunity to environment factors and ease to produce [98]. CNTs chemical bonding is based on a sp^2 orbital bond - carbon is able to form four covalent bonds with carbon or other element - which make it the strongest and hardest material documented about tensile strength and elastic modulus, respectively [99].

They have incredible electronic properties and upon their structure (diameter and helicity) can be classified as metallic or semiconducting materials [99, 102]. Thus, their use in polymeric composites improves their mechanical and electrical properties [103, 105]. Usually, CNTs have lower conductivity comparing to coper and other metals used for the conductive applications, although it is common to use techniques which allows the increment of this property such as doping, threading/ bundling of multiple CNT tubes and its hybrids [98]. Therefore, the used of CNTs instead of cooper and costly silver and silicon in electronic equipment has a high impact to the relieving of heavy metal consumption and environmental pollution [108].

Despite composite materials, CNTs are also a promising material for nano-electronics [102], nano-sensors applications [100, 102], electrochemical sensors [105], nanoprobes [100], flat panel screens [100], smart materials [102], energy and storage devices [100, 102], biological application [102], medicine industry [102], water and air purification systems and into vast fields [102]. In almost all the CNTs application cases they act as a reinforcing nanofiller in order to create lightweight high strength nanocomposites materials/ structures for applications in aerospace, automobile, sport and medical field [102].

CNTs physical and chemical properties highly depends on the manufacturing methods, being an important factor to CNTs morphology [111] To synthetise these nanoparticles there are some promising techniques such as arc discharge (AD), laser ablation (LA) and chemical vapor deposition (CVD) (induce the catalytic growth) [99, 102, 103, 112]. The growth of MWCTNs occurs at both lengthening and thickening, and during the growth the nanotubes tend to keep open but at some point, due to the pendent bond at the extremities they tend to close themselves. The growing edge is stabilized through the connection of the carbon atoms and consequently prolonging the life of the open structure [103].

Table 2.8 shows the differences between both SWCNTs and MWCNTs.

Table 2.8. Comparation between MWCNTs and SWCNTs adapted from [98].

SWCNT (Single wall carbon nanotubes)	**MWCNT (Multi-wall carbon nanotubes)**
Behaviour between metals and semiconducting materials	Behaviour like metallic materials
Diameters on the range of 0,7 to 3 nanometres	Diameters on the range of 4 to tens nanometres Distance between carbon sheets around 0,34-0,39 nm
Length in the order of hundreds of micrometres	Length up to a few millimetres

SWCNTs are made of a simple sheet of graphene wrapped on itself and depending on the way the graphene sheet is rolled up a SWCNT can have different mechanical and electric properties (Figure 2.9-g). They can be classified as chiral or achiral, in which chiral are symmetric and are divided into armchair or zigzag. While all conductive SWCTNs have an armchair structure the semiconductive possess a chiral or zigzag structure, as represented in Figure 2.9-h.

MWCNTs has advantages over SWCNTs since it has lower cost, ease of mass production, easy functionalization, and higher stabilities. For sensors applications the MWCNT has

advantages due to its morphology, high interfacial bonding with polymeric matrix since it promotes the tendency of the material to turn back to its original form, even with the presence of micro-cracks created under strain forces. Even SWCNTs being structurally a simpler material, the use of MWCNT has been popularized due to its higher degree of functionalization and comparing to SWCNTs it also minimized the tendency to form agglomerates [101].

MWCNTs has been an important piece for the fuel cell since it has been used to electro-catalyse an oxygen reduction reaction [103]. It can be used as proper intermediate between electrodes and enzymes, due to their high surface area, high surface volume ratio and to the commune electrical, conductive and mechanical properties of all CNTs. MWCTNs have the capability to improve electrocatalytic activity since it has in its structure an edge-plane-like site situated at both extremities and into at the defect region. These nanoparticles do also create changes into energy bands near to the fermi level and have recently been used for the manufacturing of electrochemical biosensors [106]. In MWCNTs only the outer graphitic shells do participate on the material strength. Otherwise, the inner layers almost do not contribute to carry the load and only decrease the strength per given volume [113]. As MWCNTs are usually hydrophobic they are not readily dispersed in water. Sonification is a useful tool to help the dispersion, but without the addition of a surfactant then MWCNTs would fall out of the water dispersion in a few minutes. The properties of the surfactant should be considered along with the intrinsic properties of the MWCTs [114].

CNTs conductivity occurs due a free and dislocated electron which can travel into all nanotube network and conduct electricity along the surface. As been unidirectional materials the charge transportation does not spread for both SWCNT and MWCNT [109]. In CNTs the charge transportation depend on a number of parameter as defects [107], doping of tubes [107], number of tubes junctions [107], tube-tube interaction [107], number of walls[107], scattering centre [107], dimensions of tubes [98], helicity [98], purity of carbon material [98], semiconducting/metallic nature [107]. These parameters interfere into the determination of transport behaviour, which can varier from ballistic to diffusion, as for example at room temperature the estimated resistivity for 10 and 18 nm are 10 and 50 mΩ.m, respectively [107].

A fact to be concern about is that CNTs tend to agglomerate and develop bundles. The creation of agglomerates is promoted by strong Van der Waals bonds. which make more difficult its dispersion on melted polymers or fluids. The insolubility in water and in organic solvents also difficult CNTs applications [109]. When dispersed in water as happens at this work, the dispersion quality is usually evaluated based on the short-term stability without needed centrifugation to remove bundled nanotubes, whose prejudice the composite properties. In order to stabilize CNTs nanoparticles into water dispersion can be used several types of surfactants [113]. Despite that, the chemical inertia of CNTs surface and weak interactions with most polymers are limitations to produce nanocomposites with good mechanical properties, which depends on the capacity to highly disperse the CNTs agglomerates as well as establish a strong CNT-polymer interface. The chemical modifications of CNTs surface have being proving to be an efficient strategy to improve the compatibility between the filler and the polymer and to improve the composite properties, being the enhancement of their dispersion possible. Some techniques as solution mixing, in situ polymerization and melt-mixing have being tried to make homogeneous dispersion of CNTs in a polymeric matrix [104].

This surface modification to improve the adhesion of CNTs-polymer by functionalization can be through either covalent or not covalent methods. While covalent modification improves the adhesion and chemical properties, it disturbs, to some extent, the graphic structure of CNTs walls. In the case of non-covalent functionalization, it increases modulus and strength of the composites and both nanotubes graphitic structure and properties remain without initial changes [105].

Despite functionalization, which can damage the CNTs structure with the increment of dispersibility, made at the cost of mechanical and electrical properties when introducing the polar groups, non-covalent physical adsorption of surfactants and polymers can also be used, in order to disperse CNTs in aqueous medium. It is widely used to overcome the van der Waals interaction and to enhance the dispersibility of CNTs, without changing the chemical structure of CNTs and stabilizing the dispersed CNTs by electrostatic repulsion or steric hindrance of the micelles created around them. Independently of these, sonication is a recognized method to break up bundled or entangled CNTs. The common methods of sonification used are bath and tip sonification and provide mechanical energy to disperse the suspended CNTs. Although it is

always related to a certain degree of damage to the CNTs from their breakage and may induce defects to their sidewall structure [82].

When applying surfactants molecules to change surface energy of CNTs, it prevents the destruction of π electronic system of the sidewall graphene structure, which usually occurs with the use of aggressive chemical modification. The surfactant in contact with CNTs, the hydrophobic part of the surfactant is oriented toward the CNT surface and the polar part interacts with the outside zone which is the solvent molecules [105].

Some distinctive surfactants were used as dispersion support for MWCNTs by several research groups, such as sodium dodecyl sulphate (SDS) polyethylene glycol sorbian (Tween series) or hexadecyl trimethyl ammonium bromide (CTAB) [105].

It is also important to explore the potential release of MWCNTs and evaluate the exposure as part of any environment, health and safety risk assessment [110].

2.4.4. Barium titanate

Barium Titanate, $BaTiO_3$ (BTO) is one of the most common ferroelectric perovskite materials, and it has a formulation type ABO_3 [115-122]. It is known as a biocompatible material with good piezoelectric and electro-magnetic properties [120, 121, 123]. It also possesses large non-linear optic and electro-optic coefficients [117, 118, 120], high dielectric constant and polarization, and lower values of dielectric losses [117, 119]. The position of ions Ba^{2+}, Ti^{4+} and O^{-2} are the factor which provides large amount properties and applications [115]. The fact of being a lead-free ferroelectric ceramic makes it an environment-friendly material [124], which due to the excellent dielectric, pyroelectric and ferroelectric properties makes it be mainly used on multilayers ceramic capacitors (MLCCs) [119, 121, 125], sensors and actuators, electro-optic materials [119, 121, 125], integral capacitors in printed circuit boards (PLBs)[125], temperature-humidity gas sensors [119, 121, 125], memory applications [125], positive temperature coefficient of resistance (PTCR) [119, 121, 125], energy storage, capacity [124], microwave absorbers [124], semiconductors [124], among others.

It seems that hollow structures can enhance the dielectric properties of BTO NPs. From the past decades some approaches in order to produce BTO hollow nanostructures have being developed, which are layer-by-layer colloidal templating, molten hydrated salt, and doping

methods. However, these methodologies are complicated and simpler processes are needed [124].

Ferroelectric materials are a subgroup of pyroelectric materials, which are crystalline and polar materials which have a range of temperatures where they have a spontaneous polarization, i.e., even at absence of an external electric field, the dipole's moments per unit of volume tend to align themselves. The difference on the ferroelectric materials is the fact that its polarization can be inverted when an electric field is applied. So, in order to the material to be called as ferroelectric it must have both, a spontaneous polarization and a reversible polarization. The ferroelectric behaviour is given trough a small distortion of the paraelectric phase from its crystallographic structure [116]. Piezoelectric ceramics are ferroelectric materials with the difference that the ferroelectric behaviour is not observed above the curie temperature (around 120 °C) (Tc).

Lead-free piezoceramics have some problems associated, in the case of BTO based piezoelectric it reveals stable piezoelectric properties, although the problem is the lower Curie temperature, which is ≤100 °C and lower coercive field which leads in more temperature dependent proprieties, a lower polarization stability and even difficulties when polishing [120].

Piezoelectric ceramic materials have a large number of the unit structures with the same polarization direction, which are the domain. Without the presence of an external electric field, the material domains remain zero, when applied the domains align in parallel way to the direction of the applied electric field, as the positive side of the electric dipoles facing the negative electrode and the negative side facing the positive electrode. If applied into polymer matrixes it significantly improves the dielectric properties, electrical conductivity, magnetoelectric effect, and electromagnetic interference shielding effect (reported to nanospheres of 16 wt.% with grain size of 20 nm in poly vinylidene fluoride (PVDF)) [123].

To specify, usually ferroelectrics have as characteristic the change of its structural phase at low temperatures, denominated as ferroelectric dominant domain [115, 118]. At higher temperatures it has the characteristic of a paraelectric, the positive charge centre does not match to the negative charges originating on an electric dipole. Lower than Curie ferroelectric temperature at ambient temperature, BTO structure transforms to a tetragonal

form, in which a great spontaneous polarization occurs and the size of crystals on structure of BTO decreases. It is at Curie temperature when the higher value of dielectric constant appears [115, 118]. If heated above 120 °C the unitary cell from BTO becomes cubic and all their ions get symmetric positions, and it is stable until 1460 °C [115, 118, 126]. Higher than this temperature the hexagonal structure is stable. This hexagonal structure can occur at room temperature if the BTO nanoparticles would be prepared from a polymeric precursor [126]. Thus, the BTO microstructure is directly related to the ferroelectric performance and consequently the devices quality [125].

If an external electric field is applied and all the domains get aligned on the same direction, and the material becomes all polarized to a maximum value, then it is called saturation polarization. If the external electric field is removed, almost all the domains remain orientated creating a memory effect, then it is denominated as remanence polarization. If the orientation of each domain gets a configuration in which all domains cancel each other, depending on the intensity of the electric field applied, that it is a coercive field [116].

The particles' size plays an important role on ferroelectric proprieties. Thin ferroelectric particles decrease their proprieties with decrement of particles size being vanished above the critical size (10-20nm) [127].

When talking about pure BTO it is an electric insulator with a high energy gap of 3,05 eV at room temperature. Although when doped with small metals, it turns into a semiconductor and allows the tailoring of its proprieties depending on a specific technological application.

2.5. Green electronics: relevant works

To be recognized as green electronic device there are some requirements that should be fulfilled. The design of the product must be taken into consideration, including the materials from matrix to filler and solvents used, the manufacturing process and consequently the amount of energy used at all processing, use, and disposal/recycle.

To implement this idea, especially in printed electronic, it is needed to apply greener subtracts, inks, through the applications of biodegradable materials as through application of new methodologies. Although, there are some degradable synthetic materials which also have

been applied in order to decrease the environmental impact [128]. Bio-origin materials has advantages for the high-performance and functional electronic devices for being non-toxic, due its biodegradable [129, 130], having excellent mechanical properties [129, 130], low-cost, and usually biocompatible [129, 130] or bioresorbable in case of biomedical application, and suitable to be used as gate electrode insulators for organic field effect transistor (OFET), including solar cells, light-emitting diodes (LEDs), batteries, applications since many of them have excellent isolator proprieties and easy to process [128, 130].

Lead-free compounds have been studied since it is considered one of the most hazardous materials. Baraskar *et al.* has successfully created a superior quality high dense microstructure $BaTiO_3$ lead-free electro-ceramic material with their Ferroelectric and Piezoelectric Properties Tuned by Ca^{2+}, Sn^{4+} and Zr^{4+}, for electro-strictive device application [120].

In biodegradable substrates the paper has been widely applied, which derives from cellulose, a low-cost biodegradable material, non-toxic and which has biocompatibility properties, also being readily degradable by bacteria in soil [128]. To show the potential range of applications for paper-based green electronics, Zhu *et al.* have described a method for the preparation of transparent paper substrates right from thin (400 µm to 1 mm) wood slices cut perpendicularly to the direction of growth [131]in an easier way.

Chen and Ye *et al.* produced a cellulose-based nanocomposite by the addition of cellulose nanocrystals (TCNCs) to O-(2,3--dihydroxypropyl) cellulose (DHPC) in order to synthesize a cellulose-based flexible paper substrate with a high transparency [132]. Ma *et al.* added cellulose to AgNW to produce a transparent conductive film to apply as a substrate in PSCs [133]. Jin *et al.* developed a transparent substrate based on chitin (poly-β-(1,4)-*N*-acetyl-D-glucosamine) nanofiber-based transparent paper to use as substrata on OLED devices [134]. Rincón-Inglesias made a magnetically active material based on a three-water soluble cellulose derivative and cobalt ferrites nanoparticles by a 2D printing process, a screen printing approach [135]. Recently, Lei *et al.* reported an ultrathin, ultralightweight cellulose substrate which is a biocompatible and totally disintegrable semiconducting polymer for transient electronics [136].

Jia *et al.* developed a "top-down" method to produce an anisotropic flexible paper which exhibits both transparency and haze from pre-delignified wood materials by shear pressing technique [137].

Within engineering of paper-like electronic substrates silk fibres and films are also a suitable natural material with biocompatibility and biodegradation rates, low-cost and easy to process. From an insoluble protein in silk is fibroin by a diversity of moth genera and insects is produced which has potential to be implemented in the production of paper-like substrates for green electronics, and also have remarkable biocompatibility, ease of chemical modification, slow degradation in vivo, and processability from both aqueous solutions and organic solvents [128]. Recently, Ji *et al.* showed the used of paper-like fibroin films as substrates for being applied in memory devices, which can degrade in 24 hours in a phosphate-buffered saline solution [138].

Among the class of semiconductors has surged another derived from the π-conjugated molecules, achieved directly or via natural inspired synthetic material [128]. Irimia-Vladu in 2010 produced thin film transistors by the use of a series of natural or natural-inspired material, which were all biodegradable and significantly less toxic [139]. Irimia-Vladu *et al.* reported transistor devices with good electrical properties which have been produced from some distinct organic semiconducting materials supported by shellac and hard gelatine substrates. Both shellac and hard gelatine used as substrates is still at its initial stage [139].

In another report of Jin *et al.* was used chitosan as a biodegradable substrate by deposing AgNW onto an antioxidant acid-modified chitosan polymer and produce transparent bottom electrodes for the PSCs. To avoid the degradation of perovskite precursor it can be protected from modified polymer without blocking the charge carrier drift by the interface of the insulating polymer [140].

Seck *et al.* used a water-soluble almond gum, freshly extracted from the almond tree, which is a natural biodegradable material to produce a bottom gate/bottom contact organic field-effect transistor, where the almond gum acts as the gate dielectric [141].

Some synthetic polymers, interesting due to their biomedical implants, have also been identified as a potential material to make film-like substrates for green electronics. One example of this is PDMS which have been approved for use by the National Heart, Lung and

Blood Institute of the United States, been proved to be a remarkable substitute substrates in flexible and stretchable electronics [128].

It is also possible to introduce biodegradability into synthetic polymers via commonly hydrolysable linkage as ester, imide and urethane bonds. Lei *et al.* reported a totally disintegrable semiconducting polymer from the use of imine bonds as conjugated linkage DPP and *p*-phenylenediamine moieties [136].

Advances in techniques are also important for electronics to consume less energy, with lower costs and use fewer toxic materials in the process. For example, Lin *et al.* used a fully green vapor deposition to produce stable and scalable 3D-2D planar PSCs [142]. To avoid a big energy consumption of vacuo-deposition Chen *et al.* has proposed a solvent and vacuum-free rout in order to offer a fully green processing of non-toxic or solvent-free, low energy consumption and heavy metal-free in future PSC industry [128, 143]. In the batteries field, which has been studied since everything is more about electric devices which need new, better, and greener batteries. Huang *et al.* reported a high-performance, biodegradable battery as in vivo on-board power supply using a dissolvable Mg anode, which has high theoretical energy density and remarkable biocompatibility [144]. Another report on the battery field was made by Fu *et al.* about a biodegradable transient lithium-ion battery involving a high-capacity origami cathode with large mass loading, a three-layer anode with integrated structure, and a bilayer battery packaging [145]. Chen *et al.* demonstrated chitosan as being a highly effective additive for lithium–sulphur batteries, enhancing cycle performance and the discharge–charge capacity [146]. Edupuganti *et al.* successfully produced a biodegradable battery using Mg as the anode and Fe as the cathode. The battery was made from different processes, first the production of the biodegradable substrate by a thick film of chitosan which was spin coated on a silicon wafer. Then by laser micromachining of Mg foil a contact mask and spiral was formed, which was placed onto the chitosan layer with clips in order to avoid misalignment [147].

The use of carbon has also grown due to its remarkable properties, either mechanical, electrical, and chemical stability. For example, Mashkour *et al.* reported a multi-walled CNTs (MECNTs)-coated cellulose as electrically conductive cellulose nanotapers [148]. Using water as a solvent Babayigit *et al.* prepared a yellow carbon quantum dots (Y-CDs) being the o-phenylenediamine the carbon source [149].

There are already some works about the 3D techniques on electronics connected with the use of biodegradable materials. The use of micro-contact printing technique was used by Mizutani *et al.* to implement e bovine serum albumin (BSA), cytochrome c and BSA-fluorescein isothiocyanate as the charge injection and transport layers in OLEDs [150].

To implement 3D techniques as inkjet printing and similes the enhancement of bioinks is required, since some natural materials have already been used in electronics. Hu *et al.* prepared a novel supramolecular hydrogel-based bioink composed of PEGylated chitosan, gelatine, α-CD, and β-GPS through dual physical crosslinking constructed by a 3D bioprinter. This process was performed without a toxic by-products or hazardous components, and the manufactured bioink has shown both biocompatibility and tuneable strength [151].

Carrageenan, a promising natural polymer, has started to be studied, despite there being more works about k-carrageenan due to its properties and rheology. K-carrageenan has been the one used into 3D printing techniques since 3D printing induced the in-situ jellification of k-carrageenan aqueous solution. Diañez *et al.* has used a RepRap 3D printer with modification to be able to in situ jellifies carrageenan-in-water dispersions [152].

On electronics, ι-carrageenan started to be studied to be used as a polymer electrolyte. Moniha *et al.* accomplished a conductive biopolymer electrolyte NH_4No_3 with ι-carrageenan via solution casting technology to apply into electrochemical devices [70]. Moniha *et al.* also produced a biopolymer of ι-carrageenan with different compositions of NH_4SCN by solution casting technique, being the amorphous nature of the polymer electrolytes confirmed. The polymer electrolyte with higher conductivity has been employed to a primary proton battery [153]. Sugumaran *et al.* prepared a gel polymer electrolyte based on ι-carrageenan polymer, sodium iodide (NaI), 1-butyl-3-methylimidazolium iodide (BMIMI) and iodine as a redox mediator. It was produced into a Dye-sensitized solar cell (DSSC) [154]. Arof *et al.* has used in an electrical double layer capacitor (EDLC) a chitosan/ ι-carrageenan polymer electrolyte where the chitosan/ι-carrageenan combined film ionic doped with orthophosphoric acid (H_3PO_4) and used a poly (ethylene glycol) (PEG) as plasticizer to act as a separator and electrolyte [155]. On sensors Bener *et al.* developed a novel biopolymer-based optical sensor using as the support material to the sensor ι-carrageenan [156].

DIW is becoming the most flexible approach to make 3D electronic components, 3D electrodes and even integrated devices because of the easy printing strategy and fabrication

process. On electrodes manufacturing Zhu *et al.* used graphene oxide and silica powders suspensions to produce the ink to print 3D periodic structures [157]. Lacey *et al.* added holey graphene oxide to green solvents as water, to produce additive-free inks with suitable rheology, to be employed to print lithium–oxygen cathodes with the similar structures to Zhu *et al.* [158]. Sun *et al.* reported patterning viscous graphene oxide ink as interdigitated microelectrodes via DIW on the PET film and creating the symmetrical micro-supercapacitor. It showed a capacitance of up to 19.8 $mF.cm^{-1}$, and excellent flexibility, mechanical robustness and cycling stability [159].

Into printed circuits Zhang *et al.* melt-blended reduced graphene oxide and poly (lactic acid) (PLA) as printable inks for printing 3D circuits [160]. Hu *et al.* produced a particle-free composite ink, mainly by soluble silver salt and adhesive rubber for DIW, and preparing highly conductive stretchable circuits [161]. To functional components, sensors for instance, Vatani *et al.* and Abas *et al.* adopted the method of DIW first followed by packaging to produce layered resistance sensors [162, 163]

Chapter 3 - Materials and methods

3. Materials and methods

3.1. Materials

3.1.1. Hydrogel preparation and printing

ι-Carrageenan was purchased from *Alfa Aesar* into powder form. Ultrapure water was provided by Minho University. The particles used $CoFe_2O_4$ NPs with 35–55 nm particle size, were purchased from NanoAmor, Multi-Wall Carbon Nanotubes (MWNT), Nanocyl-7000 with 90% C purity with average diameter of 9.5 nm and an average length of 1.5 µm particle size were purchased from *Nanocyl sa,Belgium.* $BaTiO_3$ with 100nm particle size were purchased from SkySpring Nanomaterials. The surfactant Triton X-100 (aqueous) was purchased from Sigma-Aldrich.

3.2. Experimental methodology

3.2.1. Hydrogel synthesis

The solution of pure ι-Carrageenan was produced by dissolution of 3% wt. of polymer into ultrapure water at ambient temperature, by magnetic mixing. The solutions of I ι-carrageenan and CFO NPs were produced for a concentration of 0,5 wt.%, 1 wt.%, 5 wt.%, 10 wt.%, 20 wt.% and 30 wt.% CFO NPs.

First a surfactant (Triton X-100) was added into the ultrapure water to help on the particle's dispersion (Figure 3.1 - 1st step). Then, the particles were added and placed into the ultrasound for 3 hours (Figure 3.1 – 2nd step). Next the natural polymer was inserted, and the mixture was mixed by mechanical agitator for another 3 hours (Figure 3.1 – 3rd step).

The solutions of ι-carrageenan and MCWNTs were produced to concentrations of 0,25%wt, 1%wt, 5%wt and 6%wt MWCNTs. The solutions of ι-carrageenan and $BaTiO_3$ (BTO) concentrations were 1%wt,5%wt,10%wt,20%wt,40%wt BT. Both were performed in a similar way as CFO particles. Although as mechanical agitation was not necessarily needed to MWCNTs and BTO when introducing the polymer, magnetic agitation was used once it only would have influence on magnetic particles. The magnetic agitation was performed at around 50 rpm overnight.

With MWCTNs this percentage was chosen due to the electrical percolation. The percolation threshold is round 1 wt.% CNTs. Higher than this concentration, mechanical

properties decrease as result of increasing agglomerates and wetting of CNTs agglomerates by the polymer gets worse [164, 165]. The best energy harvesting performance has found to nanocomposites samples with 20 wt.% BTO filler contents of 10nm particles size and for 5 wt.% BTO content for the 100 and 500nm. All percentages higher than 5 wt.% BTO allowed the study of the properties given to the composites considering the used filler size [166]. The 20 wt.% CFO composite data is plotted as representative for all composites [167]. Thus, all percentage higher than 5 wt.% BTO and 40 wt.% CFO were made to evaluate if the properties achieved compensate the amount of extra material used. The concentrations of CFO NPs lower than 20 wt.% CFO were made to see how the properties change during the filler addition.

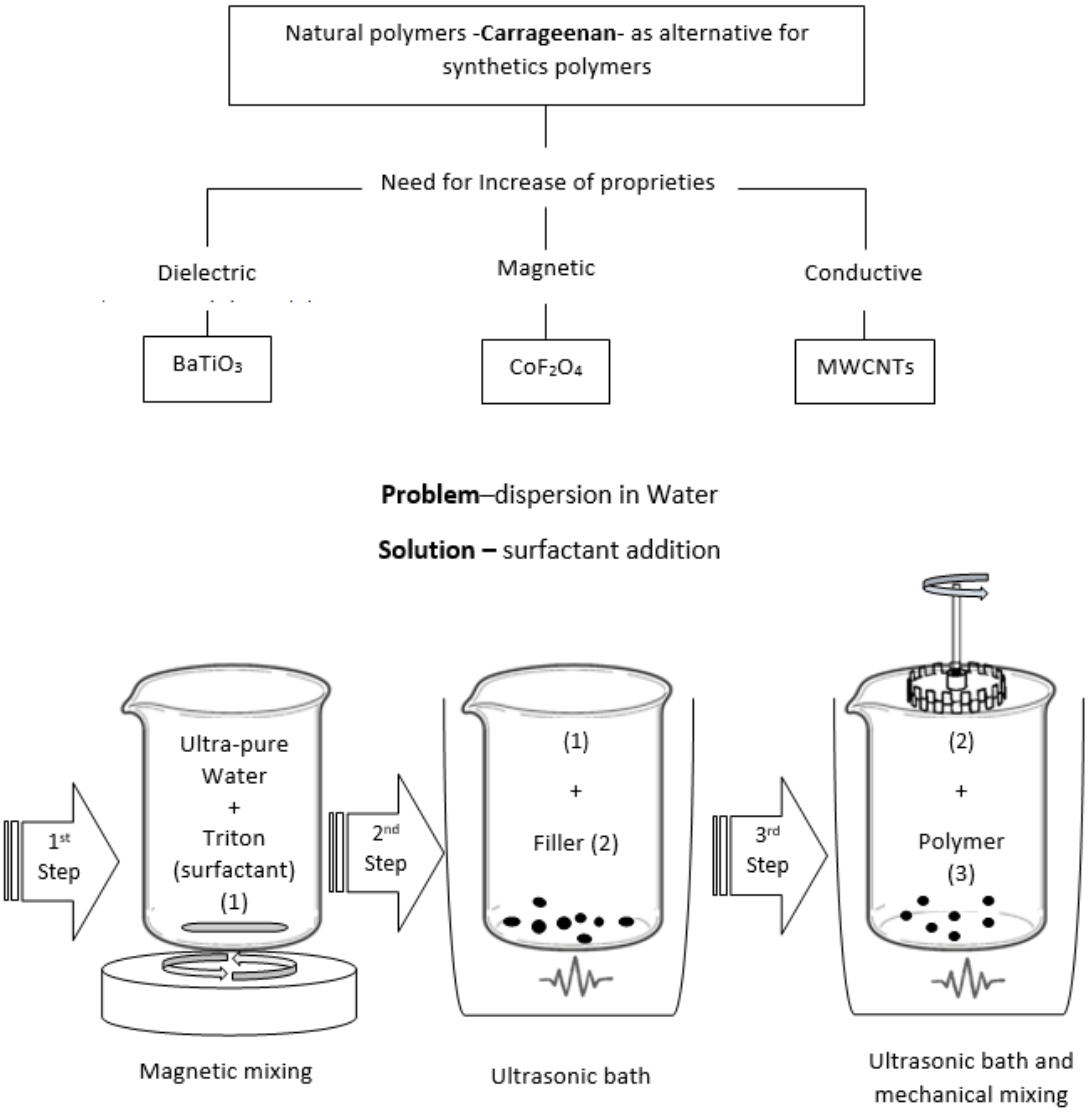

Figure 3.1. Scheme of ink solution methodology process.

3.2.2. Printing process

The ink solution was transfer into the syringe and isolated with a parafilm on the entrance of the piston and on the entrance of the needle with a little polymeric stopper. Then it was inserted into a falcon and the correspondent weight measured, so it was possible to have a similar falcon with water. Then, using a centrifuge at 2500rpm for 15minutes it was possible to remove the bobbles within the ink solution. Next, the piston was inserted back into the syringe, carefully to avoid the creation of new bobbles. The syringe with the ink was put into the bioprinter and after calibration it was ready to print, according to the respective design and parameters programmed. The printing parameters used were a needle of 0,41mm, with a space line of 0,51 to avoid overlay of lines on the same plane, with retraction, at 300mm.s^{-1} and 0,008 extrusion multiplier.

3.3. Characterization techniques

3.3.1. Scanning electron microscopy

Scanning electron microscope (SEM) consists of a focused beam of electrons to scan a surface rectilinearly. While it happens, simultaneously, the signal from the interaction between material surface and the beam are detected from a microscope and converted into the glowing points according to the amount of detected electrons. Then it is displayed on a video screen, showing the respective electron image, and providing information about the sample's topography or composition. These microscopes are equipped with magnetic lenses instead of optical ones and can have multiple detectors, each able to analyse a different type of signal [168-170]. Thus, SEM provides high-magnified, high-resolution images of the under investigation particles' surface [170]. The scheme with this technique system is shown in Figure 3.2-a.

SEM will be fundamental to analyse the detailed picture of the material's surface as well as the cross section by a cut on the samples. It is possible to see if the sample's surface has some granules or irregularities and study the morphology between layers by cross section morphological analysis. This kind of parameters are usually not perceived by naked eye.

To proceed to the analysis a small portion from the sample was cut and then coated with a 15nm thick layer of gold. The morphology of the samples was made by Nano SEM – FEI Nova 200 (FEG/SEM)), at Basque Centre Materials, Applications & Nanostructures

(BCMaterials). It was made to the sample's surface and cross-section, with amplifications of x0,5, x2,5 and x10.

3.3.2. Energy-dispersive X-ray analysis

Energy-dispersive X-ray (EDX) analysis acts as an addition to imaging sample's surface structure and morphology, since this technique can give information of elemental analysis with an EDS detector [170, 171]. The analytical information from EDS or EDX results from radioactive and respectively non-reactive decay events of core holes. Core holes are made by the ionizing interaction between primary electron beam and atoms of the samples. Typical X-Ray photons can travel across at the micrometre scale and so almost all information is delivered by EDX with electron excitation.

An electron beam made by an electron microscope cathode is needed. When the primary electron beam hits the sample's surface, it creates different interactions, one of them X-ray. This method can give qualitative information's about elements and also their spatial distribution in the samples, being able to form an elemental mapping [170]. Figure 3.2-b has an illustration of this equipment.

SEM with EDX can also provide semi-quantitative information from the surface and subsurface layers due to its high penetration depth (approximately 0,5 µm to 3 µm) depending on the procedure conditions [172]. Thus, it will be useful to analyse the presence and the elemental distribution of the particles within the samples.

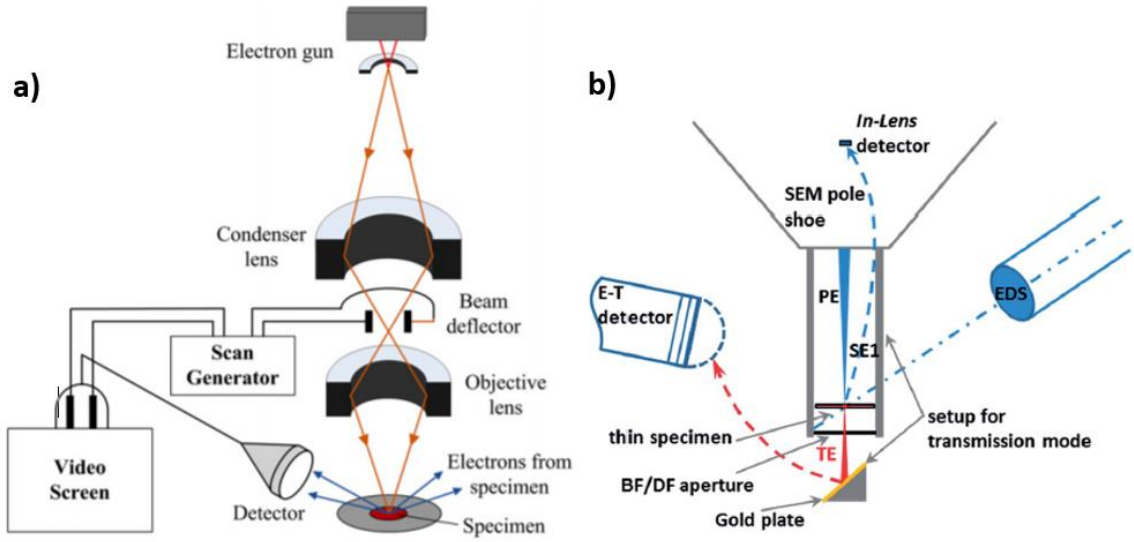

Figure 3.2. Scheme of a) SEM and b) SEM/EDX [171] technique.

In addition to SEM, the complementary EDX analysis was performed by Hitachi Tabletop Microscope TM 3000, as well as SEM to the surface samples and cross section. It detected the existence of oxygen (from polymer and water, solvent) iron and cobalt (both from CFO NPs) in CFO NPs samples, in BTO particles oxygen (from polymer and water, solvent), barium and titanium (both from BTO particles). In the case of CNTs NPs, it would not be useful since carbon, which is the main difference between particles and the rest, will be everywhere and the images would return in black. Like SEM analysis, EDX was performed at Basque Centre Materials, Applications & Nanostructures (BCMaterials).

3.3.3. Dynamic thermogravimetric analysis

Dynamic thermogravimetric analysis (TGA) is a technique that consists of a measure of mass loss (or weight) of a material as a function of temperature increase, at a constant heating rate, over time, on a controlled temperature program in a controlled atmosphere. The scheme below in Figure 3.4-a exhibits the mechanism of a scale used on TGA analysis [173].

The atmosphere control is made by a purge gas, nitrogen or oxidizing atmosphere such as air or oxygen, introduced through the scale which creates an inert atmosphere. The possible moisture within purge gas can be controlled by a range of temperatures between dry and saturated. Usually, samples' size range can vary from less than a milligram to a gram or more.

Thermosets usually shows mass loss, and yields information about three categories, volatile components (absorbed moisture, residual solvents, additives/oligomers from ambient to 200°C), reaction products (cure of phenolic resins, blocked catalysts from 100 to 250°C) and decomposition products (250 to 800°C). This information can be related with moisture content, residual solvent, composition, magnitude of cure and thermal stability. The cure and aging of the materials can be standard and predicted by determined kinetics of these processes, namely because of thermal and thermo-oxidative processes. The study of these measures are mainly used to determine the composition of polymer products and precursors, they can also be used to measure thermal stability and analyse the influence of some additives such as anti-degradants on thermal property [173].

Therefore, this technique will allow the study of the material mass loss due to the loss of intrinsic water or polymer degradation as a result of temperature increase [174]. The advantage of this Knowledge is to be aware of the temperature at which the material can be used without being destroyed.

TGA measures were performed in a *Thermal Gravimetric Analyzer (TGA) TGA/SDTA 851e Metter Toledo Apparatus* equipped with a thermo-scale, at Basque Center Materials, Applications & Nanostructures (BCMaterials). Each sample is tested one by one, the sample is introduced into a bowl and fixed in a hook. The mass measure is performed by the equipment itself. The samples were heated from 30°C to 600°C at a rate of 10°C.$^{-}$min^{-1} with a nitrogen flow rate of 50ml.min^{-1}. The software used to retrieve the data was *Pyris* and to make the TGA graphs to analyse was Origin.

3.3.4. Differential scanning calorimetry

Differential scanning calorimetry (DSC) consists of the measurement of the heat flow into or out of a material as a function of temperature or time. DSC scanning calorimetry can provide detailed information of both physical and energetic properties [175]. In this technique the both, crucible with the sample and reference crucible, are slowly heated, and it is analyse the endothermic and exothermic events and the difference between the energy needed to increase the temperature of both crucibles, and thus determine the heat flow of the material, and as a result its thermal properties [168]. The endothermic events can result from a loss of

a low molecular weight substance, such as water or a solvent, from the sample due to its volatility, from stress relaxation or even from melting of a crystalline structure within the matrix. The exothermic changes can occur from development of cross-links due to a chemical reaction, from decomposition of a sample due to anaerobic or oxidation degradation, from decomposition of a sample by chemical degradation and from formation of a crystalline structure within the sample [176, 177].

An example of a standard result from DSC analysis is shown in Figure 3.3.

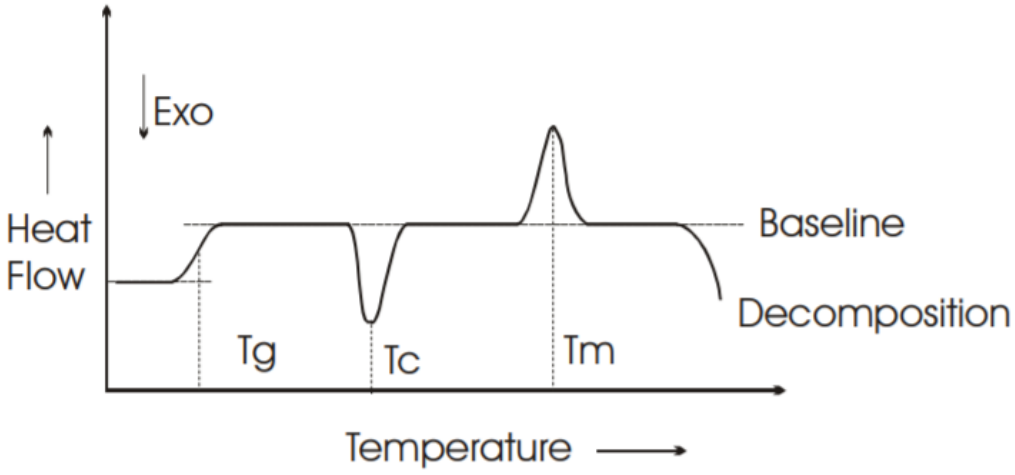

Figure 3.3. Standard DSC curve for a polymer with glass transition (Tg), crystallization temperature (Tc), melting temperature (Tm) and finishing with decomposition of the polymer adapted from [178].

The glass transition, Tg, is the temperature below which the molecular movement ceases, only vibrational movement is detected. This is a kinetic transition [4]. The crystallization temperature, Tc, is the temperature of transformation during the cooling process of an isotropic liquid to a crystalline solid. For a material with low molecular mass and high purity, Tc corresponds to the intersection of the baseline and the minimum point of the exothermic curve. The melting temperature, Tm, is the temperature at which the material changes from a crystalline solid into an isotropic liquid [178].

Moreover, it can also give information about other thermo-events of polymers as identification of crystalline polymers and polymer blends trough their melting points, whose endotherm areas and references from standard materials can give a semi-quantitative information. It is possible to identify polymers by their glass transition temperature (Tg) and

investigation of events that can affect both Tg and transition temperature (Tm) such as thermal history, additives, or molecular weight. DSC also allows a cure study on rubber compound, cross-linking analysis on thermoplastic, thermal stability testing, and crystallisation kinetic studies on crystalline plastics [176, 177]. The scheme of DSC principle is shown in Figure 3.4-b. In DSC technique it is possible to use both oxidising, for oxidation stability tests, and inert atmospheres (usually nitrogen). For compositional work an inert atmosphere is preferred to ensure that the data achieved is stable and representative of the material. Like TGA, the samples' size used on testing are relatively small (5 to 10 mg). For the tests semi-open aluminium pans are used, with sealed pans capable to hold the internal pressure and they are only used for curing studies, where endothermic response that would interfere with the curing exotherm caused by loss of volatiles from the sample [176]. The scheme of this technique is shown in Figure 3.4-b.

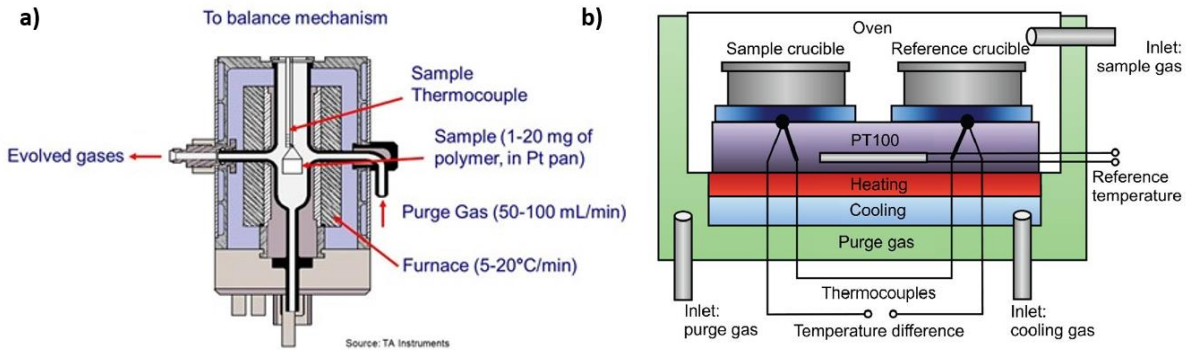

Figure 3.4. Principles of a) TGA balance [173] and b) DSC techniques [179].

Thermal properties of the sample by DSC were performed using a Mettler Toledo DSC 822e equipment equipped with a sample robot under nitrogen flow of 50 ml.min^{-1}, at Basque Center Materials, Applications & Nanostructures (BCMaterials). STAR software was used to retrieve and analyse the data. The samples sizes used on the test were between 6 and 10mg. The scans were made from 20°C to 150°C at a heating rate of 10°C per minute. The samples were weighed and compacted in an aluminium crucible, in which a small hole on the top of it was made, so any gas originated on the heating process would safely escape without exploding the crucible due to the increase of internal pressure.

3.3.5. Vibrating sample magnetometer

Vibrating sample magnetometer (VSM) is based on Faraday's law which defends that a change in a flux through a coil creates an electromagnetic force [180]. This technique allows the analysis of material's magnetic properties, such as coercivity, permeability or magnetization, as a function of magnetic field, temperature, and time. Nevertheless, this technique is commonly used at ambient temperature for hysteresis loop determination [168].

CFO NPs is a ferromagnetic material, which means that it is permanently magnetized even without the existence of an extern magnetic field, thus it fixes into the group of the hard magnetic materials. There are needed products as magnetic information-storage media and permanent magnets. For the magnetic state of these materials not to be easily distorted by an external magnetic field, they should have high coercivity and great anisotropies. As a result, when in contact with an external magnetic field the magnetic state would not be easily distorted [89].

The saturation magnetization is the maximum magnetic strength of the material when an external magnetic field is applied. This happens when the driving line approaches without pass through the horizontal magnetic line [181].

The remanence is the measure of the remaining magnetization when the running field drops to zero. Remanence also is the remaining magnetic field within the material after the magnetic field being removed. So, to a soft magnetic material it assumes much value loss since these do easily lose their magnetic energy when the applied field drops to zero. To hard magnetic materials it should assume high level of permanent magnetism after realising the magnetic field [181].

The coercivity corresponds to the needed field to decrease the magnetization to zero when saturation passes. It is dependent on the magnetization process, and can be denominated the nucleation field, domain wall coercivity or anisotropy field. For the magnetic films it becomes a more and more complicated parameter since it is related to the reversal mechanism, the magnetic microstructure as dimensions and shape of the crystallites, the surface and initial layer proprieties, nature of the boundaries, and so on [89].

In practice, a small sample from the material is holding by a rod between two large electromagnets, which applies a uniform field. Then the sample is put under mechanically vibration by the magnetic field generated by the electromagnets, which induce a voltage in

the sensing coils proportionally to the magnetic moment of the sample. This approach is shown in Figure 3.5-a.Usually, the oscillator operates with a known frequency, between 50 and 100 Hz, and at a fixed amplitude somewhere around 1–3 mm [168, 182]. The different magnetic properties of the material under study can be determined when recording this technique for various strengths of the applied magnetic field [168].

Magnetic analysis to the samples of ι-Carrageenan with CFO NPs were performed by measuring the magnetization loops between -18kOe and 18kOe and the hysteresis cycle is seen. The equipment used was Micro- Sense EZ7 VSM at Basque Centre Materials, Applications & Nanostructures (BCMaterials). The measurement of the mass sample is essential to allow the accomplishment of the following calculations. This test was made at different temperatures (20°C, 50°C and 100°C), in order to verify if there is some dependence on magnetic proprieties with temperature increasement.

3.3.6. Fourier transform infrared spectroscopy

Fourier transform infrared (FTIR) is a non-destructive technique which provide quantitative and qualitative information to organic and inorganic materials [183-186]. It identifies chemical bonds through the absorption (or transmittance) over a range of wavelengths (or frequency) from a material, and the plot of absorption versus wavelength is an IR spectrum providing a profile of the sample. It is possible because every material with chemical elements along with functional groups which vibrate together with rotational movements associated to specific infrared absorption bands, as a material fingerprint [183, 185-187]. Despite being an analytical instrument to detect functional groups, it is also able to characterize covalent bonding data [183, 185].

FTIR methodology consists of collecting an interferogram, a pattern formed by a wave interference, of a sample signal through an interferometer, followed by the performance of a Fourier Transform, which is a mathematical algorithm. It only requires tens of micrograms of a sample and if smaller particles need to be analysed, for example 10mm in diameter, it is possible to couple spectrometers to microscopes [188]. This technique is useful to determine the composition and structure of the sample as well as to know the quantitative amount of radiation absorbed on each certain wavelength of the band [168]. FTIR technique approach is represented in Figure 3.5-b.

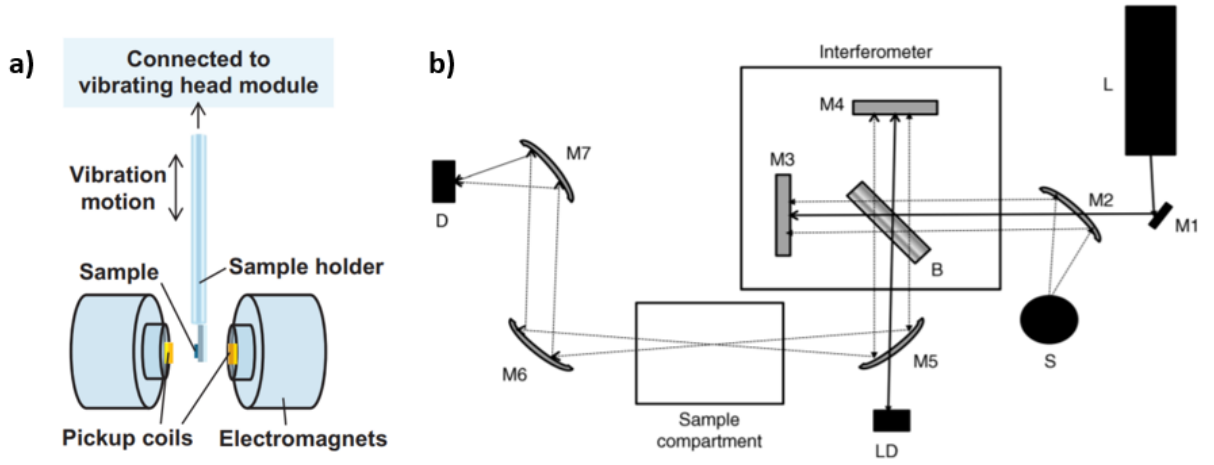

Figure 3.5. Scheme of a) VSM [182] and b) FTIR [186] techniques.

The equipment used to FTIR measurements was Jasco FT/IR-4100 system apparatus at Basque Centre Materials, Applications & Nanostructures (BCMaterials). The samples pure (ι-Carrageenan) and with the respective added particles (CFO, CNTs and BTO) were placed in the deuterated triglycine sulphate (DTGS) sensor and their transmittance was measured at room temperature, in attenuated total reflection (ATR) mode, between 600 cm^{-1} a 4000 cm^{-1} using 64 scans at a resolution of 4 cm^{-1}. ATR decreases the noise from the test which make the peaks from the FTIR curve more perceptive, but in the other hand the total peak intensity also decreases. The sensor was cleaned and zeroed between measurements.

3.3.7. Electric characterization

Materials can be defined as conductors, semiconductors or isolators. Conductive materials have no resistance to the passage of current in their internal structure. Once the conductive layer and the valence layer are united or really close to each other, it is possible for the charge to easily pass through from one to another. Usually, metals are the best definition of conductive materials, and their conduction decreases with the temperature increasement. This occurs because of the augment of molecular movements, which blocks the passage of electrons (charge) or holes due the collisions with metallic atoms within material structure, when an electric field is applied. In isolators the energy gap is so big that the charge is not able to pass from the valence layer to the conductive layer. These materials are mostly associated to ceramics, wood and cork. In the case of semiconductors, they behave as an

isolator, but they do not have an energy gap as big as real isolators, and when enough energy is provided the electrons or holes (protons), depending on if it is a *n* or *s* type, can pass to the conductive layer. Germanium or silicon are the most common semiconductors [189].

To distinguish conductor from semiconductor materials there are two main techniques, the Hall effect and the temperature dependent effects. To semiconductors and for common measurements the contactless measurement is usually done [190].

To study the dynamic of bounds or mobile charge to the impedance spectroscopy is used [189].

To analyse the conductivity of materials the flow resistance of electricity (ρ) of a material can be measured, and this is designated as electric resistivity of a material. If the material can easily let the flow of electricity pass through, like a conductor material, it corresponds to a low electric resistivity (around 20 nW m). Otherwise, if the material has difficulties in letting the flow of electricity pass, as it is the case of isolators, then it has a high electric resistivity. Usually, the Ohm's law is used to calculate the resistance (R, ohm). IA voltage (v, volt) is applied across the sample and the current (I, Amper) flows through it. When obtaining the result of resistance by Ohm's law, it is possible to determine the resistivity, and then the conductivity. The techniques to execute this kind of tests are the two-point technique, the four-point technique and the sheet resistance technique, van der Pauw technique [189, 191].

For the execution of the analysis to be possible, first, all samples must be subjected to a deposition of electrodes in both sides of the films, by a technique of sputtering by plasma. The equipment used was *BOC Edwards Scancoat Six* Sputter Coater, represented in Figure 3.7-a. It was made a deposition of gold, into an atmosphere of argon, 2 minutes (120 seconds). To begin this technique first the pressure in the chamber must be reduced and air introduced, so it can be opened to introduce the samples. All samples must be organised and numbered so they can be identified at the end. Then the chamber is closed, vacuum is created and at the same time argon introduced until the moment it achieves the ideal pressure. For the chamber to be clean from impurities and other particles it must be waited a minute. The cleaning of proves is important to a successful deposition since the presence of impurities and other particles except argon would create a high number of collisions and consequently make it more difficult, so could make it into the sample's surface. In this case, argon works as a transportation vehicle from the source to the sample. Next a purple "cloud" of plasma is

created in which the deposition happens. It is normal to verify an increase of temperature inside the chamber.

So, the measuring is done by inducing a difference of potential on the top and bottom of the sample, and then measure the response of the sample. This response is verified by a graph of current by function of the induced DC, especially if it analysed some conductive behaviour on the sample. The equipment used is from Figure 3.7-b, which name is *Model 6487 Picoammeter/Voltage Source*. The IV curves were made to a range of voltage from 0V to 0,4V with a step of 0,04V to obtain a linear curve.

3.3.8. Dielectric characterization

Dielectric material starts to be described as the behaviour of an isolator when positioned between two parallel plates of a capacitor. The dielectric constant (or dielectric permittivity) of a material is its ability to store electric energy when an electrical field is applied [192].

Dielectric analysis, DEA, is strongly recognized due to its effective analysis approach for studying condensed- and soft-matter dynamics. DEA consists in a bunch of techniques which measure some specific changes in different physical properties of a polar material as polarization, permittivity, and conductivity as a function of temperature or frequency. The analysis is done when an alternating-current (AC) is provided, which corresponds to an oscillating electric field when the reorientation of dipoles and the translational diffusion of the charged particles occurs. This makes a variation on the dielectric constant and in the polarizability of the material, which can be easily detected while the phase transition and secondary transition occurs. In other words, this technique measures the ability to store electric energy when provided AC, from low to high frequency of current. Usually, it is easily at first but sometimes, as frequency increases then the time of response from the material shrinks to the current changes, until it only conducts and no longer stores electrical energy [192].

This technique has the same first procedure as electric characterization. Thus, the deposition of electrodes must be done to enable the analysis. The structure where the samples is inserted is the same as electric characterization, except that the equipment is provided with the source and receives the material response. This analysis measures the complex relative permittivity (ε_r) and complex relative permeability (μ_r) [192]. The complex

dielectric permittivity (ε*) consists of real (ε') part and imaginary part (ε''), which are given with the knowledge of thickness of the sample and the area of the electrodes, which are introduced as parameter in the computer software. Among those it is given the value of tangent, frequency and capacitance. The equipment where dielectric tests was performed, *Series 1920 Precision LCR Meter,* is shown in Figure 3.7-c.

3.3.9. Mechanical characterization

Mechanical characterization by traditional methodologies is made through tensile or compressive tests. It leads to the determination of Young's modulus, sample deformation, and tensile/compressive strength. With the analysis of these parameters the toughness and elasticity of the material can be deduced as well as the resilience and tenacity. There are some points of the nominal stress–nominal strain curves as rupture strength, yield strength, elongation at yield and maximum elongation (at break) (Figure 3.6) [193-195].

In practice, the equipment is based on claws that fix the two extremes of the test piece of the sample. Then, a compressive (push) or tensile (pull) force is applied in both extremes of the sample [193, 194]. Usually, the curve obtained is not equal to the engineer stress-strain curve, since it does not have in consideration the decrease of the transversal section area during the test, which results on an increase of elongation to the stress applied or a decrease of applied force to the elongation per second stipulated. If the material has some deformation capacity, it is possible to observe a neck formation, usually in the middle of the sample, where it is more fragile, at the plastic region of the diagram close to where the rupture occurs [194, 195].

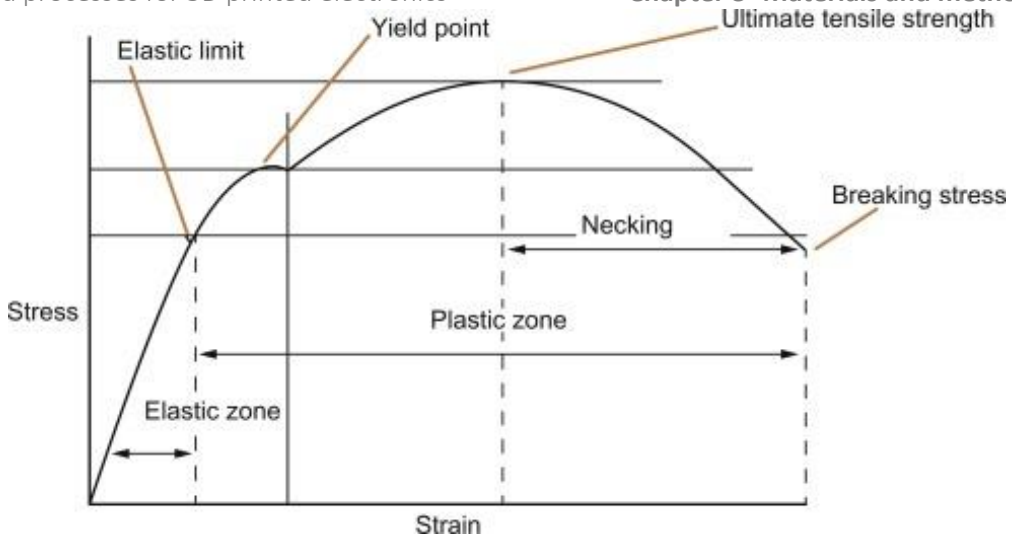

Figure 3.6.Engineer stress-strain curve and some parameters of mechanic properties [196].

Mechanical tests were performed into a system of a mechanical mechanism connected with a computer with software which allowed the monitoring during the test. The deformation defined was 15 µm/s, which depending on the material, will interfere on the necessary force to be applied to produce this deformation, and the load cell must be switched from 20N to 200N to enable the test of the sample. The equipment where the mechanical tests were performed in a *Linkam TST350 stage*, represented at Figure 3.7-d.

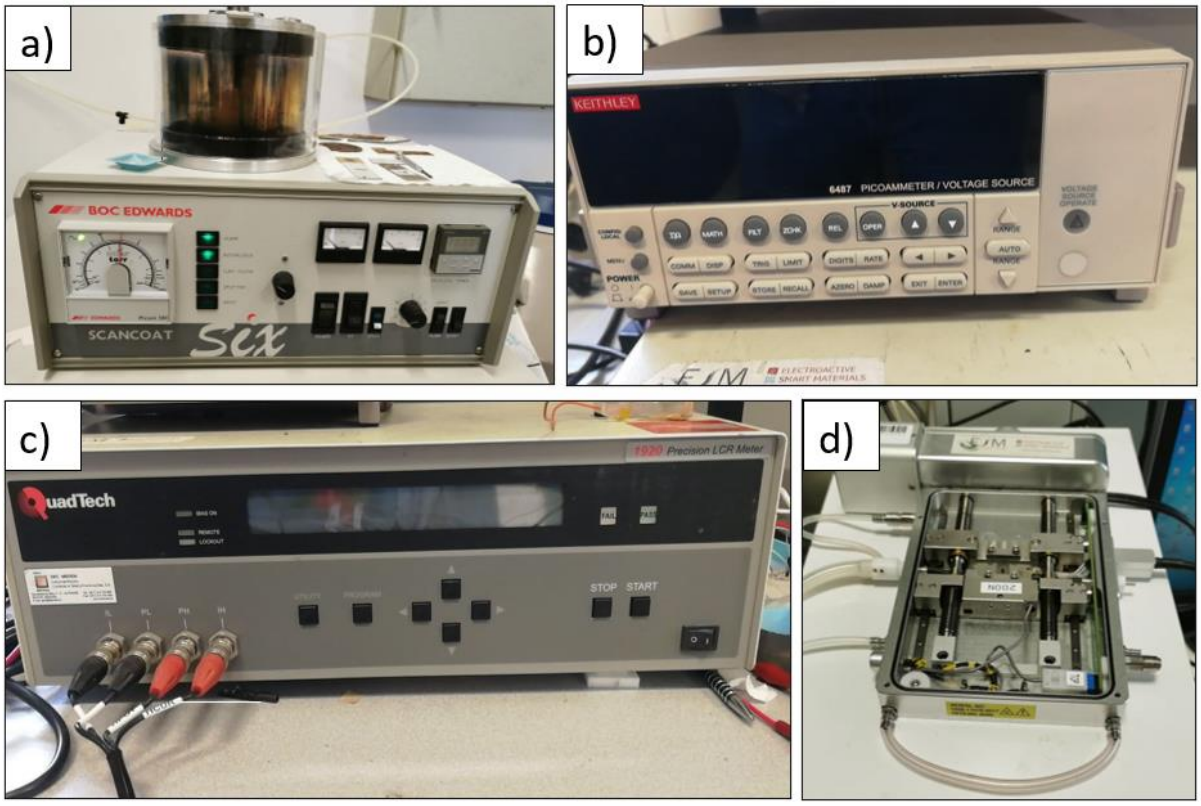

Figure 3.7. Equipment of a) was BOC Edwards Scancoat Six *Sputter Coater, b) Model 6487 Picoammeter/Voltage Source, c) Series 1920 Precision LCR Meter and c) Linkam TST350 stage.*

Chapter 4 – Results and discussion

4. Results and discussion

4.1.1. Morphological Features

For each sample, pristine ι -carrageenan and ι -carrageenan with filler addition (CFO, MWCNTs and BTO), various SEM images were obtained, with amplifications of 0.5 kX, 2.5 kX and 10.0 kX. Are prfesented in Figure 4.1 the SEM images of pristine ι -carrageenan, and in Figures 4.2 and Figure 4.4, SEM and EDX imagens of CFO, and BTO samples, respectively and, WCNTs SEM images in Figure 4.3. The chosen amplifications were of 2.5 kX, since they show the sample's morphology better.

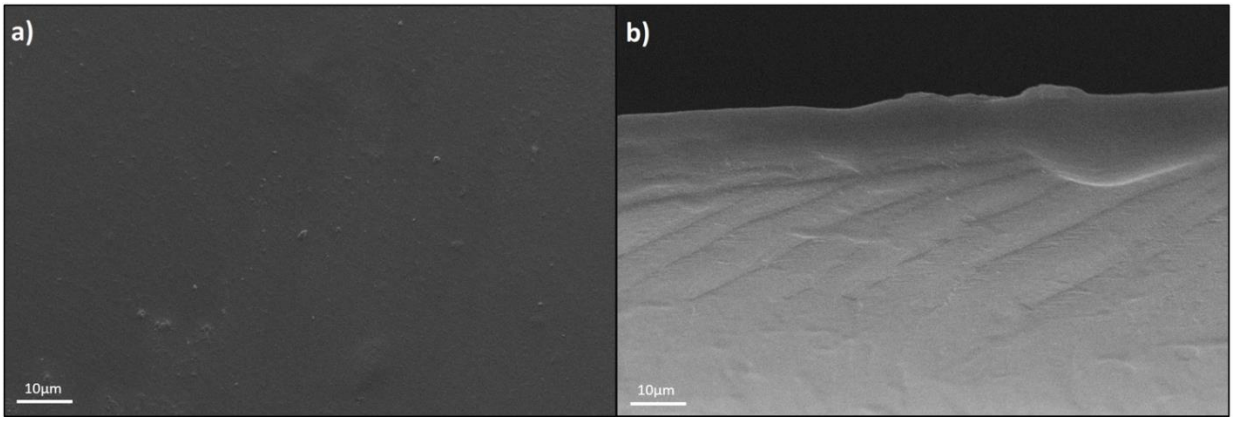

Figure 4.1. SEM images of pure ι-carrageenan on the a) surface and b) cross-section of the sample.

As it is possible to see in Figure 4.1-a, agglomerations of ι-Carrageenan at 2.5kX was not detected. In Figure 4.1-b the cross-section of the samples shows some irregularities due to the cut. The EDX analysis has only detected the presence of oxygen, within chemical structure of carrageenan and ultrapure water.

SEM and EDX images are represented in Figure 4.2 and 4.4, both with ampliations of 2.5kX. Among all EDX images, i.e., from detection of oxygen, Iron and cobalt to CFO and barium, titanate and oxygen to BTO, the most representative were selected. For CFO the distribution of iron (yellow) and to BTO the barium element (blue) was selected. In Figure 4.3 the EDX images are incorporated into SEM images, so it is easier to see if the surface particles derived from filler or not.

SEM and EDX

CFO + ι-Carrageenan	
Surface	Cross-section
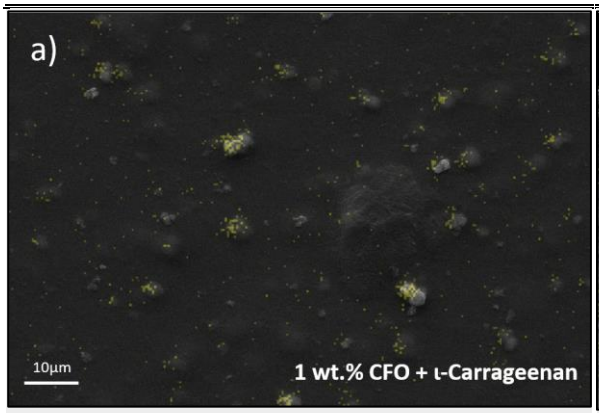	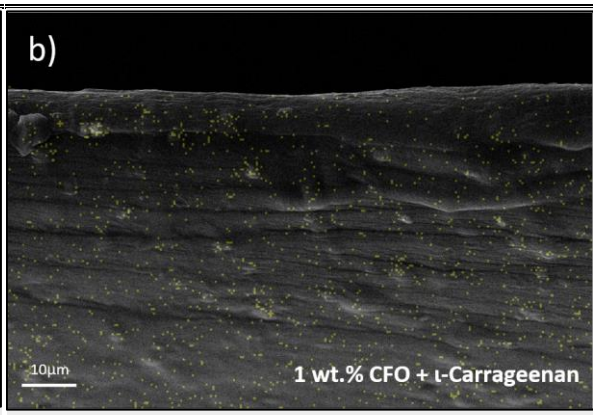
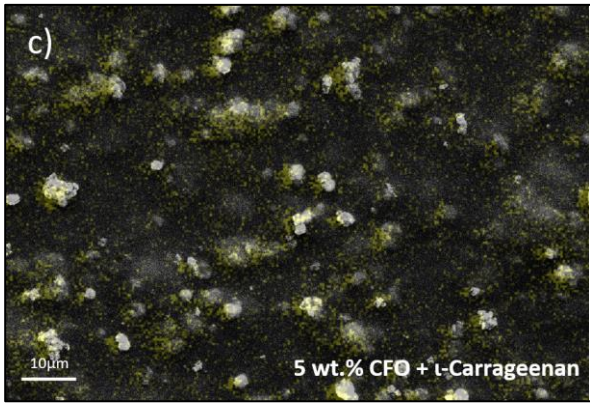	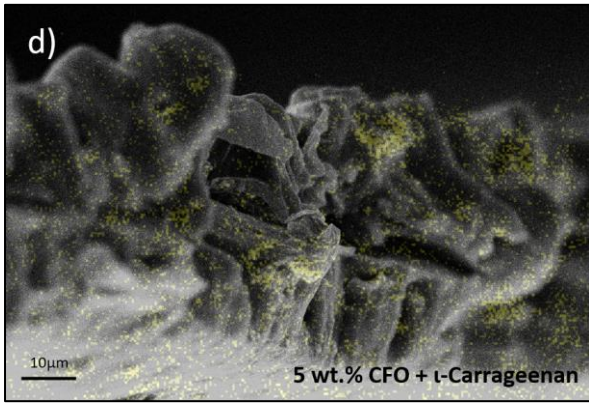
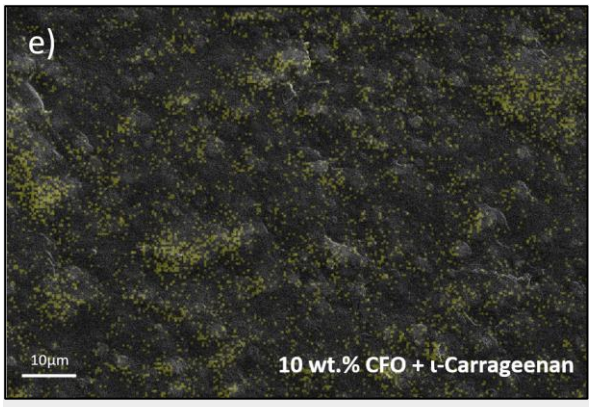	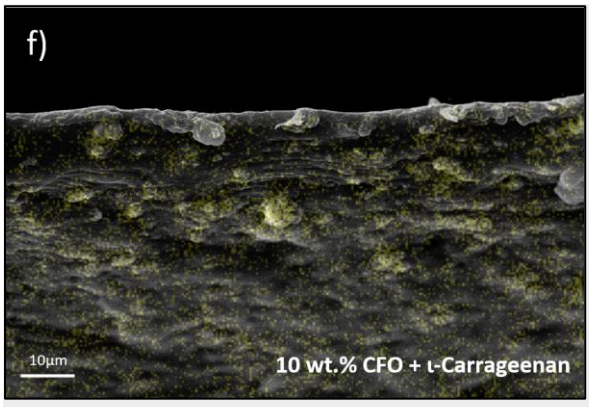

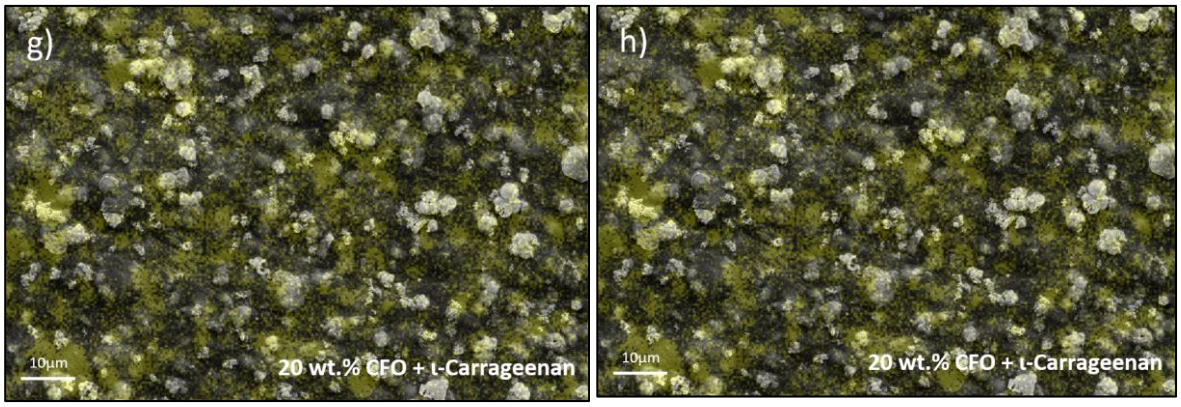

Figure 4.2. SEM and EDX images from 1 wt.% CFO,5 wt.% CFO,10 wt.% CFO and 20 wt.% CFO filler addition into ι-carrageenan polymeric matrix.

When analysing the sample's morphology of samples with CFO particles (Figure 4.2) it is can be seen that the amount of particles detected has intensified with the increase of CFO NPs percentages. Trough analysis of EDX imagens, the particles present on morphology are mostly related to the CFO NPs. With lower percentage the CFO NPs tend to agglomerate as seen in Figure 4.2, and with the increase of it the particles seem to get a better dispersion. These particles on the sample's surface can be related to the CFO NPs, to random impurities, or to a possible not completely dissolved carrageenan, since it is partially soluble in water at ambient temperature.

In SEM imagens an interface region between layers is observed, especially in Figures 4.2-d. This region could be formed during the printing process since it was given waiting a time so the material of the previous layer could colder/plasticize for a bit. In the samples with lower percentage of fillers the interface between layers was not so perceptive. There is a rise of irregularities in the sample's surface with the increase of CFO NPs in the matrix.

Figure 4.3 presents the results of SEM analysis on MWCNTs samples with amplifications of x2,5k.

SEM	
MWCNTs + ι-Carrageenan	
Surface	**Cross-section**

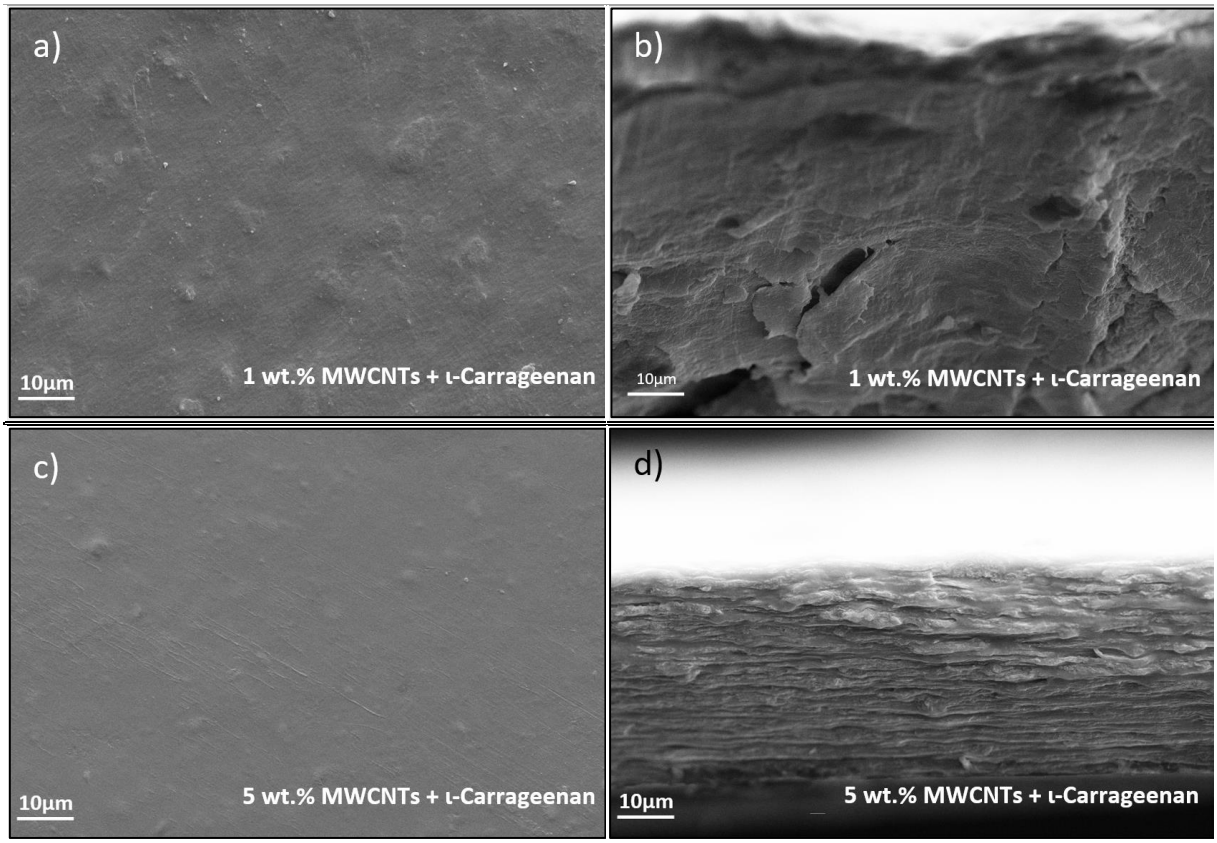

Figure 4.3.SEM images from 1 wt.% MWCNTs and 5 wt.% MWCNTs filler addition into ι-carrageenan polymeric matrix.

From SEM images of Figure 4.3 analysis, it can be seen, that all MWCNTs surface morphologies are similar. MWCTNs morphologies from the cross-section are the ones which have significant changes. In Figure 4.3-b the sample's internal morphology seems like scales with vertical ruptures. Some of those breaks seem to be caused due to the cut.

EDS analysis had not been done, since it would not be precise, the image would return all black due the interaction of photon on EDX radiation with the carbon on MWCNT, which is a conductive material.

Images from Figure 4.4 are the result of SEM and EDX analysis of BTO samples with amplifications of x2,5k.

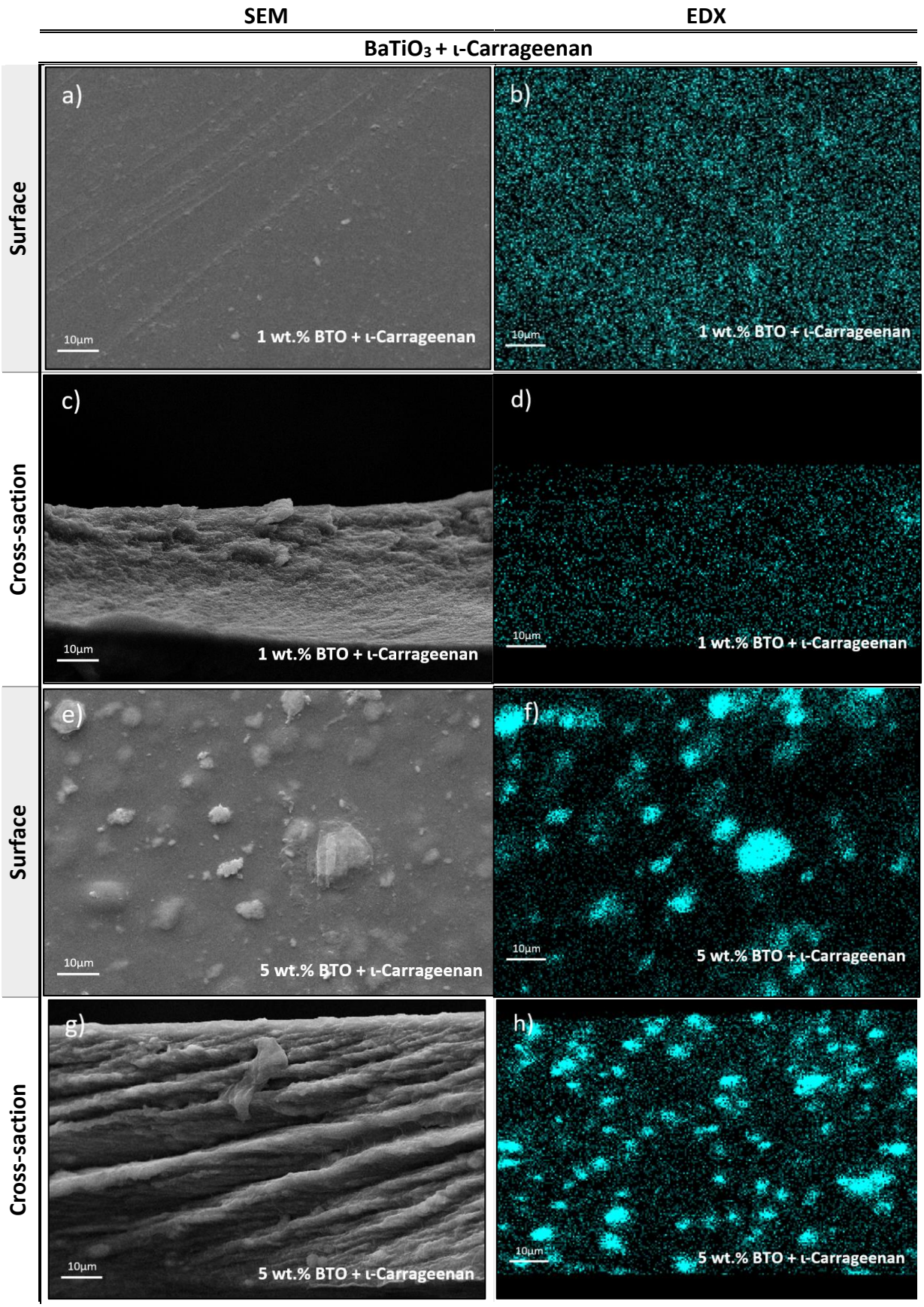
SEM
EDX
BaTiO3 + ι-Carrageenan
Surface
Cross-saction
Surface
Cross-saction
a)
b)
c)
d)
e)
f)
g)
h)
10µm
1 wt.% BTO + ι-Carrageenan
5 wt.% BTO + ι-Carrageenan

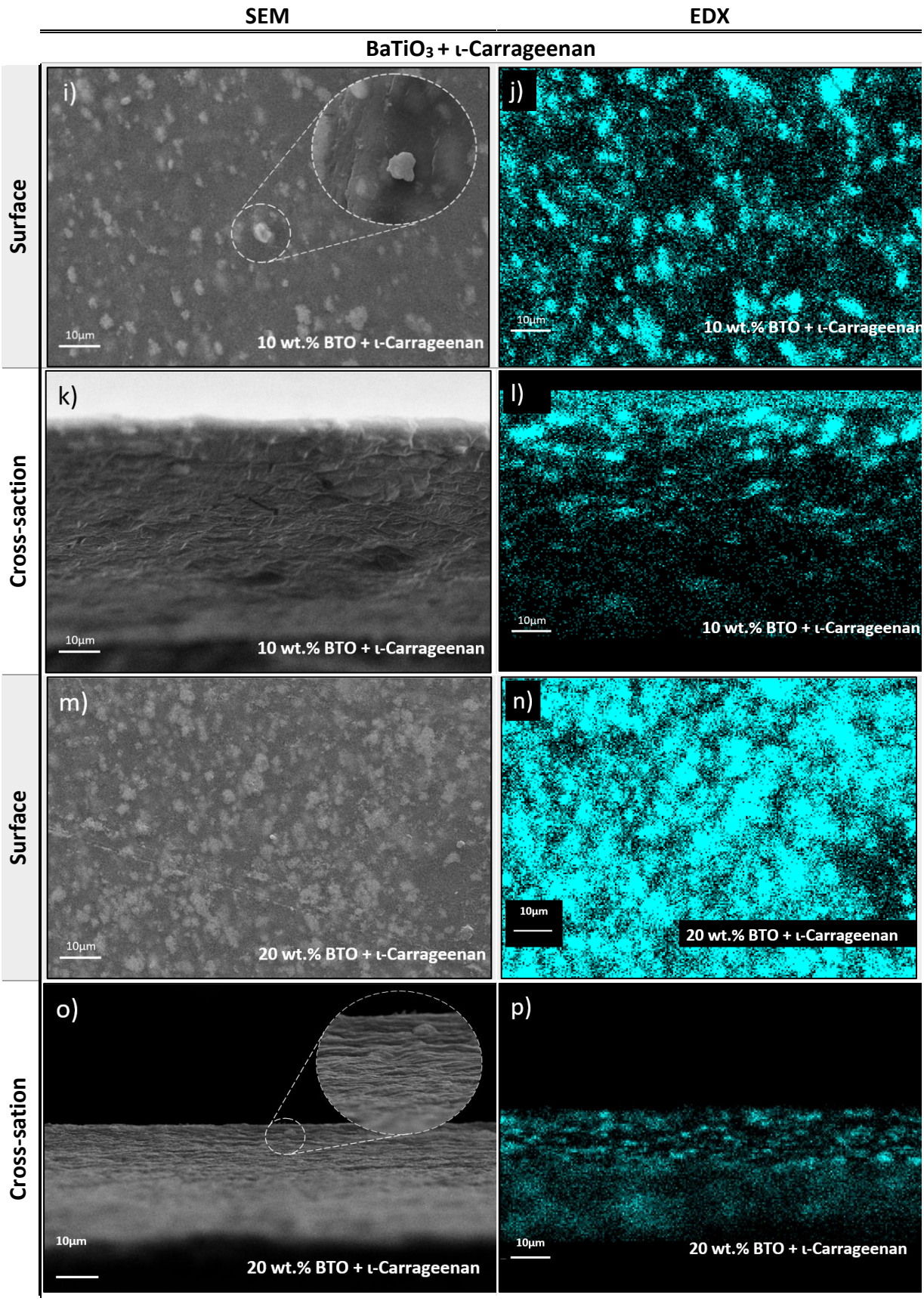
SEM
EDX
BaTiO3 + ι-Carrageenan
Surface
Cross-saction
Surface
Cross-sation
i)
j)
k)
l)
m)
n)
o)
p)
10µm
10 wt.% BTO + ι-Carrageenan
20 wt.% BTO + ι-Carrageenan

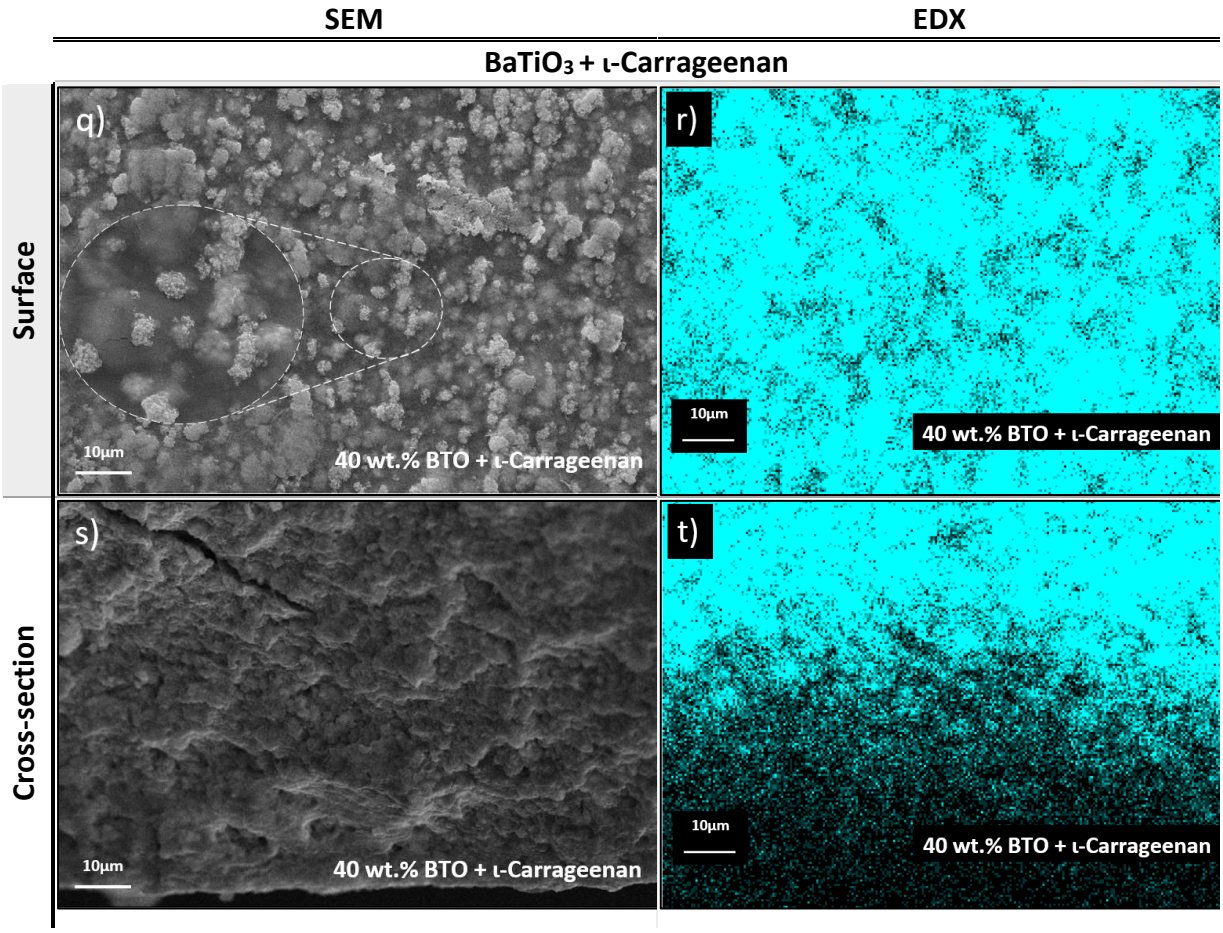

Figure 4.4. SEM and EDX images from wt.% BTO filler addition into ι-carrageenan polymeric matrix.

From SEM images of BTO samples, as from the others, it is shown that the density of qualitative roughness due to particles' presence increases with the addition of particles. In image-e and f from Figure 4.4, associated to 5 wt.% BTO NPs surface SEM and EDX respectively, has seen that has some agglomeration of BTO particles. The nature of these agglomerations was confirmed by EDX images, whose blue points correspond to Ba element present on BTO composition. In general, all EDX imagens show a good dispersion. The dispersion seems to be better at low concentration of added BTO NPs.

It was expected to have more holes in the internal structure of CFO samples since CFO based ink created more bobbles than MWCNTs and BTO samples. From CFO and BTO samples were represented concentrations of 1 wt.%, 5 wt.%, 10 wt.% and 20 wt.% filler and from MWCNTs samples were represented 1 wt.% and 5 wt.%, to easily compare how the distinctive nanoparticles do interfere into the morphological structure.

At 1 wt.% filler addition MWCNTs samples have the most homogeneous surface, comparing to MWCFO and BTO samples at same application. The cross section at 1 wt.% the CNTs and BTO samples had shown some kind of scale form being more significant to MWCNTs samples.

At 5 wt.% filler, MWCNTs samples still have a more homogeneous surface, and BTO shows some agglomerations of NPs at its surface. On cross-section all CFO, MWCNTs and BTO samples had shown a more defined layer deposition with filler concentration, where the superposition of layers can be seen. Between layers there is a slight impression of a line caused by the printing movement and layers deposition. Perhaps due to the viscosity increment, the line is thinner and has suffered more shear stress, creating more surface tension. This was predictable since the increment of all CFO, MWCNTs and BTO concentrations increases the viscosity of the ink. This can lead to defects (irregularities) by shear stress.

At 10 wt.% filler and 20 wt.% filler both CFO get a better dispersion with filler addition and BTO gains some agglomerates with it, having the layer more refined superposition.

Figure 4.4 shows all concentrations of BTO addition in order to analyse with more detail the intervention of filler addition into both surface and cross-section morphology, specially being the sample with more risks or agglomeration to occur.

To all added particles no negative change into the structure of the composite was found, which is a good and aimed result.

4.1.2. Dynamic thermogravimetric analysis

TGA allows the study of the thermal stability of the material and indicates the onset temperatures in which the material starts do degrade and in which way the change in the composition affects the thermal stability. Another important information that this technique can offer is the quantification of the interface between polymer and nanoparticles [197]. This information is relevant since it has impact on the properties being related to agglomerate issues. Usually, interface parameter decreases when agglomeration of particles occurs. In Figure 4.5 are the graphs associated to the TGA measurement of each one of the three kinds of samples.

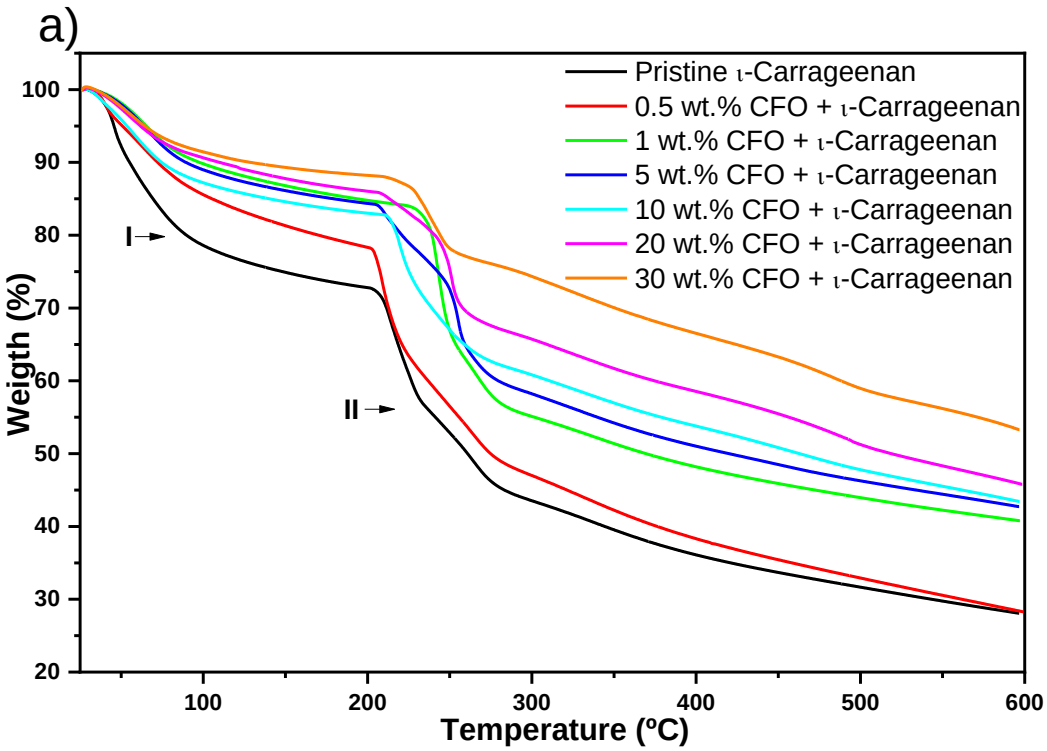
a)
Pristine ι-Carrageenan
0.5 wt.% CFO + ι-Carrageenan
1 wt.% CFO + ι-Carrageenan
5 wt.% CFO + ι-Carrageenan
10 wt.% CFO + ι-Carrageenan
20 wt.% CFO + ι-Carrageenan
30 wt.% CFO + ι-Carrageenan
I
II
Weigth (%)
Temperature (ºC)
100
90
80
70
60
50
40
30
20
100
200
300
400
500
600

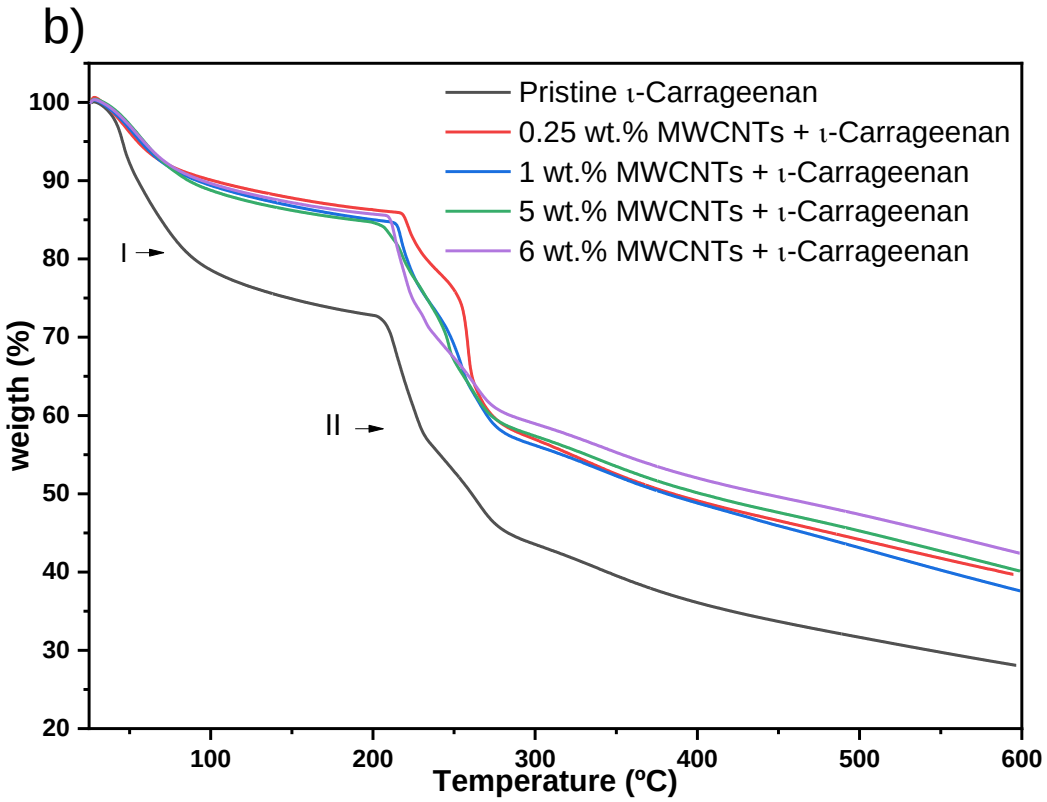
b)
Pristine ι-Carrageenan
0.25 wt.% MWCNTs + ι-Carrageenan
1 wt.% MWCNTs + ι-Carrageenan
5 wt.% MWCNTs + ι-Carrageenan
6 wt.% MWCNTs + ι-Carrageenan
I
II
weigth (%)
Temperature (ºC)
100
90
80
70
60
50
40
30
20
100
200
300
400
500
600

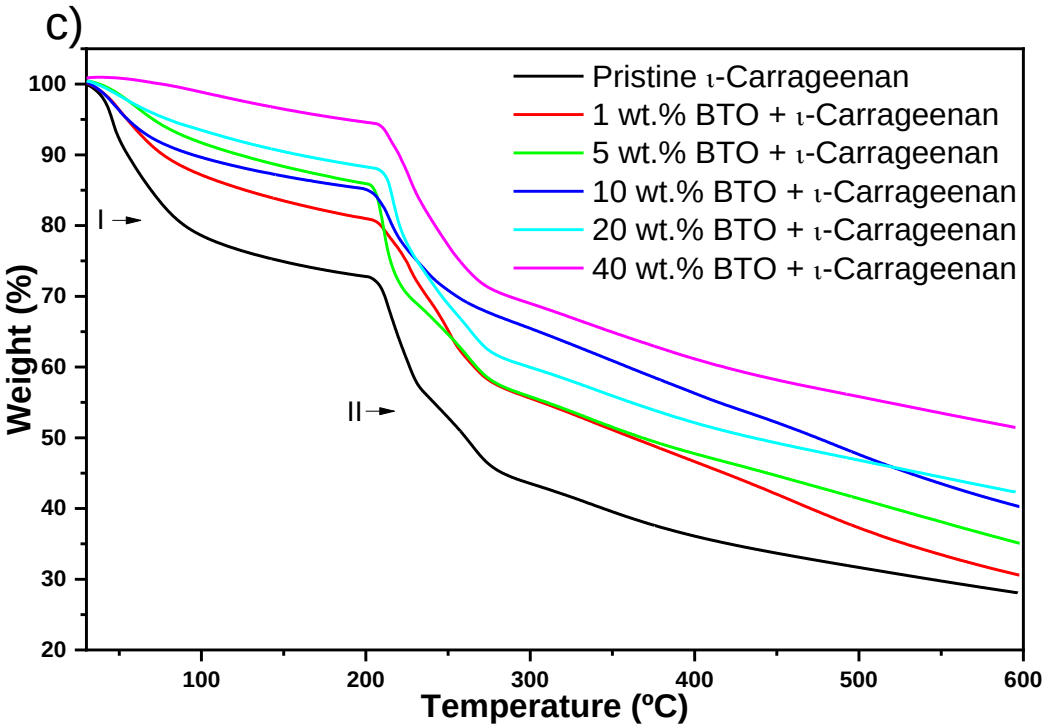

Figure 4.5. TGA Graphs from a) CFO, b) MWCNTs and c) BTO filler addition on ι-carrageenan polymeric matrix, being I- first degradation, II- second degradation.

To the pritine ι-Carrageenan the first degradation is associated to the evaporation of moiture, and occur from 14°C to 114°C of aroud 27% weight loss. The second weight loss is around 28% degradation, starting from 206°C to 282°C corresponding to the maximum peak in DTG curve at 203 °C [198]. Around these temperatures the decomposition of Triton X-100 is also related, but due to its lower concentration into the ink it has not a significant impact on the curve [199]. The addition of all particles decrease the amout of weight loss at first degradation, being gradually by BTO concentration, not linear to CFO concentrations, and more significative and close values to MWCTNs. In the second degradation the nanoparticles have the same influence, but the 20 wt.% CFO and 30 wt.% CFO samples decrease the wight loss the most. The time span of defradation also seems to get shorter.

In Table 4.1 are the temperatures where decomposition begins, also designated as onset temperatures.

Table 4.1. Onset temperatures from TGA analysis.

Samples	***Onset (°C)***	***Samples***	***Onset (°C)***	***Samples***	***Onset (°C)***	***Samples***	***Onset (°C)***
ι-Carrageenan	208 ±10	**0,5 wt.% CFO + ι-Carrageenan**	203 ±10	**0,25 wt.% MWCNTs + ι-Carrageenan**	218 ±11	**1 wt.% BTO + ι-Carrageenan**	204 ±10
		1 wt.% CFO +ι-Carrageenan	239 ±12	**1 wt.% MWCNTs + ι-Carrageenan**	215 ±11	**5 wt.% BTO + ι-Carrageenan**	206 ±10
		5 wt.% CFO + ι-Carrageenan	206 ±10	**5 wt.% MWCNTs + ι-Carrageenan**	203 ±10	**10 wt.% BTO + ι-Carrageenan**	206 ±10
		10 wt.% CFO + ι-Carrageenan	214 ±11	**6 wt.% MWCNTs + ι-Carrageenan**	211 ±11	**20 wt.% BTO + ι-Carrageenan**	212 ±11
		20 wt.% CFO + ι-Carrageenan	209 ±11			**40 wt.% BTO + ι-Carrageenan**	209 ±10
		30 wt.% CFO + ι-Carrageenan	225 ±11				

Through TGA graphic analysis pristine ι-carrageenan has iniciated decomposition first than the samples with NPs, and the first major decomposition, related to the water evaporation, is also higher. So, with the addition of CFO particles the humidity within the samples decreased.

Through Equation 1 [197], the interface between polymer and nanoparticles can be calculated, m_i, in which data information is gotten from the thermograph from Figure 4.5 and its first derivative.

$$m_{interface,i} = \frac{m(x)_{i0} - m_{i0}}{m_{i0}} \times 100 \quad (1)$$

From the derivative of the thermograph the mass of pristine ι-carrageenan at the temperature in which the mass loss rate is maximum (minimum pick of the curve) is acquired,

$m_{i0,}$ and from the thermograph the mass of composite ι-carrageenan with filler addition, in which the material has not degraded at m_{i0} temperature.

The higher mass loss of pristine ι-carrageenan occurs when polymer decomposition, the second major degradation, does not coincide with the particle's decomposition.

The higher rate of weight loss corresponds to the point (x= 214 y= 68) from the TGA of pristine ι-Carrageenan. Through interpolations the exact value of weight loss of the other samples with CFO, MWCNTs and BTO added particles can be determined, correspondent to 214 °C, $m(x)_{i0}$. The calculated values are exposed in Table 4.2.

Table 4.2. Values of calculated $m(x)_{i0}$ and m_i.

Sample	**$m(x)_{i0}$**	**$m_{interface,i}$**
0.5 wt.% CFO + ι-Carrageenan	61 ±3	1 ±0
1 wt.% CFO + ι-Carrageenan	84 ±4	24 ±1
5 wt.% CFO + ι-Carrageenan	82±4	20 ±1
10 wt.% CFO+ ι-Carrageenan	82 ±4	20 ±1
20 wt.% CFO + ι-Carrageenan	85 ±4	25 ±1
30 wt.% CFO+ ι-Carrageenan	88 ±4	29 ±2
0.25 wt.% MWCNTs+ ι-Carrageenan	86 ±4	27 ±1
1 wt.% MWCNTs+ ι-Carrageenan	84 ±4	24 ±1
5 wt.% MWCNTs + ι-Carrageenan	82 ±4	21 ±1
6 wt.% MWCNTs + ι-Carrageenan	82 ±4	21 ±1
1 wt.% BTO + ι-Carrageenan	78 ±4	15 ±1
5 wt.% BTO + ι-Carrageenan	75 ±4	11 ±1
10 wt.% BTO + ι-Carrageenan	81 ±4	19 ±1
20 wt.% BTO + ι-Carrageenan	86 ±4	26±1
40 wt.% BTO + ι-Carrageenan	92 ±5	36 ±2

As it can be verified in Table 4.2, there is one sample (1 wt.% CFO+ ι-carrageenan) which hasn´t followed the presumed logic that with the increase of particles added also increases the interface between particles and polymers.

Analysing Figure 4.5-a from TGA global graph of added CFO particles and Table 4.2 simultaneously, the anomaly of 1 wt.% CFO + ι-carrageenan could be explained by the amount of moisture within the sample. In Figure 4.5-a, the concentration of 1 wt.%, 5 wt.% and 10 wt.% CFO shows a lower loss of water comparing to the others. Also, the initial phase doesn´t have a linear behaviour and seems like to have a lower quantity of superficial water than intrinsic water, since the second major degradation occurs later.

Other reasons could pass by the water encapsulation inside an agglomeration of particles, since those samples have lower weight loss than the others. Thus, the weight loss form that water could be detected as NPs degradation, at very high temperatures.

As BTO NPs are ceramics they absorb more water than the others, although it demonstrates a lower first loss of water, and at 40 wt.% BTO does not even show that initial loss of weight.

In the case of MWCNTs NPs, a linear decrease of interface zones between particles/polymer is seen in Table 4.2. Usually, the smaller the particles are the more likely they are to agglomerate. When particle agglomeration occurs, the interface zone is smaller than a bunch of smaller particles, since the interface zone is surface-to-volume area of NPs. Analysing MWCNTs TGA graphics (Figure 4.5-b) this is the only one whose curves of all particle's percentage are close to each other.

4.1.3. Differential scanning calorimetry

DSC analysis helps to understand what happens inside the samples, to the chemical bonds, whether a degradation or creation occurs. As it is seen for all CFO, MWCNTs and BTO samples, the peaks on the DSC graphs are endothermic, which means that while the temperature increases a gain of energy inside the sample occurs. Usually, the gain of energy is associated to the creation of a bond, the exothermic peaks are related to the degradation of these bonds, whether to the dissociation of atoms or the material degradation. The creation bonds need energy to create new kinds of atoms and thus transform in the material molecular

structure, the endothermic peaks, although their break release energy. The enthalpy portraits exactly this, the energy necessary to the reaction to occur. In the case of ι-carrageenan the peak shown on the graphs below are related to the glass transition [70, 153].

The graph from Figure 4.6 is the measure of DSC test to CFO samples.

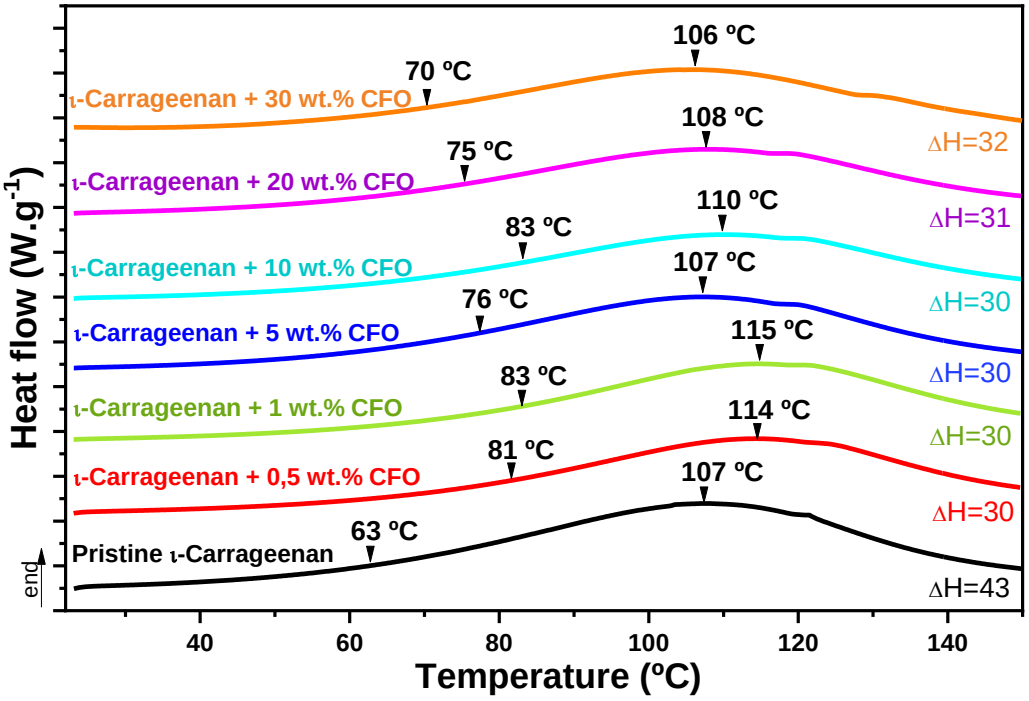

Figure 4.6. DSC graph of CFO within ι-carrageenan polymeric matrix and pristine ι-carrageenan.

The graph of Figure 4.6, 4.7 and 4.8 shows that pristine has a higher endothermic peak than the others, also seen by the enthalpy values determined by the area under the endothermic peak. The sample of 10 wt.% CFO + ι-carrageenan has a lower enthalpy value (lower peak), and from pristine ι-carrageenan, 1 wt.% CFO + ι-carrageenan retarded the reaction, and tg occurs at higher values. The following percentages anticipated a little the reaction but comparing to pristine ι-carrageenan does seem to get a significative interference.

Figure 4.7 shows the result from DSC analysis on MWCNTs samples.

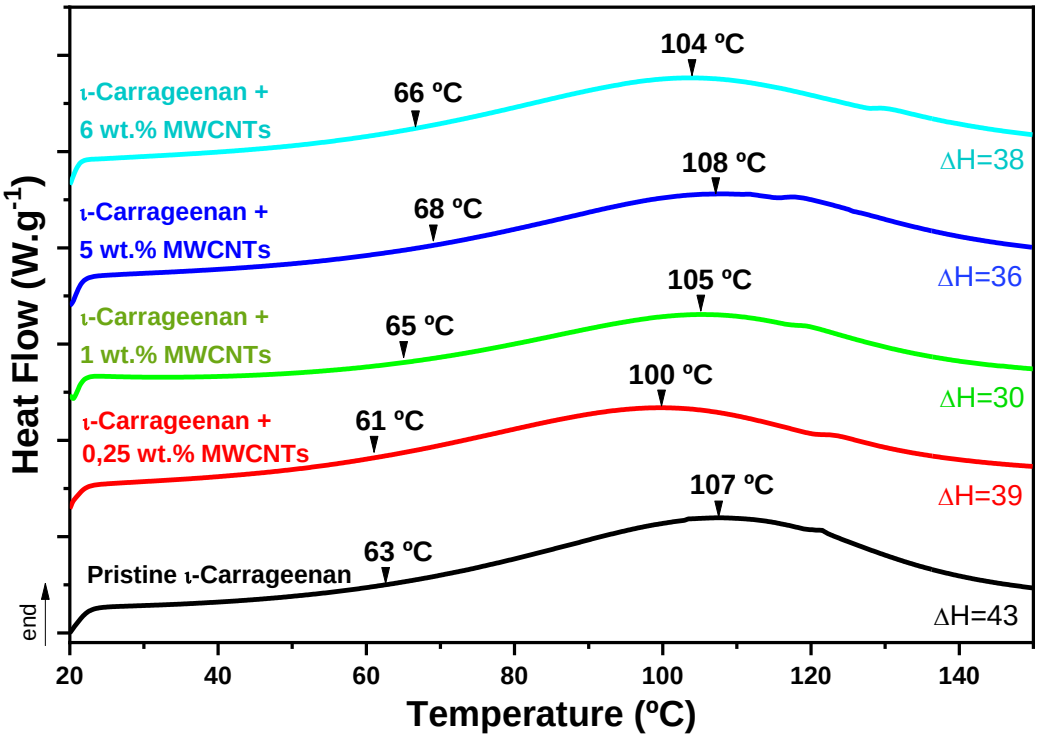

Figure 4.7. DSC graph of CNTs within ι-carrageenan polymeric matrix and pristine ι-carrageenan.

From graph 4.7 and through the data of endothermic peaks and enthalpy values it is seen that MWCNTs are the particles whose values are the closest to the pristine ι-carrageenan. The endothermic peak does also not change that much from the pristine ι-carrageenan sample, except to the 0.25 wt.% MWCNTs, whose acceleration of the reaction having happened at lower temperatures. Figure 4.8 shows the results from DSC to BTO samples.

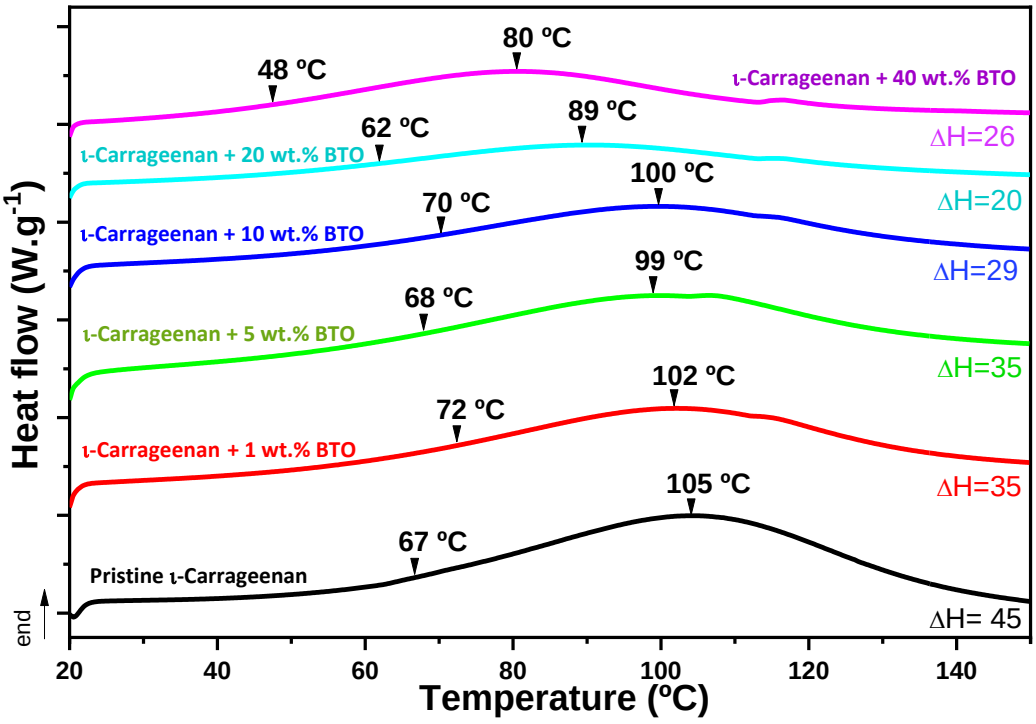

Figure 4.8. DSC graph of BTO within ι-carrageenan polymeric matrix and pristine ι-carrageenan.

From the graph of Figure 4.8 is seen that the endothermic peak tends to occur at even lower temperatures with the increment of BTO percentage on the sample, and it is significantly visible that 20 wt.% BTO + ι-carrageenan has the lowest enthalpy value.

From all graphs the analysis led to the fact that all the fillers added had influenced the endothermic peak and enthalpy, either the peak's range or intensity. Related to the polymer used and DSC analysis on the literature, a relation of quantity of ι-carrageenan and enthalpy of reaction was found[200].

4.1.4. Fourier transform infrared

FTIR analysis allowed the detection of elements within the sample and those interactions. In Figure 4.9 is the FTIR of the samples for the study of ι-carrageenan with CFO, MWCTNs and BTO NPs.

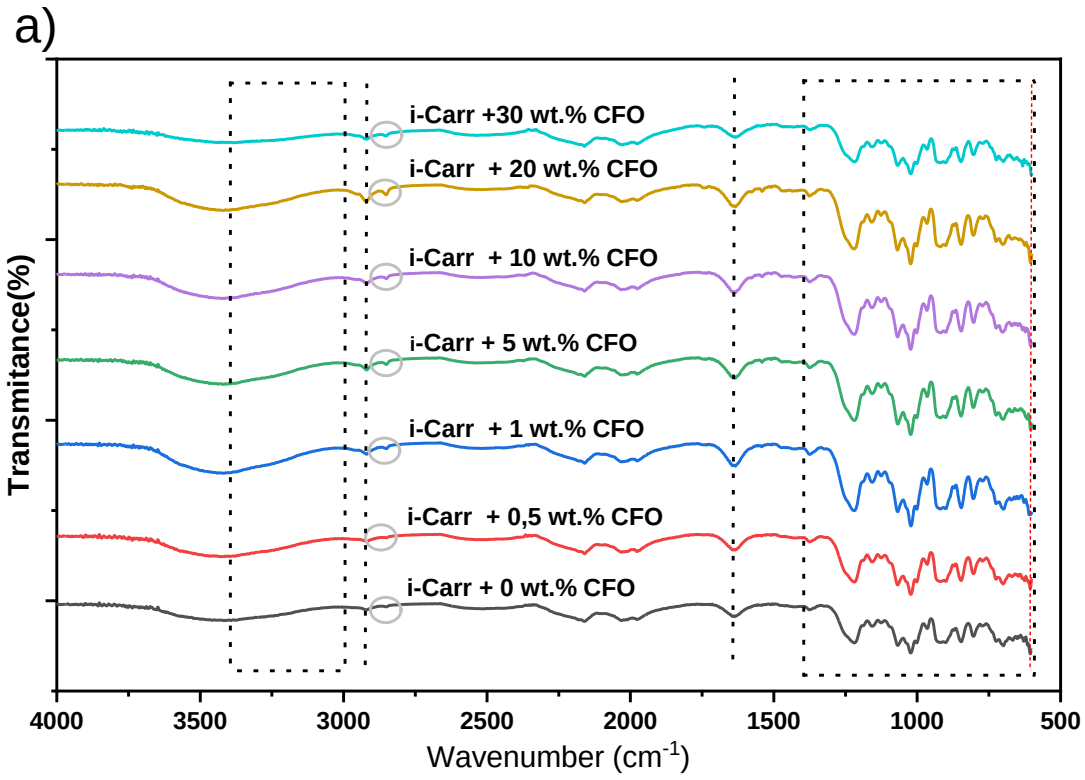
a)
i-Carr +30 wt.% CFO
i-Carr + 20 wt.% CFO
i-Carr + 10 wt.% CFO
i-Carr + 5 wt.% CFO
i-Carr + 1 wt.% CFO
i-Carr + 0,5 wt.% CFO
i-Carr + 0 wt.% CFO
Transmitance(%)
4000
3500
3000
2500
2000
1500
1000
500
Wavenumber (cm-1)

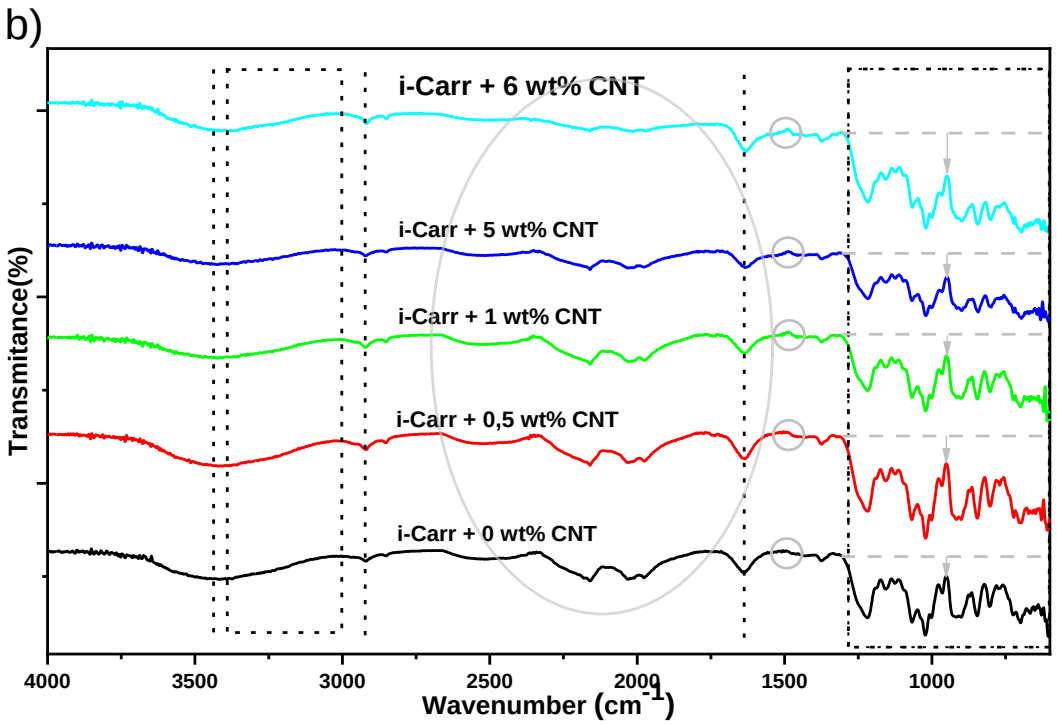
b)
i-Carr + 6 wt% CNT
i-Carr + 5 wt% CNT
i-Carr + 1 wt% CNT
i-Carr + 0,5 wt% CNT
i-Carr + 0 wt% CNT
Transmitance(%)
4000
3500
3000
2500
2000
1500
1000
Wavenumber (cm-1)

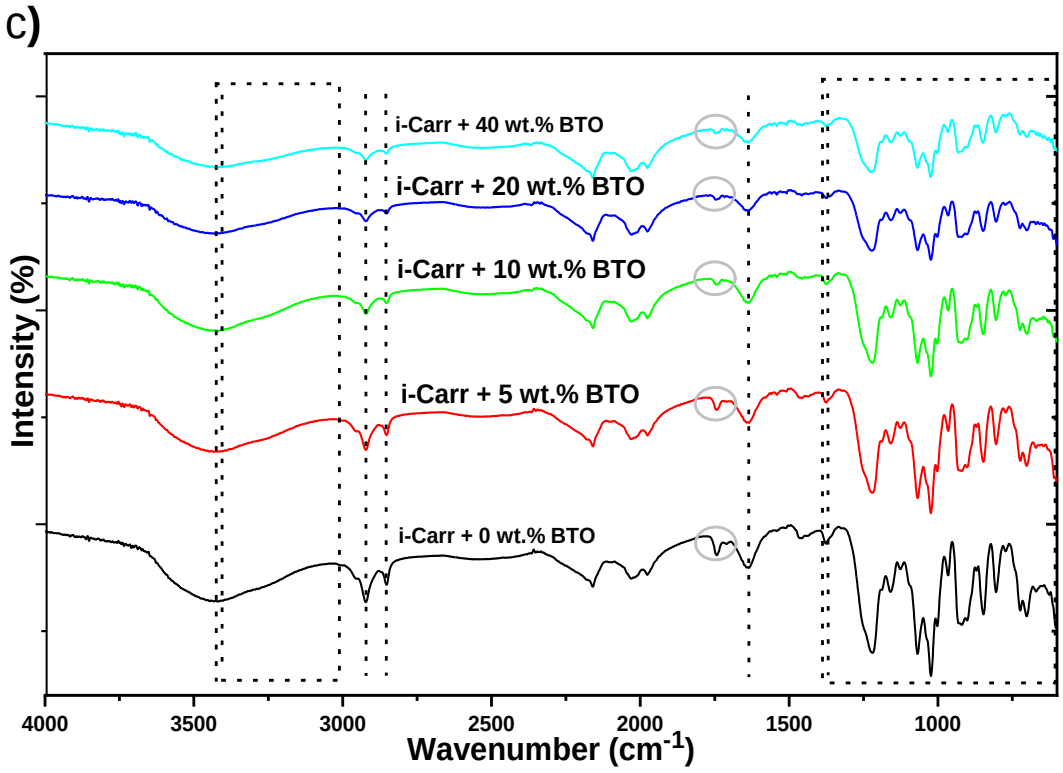

Figure 4.9- FTIR analysis of a) CFO NPs samples b) CNTs NPs samples and c) BTO NPs samples in ι-carrageenan polymeric matrix.

In all graphs of Figure 4.9 are highlighted the correspondent points from table 4.3 which correspond to the presence of ι-carrageenan.

It was expected, for all CFO, MWCNTs and BTO samples, that the main peaks found would be from the polymeric matrix, since the filler peaks are usually at very low frequencies or with extremely low intensity. As it can be seen, almost all the points characteristic to the vibration of ι-carrageen bonds can be detected, which confirms its presence. Thus, from the points correspondent to the vibration of CFO NPs bonds, only one can be slightly detected, the peak of wavenumber around 603 cm^{-1}, which represents the Fe-O bound [201-203]. On CFO FTIR had only been noticed a change in the number wave 2851 (surrounded in grey colour), with the appearance of a little peak which increased intensity until it reached the 30 wt.% CFO.

On MWCNTs FTIR analysis it was not possible to see any point related to its presence. Usually, these nanoparticles have weak absorption strength being difficult to be detected. Since the MWCNTs used are non-functionalized the peak which could be detected would be around 1568 cm^{-1}, which corresponds to the C=C bond [204]. Although some interaction may occur between polymer and filler in these samples since there are some changes on peaks

surrounded at grey. On BTO samples it also seems to occur but only at one point around 1742 cm^2 which eventually disappears with the BTO NPs addition into the polymeric matrix. To BTO samples the FTIR analysis also does not seem to capture some of the peaks associated with their presence, which would be 755 and 890 Ti-O or Ti-O-Ti vibrations respectively[205].

In Table 4.3 are the peaks related to ι-carrageenan and which appear into all the three samples FTIR.

Table 4.3.FTIR peaks associated to the presence of ι-carrageenan.

Wavenumber (cm^{-1})	**Assignments**	**Ref.**
3400-4300	❖ O-H Stretching	[67, 68, 70, 73, 198, 206-208]
2920	❖ C-H Stretching vibration of CH_2 group	[67, 68, 198, 207]
1634 and 1644	❖ Deformation of O-H band due the bonds of water of crystallization (from absorbed water)	[67, 70, 202, 207-209]
1380-1355 (~1376)	❖ Asymmetric vibration of S-O_2 group (Sulphates)	[68, 209]
1250-1230 (~1220)	❖ O=S=O symmetric Stretching of sulphated esters	[68, 70, 73, 198, 207, 209, 210]
1160-1155 (~1158)	❖ C-O-C asymmetric stretching (C-O bridge)	[67, 68, 70, 198, 208]
1125	❖ Glycosidic bonds asymmetric stretching	[68]
1080-1040 (~1068)	❖ C-O	[67, 68, 73, 198, 206, 208]
1023	❖ S-O in C_2 pseudo-symmetric ❖ (CH_2 symmetric stretching)	[68] [70]
1002	❖ Glycosidic bonds	[68]
970-965 (~966)	❖ Glycosidic bonds ❖ (C-H stretching)	[68, 70, 73]
928	❖ Galactose position, C-O-C of 3,6 anhydrogalactose	[67, 70, 73, 198, 208]
900-890 (~901)	❖ C_6 group in β-D- galactose	[68]

847	❖ C_4-O-S group in galactose (stretching) Or ❖ -O-SO_3 stretching at D-galactose -4-sulphate	[68, 70, 73, 207, 209, 210] [67, 198, 208]
805	❖ C_2-O-S in 3,6-anhydrogalactose Or ❖ -O-SO_3 stretching at D-galactose -4-sulphate	[68, 70, 73, 207, 209, 210] [67, 198, 208]
740-725 (~725)	❖ C-O-C α (1,3) (stretching)	[68]
615-608	❖ O=S=O (bending)	[68]

4.1.5. Mechanical characterization

Mechanical tests were performed to all CFO, MWCNTs and BTO particles used. Some samples needed to be cut to remove the irregularities originated during cure process which would jeopardize the mechanical test. For the particles of ι-Carrageenan and CFO, MWCNTs and BTO NPs the results are shown in Figure 4.10.

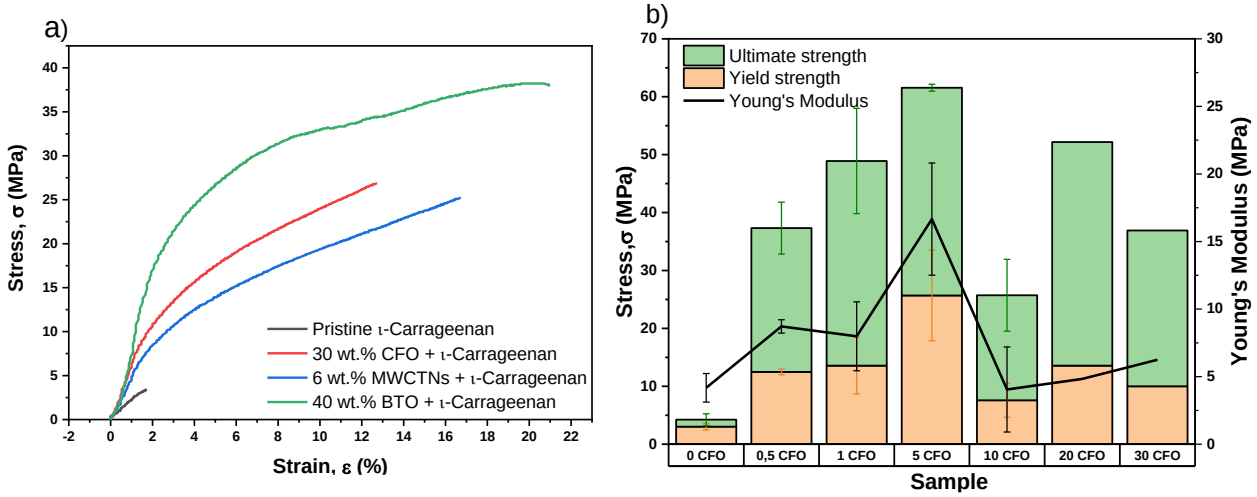

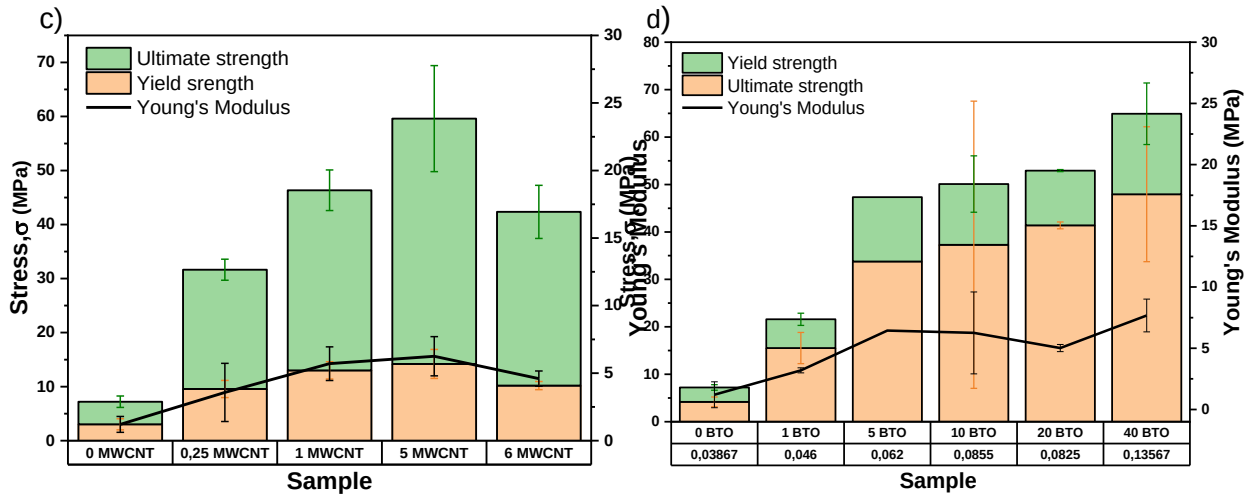

Figure 4.10. a) Stress-strain graph from mechanical test of CFO, MWNTs and BTO NPs samples within ι-carrageenan polymeric matrix, respectively. b), c) and d) Analysis of mechanical properties (Young's modulus, ultimate strength and yield strength) with samples width and thickness and filler concentration.

For CFO samples the results are not very linear, since the sample with higher Young's Modulus and yield strength as well is 5 wt.% CFO + ι-carrageenan, the one with higher ultimate strength is 20 wt.% CFO + ι-carrageenan. The only thing foreseen was the fact that the addition of particles increases the mechanical properties of the product. It was seen even to the samples with lowest concentrations, having all better properties than the pristine ι-carrageenan. In the case of CFO samples, if the final product were needed to act as a rubber or a piezoelectric, where the elastic proprieties would be essential, the best sample would be 5 wt.% CFO + ι-carrageenan (more ductile material). If the material would need to be more resistant to mechanical forces, where the ultimate strength should be the highest possible, then the better sample is 20 wt.% CFO ι -carrageenan (more rigid material).

On all Figures 4.10-b, c and d, are the average of the main properties of all tests made to each percentage of filler addition. When analysed, the properties determined that 5 wt.% CFO + ι-carrageenan seems to be the one with the best of all proprieties. It is seen that sample 10 wt.% CFO + ι-carrageenan has a breakdown comparing to the others, which can be related to defects on its structure. The dimensions of error bars are directly connected to some difficulties on the cure process which interfered into final dimensions obtained. Despite that was tried to put all samples with similar dimensions.

For the samples 20 wt.% and 30 wt.% CFO in Figure 4.10-b, considering the high CFO content, the curing process is affected by humidity during the process. For these samples,

considering this behaviour, a box with holes was used that allowed for a slow and as homogeneous evaporation as possible.

As far as samples with MWCNTs filler addition are concerned, they show a higher ultimate strength than samples with CFOs filler addition. MWCNTs NPs opposed to the CFO NPs has a more linear behaviour and the error associated to the respective property. When analysing Figure 4.10-c it is seen that 5 wt.% MWCNTs + ι-carrageenan has a higher tensile strength than any other of MWCNTs samples. The sample with higher MWCNTs percentage has the lowest ultimate strength and lowest yield strength but does not have the lowest young modulus. The main reason is that the addition of carbon increases the fragility due agglomeration factor, sported to the fact that 6 wt.% MWCNT + ι-Carrageenan has the lower interface zones in relation to the rest of the samples with MWCNTs NPs, as explained in the TGA interpretation.

The error associated to the mechanical tests is also similar for all percentages of MWCNTs addition and it is low, except to the 5 wt.% MWCNTs + ι-Carrageenan that have a bit higher error. This implies that with these particles the retraction and dimensions' changes have a more predictable behaviour and without a big deformation as occurs with the samples within CFO NPs.

At last, analysing the samples with BTO particles addition in Figure 4.10-a, these are the most rigid products, which was predictable since these particles are a ceramic. Despite that, the samples with higher ultimate strength with more rigid behaviour were 10 wt.% BTO + ι-Carrageenan and with higher yield strength was 40 wt.% BTO + ι-Carrageenan. From the graph from Figure 4.10-d can be seen that all mechanical proprieties increase until 10 wt.% BTO + ι-Carrageenan, decrease at 20 wt.% BTO + ι-Carrageenan and then retrieve.

Yield strength of BTO samples increases until 5 wt.% BTO, then decreases until 20 wt.% BTO + ι-Carrageenan, and increases again at 40 wt.% BTO + ι-Carrageenan. In the graph from Figure 4.10-d this occurs due to the error associated specially to 10 wt.% BTO + ι-Carrageenan. The dimension of the error associated to 10 wt.% BTO + ι-Carrageenan is strongly related to imperfections on one of the samples tested, which had lower properties than the others. The retraction and deformation were like the MWCNTs samples.

4.1.6. Dielectric characterization

This test was performed to samples with BTO particles, since they are known as being a dielectric material. At that moment, the material could not hold the charge and only let it pass through. After the first attempt, due to high values of dielectric constant, it was concluded that the samples still had water molecules inside the material structure, some humidity that was not removed during cure process. So, it was necessary to do a thermic treatment, which consisted of putting the samples in an oven with vacuum auxilium for 3 hours to remove the impurities. The masses were measured before and after the thermic treatment to determine the amount of water removed, which effectively assured the water presence.

Dielectric studies are important to determine the capacity of achievement and storage charges. Dielectric proprieties may be characterized by a frequency-dependence and defined by the complex permittivity ε, expressed by equation 2 [70, 154, 206].

$$\varepsilon^* = \varepsilon'(w) - i\varepsilon''(w),\ i^2 = 1 \qquad 2$$

Thus, ε' is the real part of the complex permittivity and usually known as the dielectric constant and is the capacity of a material to store charge. ε'' is the imaginary part of the complex permittivity, and corresponds to the dielectric loss, being related to the oscillating of ions and alignment of dipoles of charges for cycle of the applied electric field when energy loss occurs [70, 154, 206]. From all graphs of the dielectric tests, for low frequencies the dielectric permittivity (ε', ε'') is high, and it decreases with the increment of the frequency. This happens because the periodic reversal of field occurs at first slowly (low frequencies), therefore the sample can storage and release the charge. When the frequencies increase, the periodic reversal of field is quicker and leads to a lower diffusion of charges on the field direction since the mobile ions would not be able to orientate themselves into the direction of the applied field [70, 154, 206]. Figure 4.11 shows the graphs associated to the dielectric measurements of BTO samples.

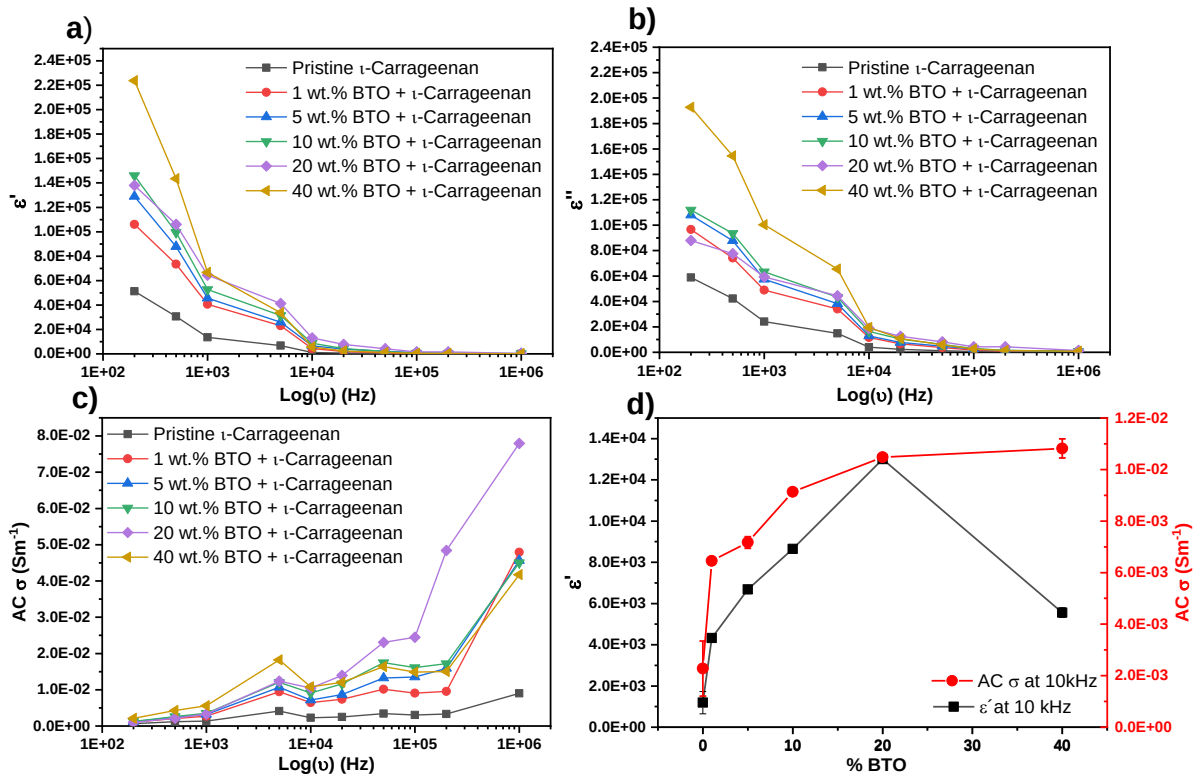

Figure 4.11. Dielectric measures of BTO NPs samples within ι-carrageenan polymeric matrix.

For BTO samples this is the most important test, once it evaluates if these samples process dielectric behaviour and if it will be good at the respective application. At low frequencies, an electrode polarization effect produced by an accumulation of charges near the electrode causes an increase of both, ε' and ε'' proprieties, with decreasing frequency, Figure 4.11-a and b. It also shows that these properties tend to increase with the increment of BTO concentration in the samples. To carrageenan dielectric measures can have some difficulties associated to the electrode polarization and the high loss tangent (can reach 10^3) due to the high DC conductivity. The increase of the charge density throughout the coil-to-helix transition led to an increase of the dielectric constant in connection with decreasing influence on the conductivity [76]. Since tan(δ)= $\frac{\varepsilon''}{\varepsilon'}$ and as this value is usually high, it means that ε'' must be high as well, which explains the elevated values obtained in the dielectric test [76, 211].

Comparing the graphs from Figure 4.11-a and b, X wt.% BTO (X>0) + ι-carrageenan has a behaviour of a dielectric material since ε'>ε'', even with a small difference. On the graph from Figure 4.11-c the AC conductivity also increases with the BTO content, except the 40 wt.% BTO sample, at higher frequencies, 20 wt.% BTO has the higher AC conductivity.

Analysing a certain frequency, e.g., 10 kHz, is easy to evaluate the evolution of ε' and AC conductivity with the increase of BTO content. On the graph from Figure 4.11-d a linear increment of AC conductivity until 20 wt.% BTO and then it seems to tend to stabilize. On graphs from Figure 4.11-a, b, c, and d 20 wt.% BTO seems to be a good sample with dielectric constant of 1.3 x 10^4 and AC conductivity of 1.05 x 10^{-3} Sm^{-1} at 10 kHz, and to 40 wt.% BTO does have a significant increase of dielectric properties. Consequently, there is no need to use the double of the nanoparticles and no need to increase expenses which do not compensate the acquired properties.

4.1.7. Electrical conductivity

This test was mainly targeted at the samples of MWCNTs NPs, which are considered electrically conductive material.

After the first attempt, due to inconsistencies during the test, and because of the causes from dielectric measures, the same thermic treatment was needed. The thermic treatment and electrodes were used for both studies. Figure 4.12 shows the results from the IV measures of MWCNTs NPs within ι-carrageenan polymeric matrix.

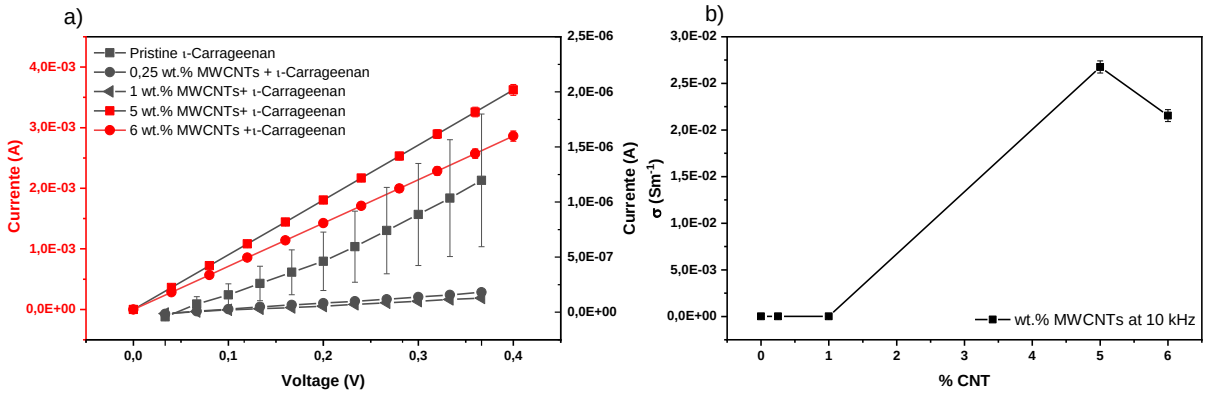

Figure 4.12. a) IV measures of MWCNTs NPs in a ι-carrageenan polymeric matrix and b) calculated conductivity of MWCNTs sample with filler addition.

Figure 4.12-a the IV's graph from MWCNTs corresponds to an Ohm's law curve since it exhibits a linear relationship between the applied voltage and the resulting electric current [212]. From Figure 4.12-b is seen that from pristine ι-carrageenan sample to 1 wt.% MWCNTs + ι-carrageenan samples, and being compared at the same scale size, they have both almost the same behaviour. Then a big increase in the conductive behaviour occurs at 5 wt.%

MWCNTs + ι-carrageenan followed by a decrease at 6 wt.% MWCNTs. The associated error from measure and calculation of conductivity is small, represented by an almost not distinguishable error bar in both graphs from Figure 4.12. From the conductivity average the more conductive sample, and consequently the best one, is the 5 wt.% MWCNTs with a DC conductivity of 0.026 $S.m^{-1}$.

4.1.8. Vibrating sample magnetometry

VSM test was performed to analyse the magnetic proprieties of the CFO particles. Watching the big picture of the hysteresis curves, from all CFO samples, in Figure 4.13-a, can clearly be seen that the addition of particles increases the magnetic proprieties i.e., increases saturation magnetization, remanence and coercivity of the samples, which is coherent since magnetic proprieties were used. The samples of 0,5 wt.% CFO + ι-Carrageenan and 1 wt.% CFO + ι-Carrageenan has shown the lowest values of saturation magnetization and remanence, being two curves very close to each other ($Mc_{0.5wt.\%\ CFO}$= (-3) kOe, $Mr_{0.5wt\%\ CFO}$= 0.1 $emu.g^{-1}$, $Ms_{0.5wt.\%\ CFO}$= 3 $emu.g^{-1}$ to $Mc_{1wt.\%\ CFO}$= (-3.1) kOe, $Mr_{1wt\%\ CFO}$= 0.3 $emu.g^{-1}$, $Ms_{1wt\%\ CFO}$.= 7 $emu.g^{-1}$). Next, 5 wt.% CFO + ι-Carrageenan and 10 wt.% CFO + ι-Carrageenan had a small increase on these proprieties and as well with values close to each other ($Mc_{5wt.\%\ CFO}$ = (-3.6) kOe, $Mr_{5wt\%\ CFO}$=1.6 $emu.g^{-1}$, $Ms_{5wt.\%\ CFO}$=3 $emu.g^{-1}$ to $Mc_{10wt.\%\ CFO}$= (-3.3) kOe, $Mr_{10wt\%\ CFO}$ = 2 $emu.g^{-1}$, $Ms_{10wt\%\ CFO}$= 4 $emu.g^{-1}$). At 20 wt.% CFO NPs the hysteresis curve highly increased, and it happened again to the 40 wt.% CFO NPs ($Mc_{20wt.\%\ CFO}$= (-3.1) kOe, $Mr_{20wt\%\ CFO}$ = 2 $emu.g^{-1}$, $Ms_{20wt.\%\ CFO}$= 11 $emu.g^{-1}$ to $Mc_{30wt.\%\ CFO}$=(-3.4) kOe, $Mr_{30wt\%\ CFO}$=6.7 $emu.g^{-1}$, $Ms_{30wt\%\ CFO}$.=16 $emu.g^{-1}$).

As seen on graph 4.13-b coercivity, comparing to the other two proprieties (saturation magnetization a remanence), does not has a significative change with the increase of the CFO wt.% from 0.5 wt.% BTO to 40 wt.% BTO, being the lowest value of 2,89 kOe and the highest of 3,57 kOe. In the other hand, the saturation magnetization and remanence increase with CFO addition, from 0.5 wt.% BTO to 40 wt.% BTO, which higher values of 40 wt.% reach 16,28 $emu.g^{-1}$ and 9,95 $emu.g^{-1}$, respectively. The increase of remanence means that the successive augment of CFO NPs on ι-carrageenan polymeric matrix increases the behaviour of hard magnetic material, i.e., allows the material to keep a permanent magnetism field after it drops to zero.

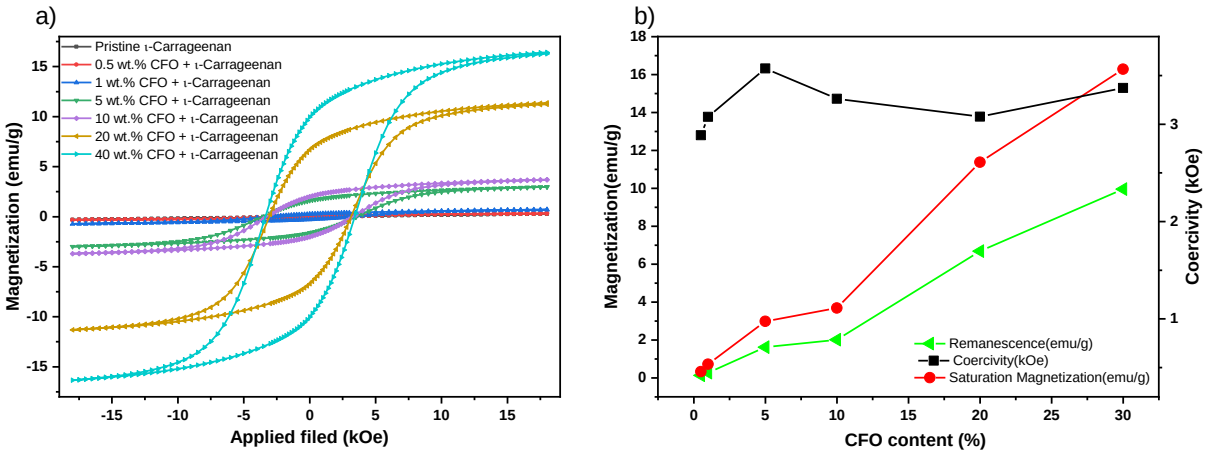

Figure 4.13.Vibrating Sample Magnetometer (VSM) a) hysteresis loop of all of CFO NPs samples within ι-carrageenan polymeric matrix and b) influence of magnetic proprieties with CFO content.

The data from these graphs allows the calculation of the effective concentration of nanoparticles. The saturation magnetization of CFO NPs is 60 emu.g^{-1}. The calculation can be expressed into 2 forms, shown on equation 3 and 4.

$$\%CFO = \frac{saturation\ magnetization\ (film\ or\ membranes)}{saturation\ magnetixation\ of\ pure\ CFO} \times 100, [213] \qquad 3$$

However, it can also be done by a three-simple rule. If 60 emu correspond to 1g, then the saturation magnetization of the sample is given. Next, the mass correspondent to the nanoparticles within the sample calculated before divided for the mass of the respective sample plus 100 is the value of the percentage of CFO on the sample.

$$\begin{array}{ccc} 60\ emu & \longrightarrow & 1g \\ \text{Sample's saturation magnetization} & \longrightarrow & X \end{array}$$

$$\frac{X\ (mass\ of\ the\ particles\ calculated\ before\ )}{mass\ of\ the\ sample} \times 100 = \%CFO \qquad 4$$

Table 4.4 below shows the value determined of the real % CFO within the samples.

Table 4.4. Values determined of the real percentage of CFO on the samples.

Sample wt.% CFO	Saturation magnetization on the sample (emu)	Nanoparticle's mass	Sample's mass	Real %CFO at 20°C
0.5	2.48×10^{-2}	4.24×10^{-2}	7.07×10^{-3}	0.54
1	22.42×10^{-2}	4.03×10^{-5}	3.40×10^{-3}	1.19
5	1.19×10^{-2}	1.99×10^{-4}	4.00×10^{-3}	4.97
10	1.62×10^{-2}	2.71×10^{-4}	4.40×10^{-3}	6.15
20	6.19×10^{-2}	1.03×10^{-3}	5.50×10^{-3}	18.77
30	4.24×10^{-2}	7.07×10^{-4}	2.60×10^{-3}	27.17

As seen in Table 4.4 the sample that has the further value from between the real and the hypotactic percentage value is sample 10 wt.% CFO + ι-carrageenan. This can explain the fact of this sample being the one with more irregular results. The rest has the real percentage of CFO on the sample near the theoretical on the experimental performance.

The saturation magnetization considering the samples' mass (emu.g^{-1}) the 30 wt.% CFO is the one with higher value of ~16 emu.g^{-1}. The gap between the saturation magnetization of 10 wt.% CFO and 20 wt.% CFO is higher (3 emu.g^{-1} to 11 emu.g^{-1}) than 20 wt.% CFO to 30 wt.% CFO.

4.2. Applications

4.2.1. Magnetic sample

Hi-Strength 90 spray adhesive from 3M was used for contact bonding between a commercial PVDF metalized with 52 µm from measurement Specialties, Inc and Material. The fabricated magnetoelectric sensor was connected to the electronic acquisition system by two golden electrodes. Figure 4.14 shows the magnetoelectric sensor in action and a scheme of data reading.

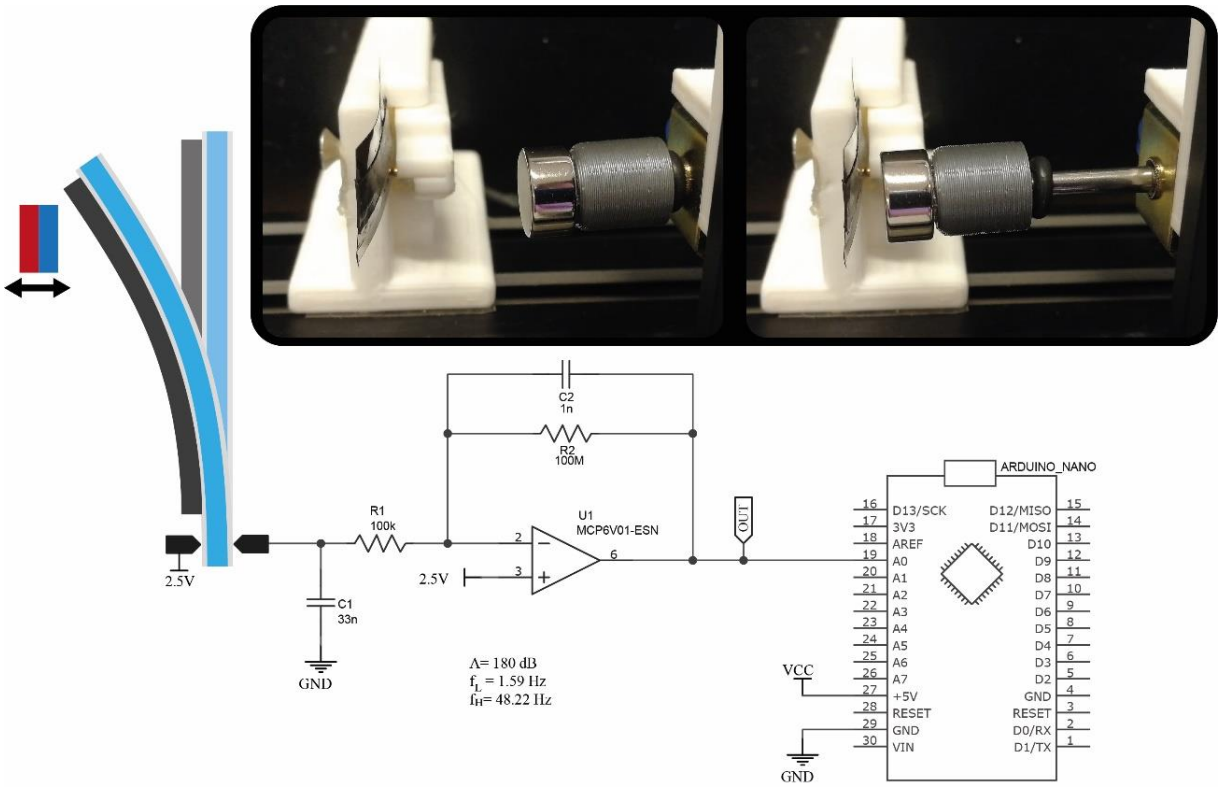

Figure 4.14. Electronic acquisition system and magnetic sensor application with magnetic field variation through magnet interference.

The electronic acquisition circuit is composed by a charge amplifier connected to the analogue to digital converter (ADC) of an Arduino nano (ATMEGA328P). The data is sent via Universal Serial Bus (USB) where an application developed in Qt 5 plots the sensor response. The charge amplifier integrates the input current and provides a voltage output proportional to the force applied on the piezoelectric material [214] via the applied magnetic field. This circuit also reduces the input noise when compared to voltage sensing. The low-pass filter composed by the resistance R1 and capacitor C1 provides immunity to high frequencies and anti-aliasing filter, the high pass filter composed by the resistance R2 and capacitor C2 limits the minimum input frequency. The reference voltage of 2.5 V provides a positive voltage offset that centre the output voltage at 2.5V allowing the signal to be read by the microprocessor ADC.

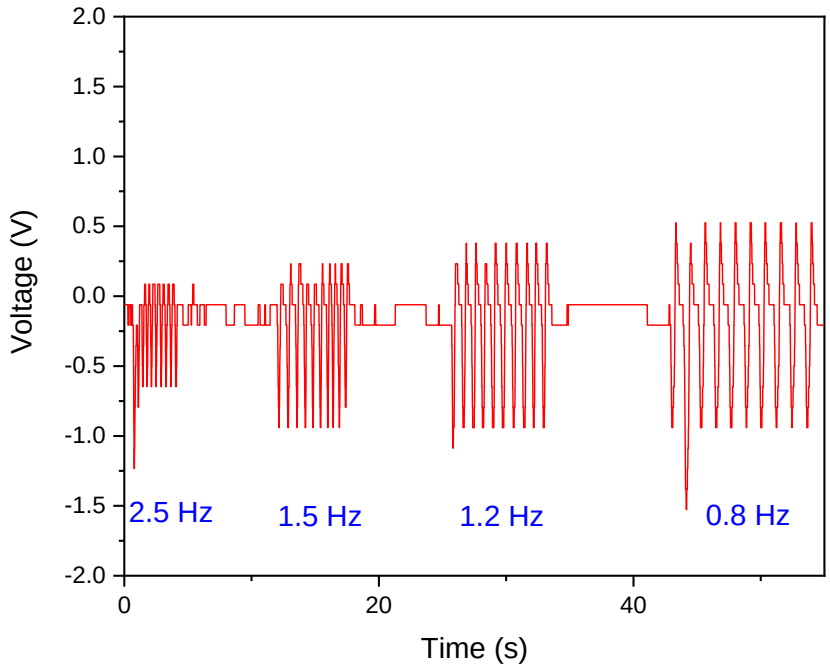

Figure 4.15. Response of the magnetoelectric sensor to magnet approach at 2,5 Hz, 1,5 Hz, 1,8 Hz, and 0,8 Hz.

Figure 4.15 shows the amplified and filtered voltage response of the ME Sensor at 4 frequencies (2,5; 1,5; 1,2 and 0,8 Hz) when the NdFeB magnet (10 mm diameter by 5 mm thickness N42 magnetization from supermagnet) approaches the sensor that gives rise to a voltage above the voltage reference of 2.5 and when is released gives a response inferior to the voltage reference.

4.2.2. Conductive samples

The sample with 6 wt.% MWCNTs was used in A resistive sensor application based on the approximation of the active material from the interdigit layer. When the active layer starts the contact with the interdigit layer, the sensor starts to change the resistance from the isolator (no contact at Figure 4.16-c) to resistive (with contact at Figure 4.16-d). In the resistive region when the pressure is increased the area of the active material with the interdigit increases, decreasing the resistance of the sensor.

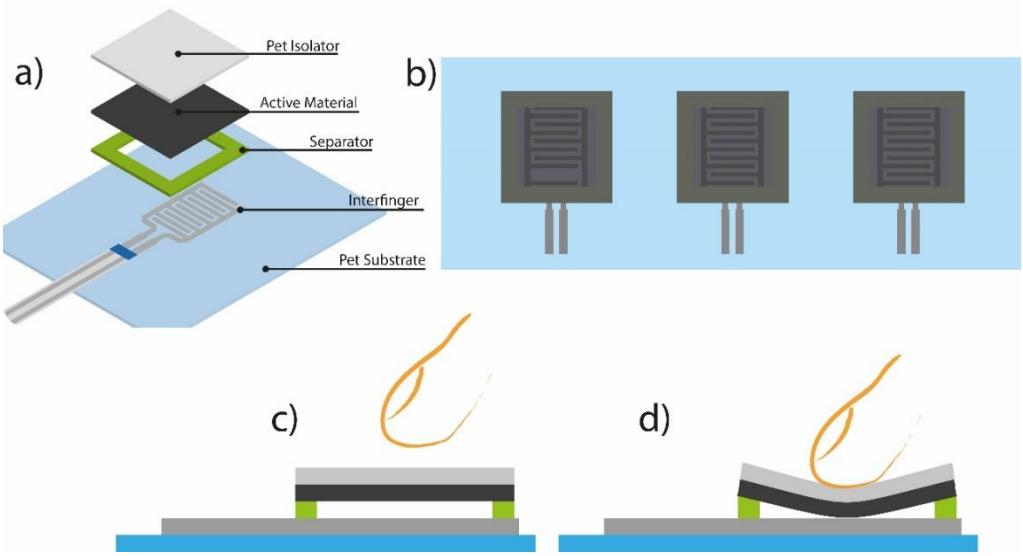

Figure 4.16. a) Constitution of the resistive sensor, b) Sensor design, c) resistive and d) isolator behaviour of the sensor.

Three sensors were constructed by gluing together the active material to a PET (polyethylene) separator and a silver printed interdigit electrode. A last PET isolator was placed on top for isolation from human skin contact (Figure 4.16-a).

The silver interdigit was printed by screen printing (with a mesh of 100 threads by centimetre) with Metalon HPS-021L silver conductive ink from Novacentrix on a PET substrate and cured at 80 °C for 60 min in the electric Convection Oven. The electronic acquisition system is schematized in Figure 4.17-a and the sensor application with a user interface in Figure 4.17-b.

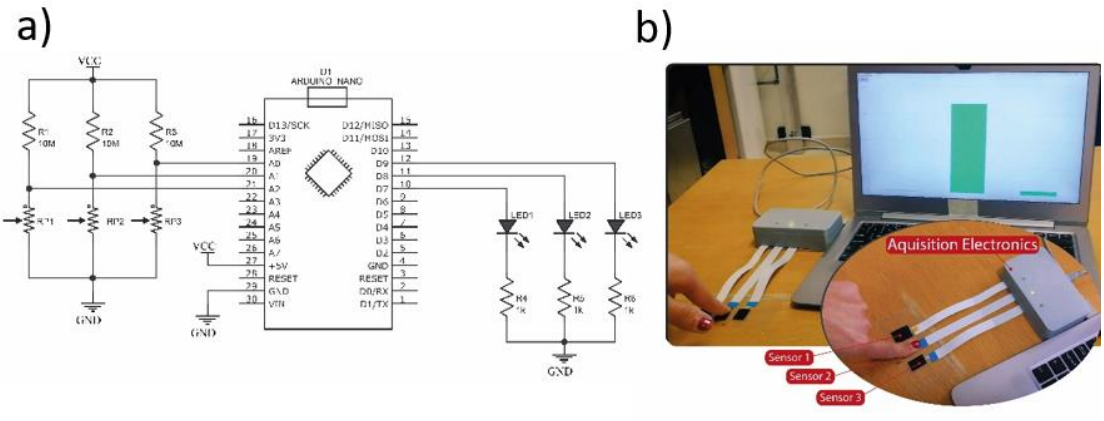

Figure 4.17. a) electronic acquisition system and b) force sensor application with user interface.

The electronic acquisition system is composed by an Arduino nano that sends the data received from the resistive sensors to the PC. The 3 resistive sensors are connected to the 10 bits ADC (analogue to digital converter) through a 10 MΩ resistor completing a voltage divider. When pressure is applied to the sensors the ADC reads the voltage variation in the voltage divider, activates the corresponding LED (light-emitting diode) and sends the data to the user interface. The user interface receives the raw data from the ADC conversion (0 to 1023) and shows the data in the bar chart corresponding to the applied force in the 3 sensors.

Chapter 5- Conclusion and future works

5. Conclusion

In this work a ι-carrageenan based ink with the addition of CFO, MWCNTs and BTO as magnetic, conductive and dielectric filler, respectively was successfully produced. Despite the use of ultrapure water as a solvent a good dispersion of all fillers into the polymeric matrix was achieved, demonstrated in the morphological analysis. The use of triton X-100 as a surfactant, whose main function is to make the dispersion easier, acts as an important factor. From magnetic analysis trough VSM the magnetic properties of CFO samples were confirmed, and as expected the one with 30 wt.% CFO sample had higher saturation magnetization 16 $emu.g^{-1}$ proportional to the amount of additional filler. In the case of MWCNTs samples it was detected a conductive behaviour, which higher conductivity of 0.27 $S.m^{-1}$ from the 5 wt.% MWCNTs sample with seems to be the best sample since 6 wt.% MWCNTs has a decrease of conductivity, having 0.022 $S.m^{-1}$. Thus, there is no need to use an additional amount of material without necessity. BTO samples have been the samples with more fragile/hard behaviour, typical of a ceramic. Due the polymeric matrix (carrageenan) it has a high ε'', which is common since carrageenan is associated to high tanδ ($\frac{\varepsilon''}{\varepsilon'}$) value. It had also shown a dielectric behaviour ε'>ε'' and 20 wt.% BTO has higher ε' value of 1300 and conductivity AC of 0.01 $S.m^{-1}$, comparing to 30 wt.% BTO (ε'=5561 and AC σ=0.01 $S.m^{-1}$)

In this work was successfully produced three different types of materials, with a good dispersion of CFO, MWCNTs and BTO nanoparticles which gave magnetic, conductive and dielectric properties to the natural polymer (ι-Carrageenan), respectively. The 3D printing was also performed, despite the final product seem to have a 2D form due to the process of solvent evaporation.

It was also possible to show the applicability of the CFO and CNTs samples, using the samples with higher percentage.

5.1. Future Works proposal

Despite this work presented promising results, further investigation is required, because even being possible to print a 3D structure this does not handle its form. Thus, the cure process needs to be studied so that after printing it can retain the three-dimensional

form. Assembling the cure process with the incorporation of other material, for example another natural polymer, in order to create some kind of backbone within the internal structure, can be a good approach to solve the problem.

It was thought not to use heat during the printing process, in order to make the process energetically optimized and with lower costs. However, if the ink based on ι-carrageen would be heated during printing, then the contact with the substrate at ambient temperature could improve the adhesion to the substrate.

Bibliography

1. Oliveira, J., et al., *Polymer-based smart materials by printing technologies: Improving application and integration.* Additive Manufacturing, 2018. **21**: p. 269-283.
2. Narita, F. and M. Fox, *A Review on Piezoelectric, Magnetostrictive, and Magnetoelectric Materials and Device Technologies for Energy Harvesting Applications.* Advanced Engineering Materials, 2018. **20**(5).
3. Humayun, M., et al., *Internet of things and ransomware: Evolution, mitigation and prevention.* Egyptian Informatics Journal, 2021. **22**(1): p. 105-117.
4. Azmoodeh, A., et al., *Detecting crypto-ransomware in IoT networks based on energy consumption footprint.* Journal of Ambient Intelligence and Humanized Computing, 2017. **9**(4): p. 1141-1152.
5. Xi, W., et al., *Material approaches to active tissue mechanics.* Nature Reviews Materials, 2018. **4**(1): p. 23-44.
6. Drossel, W.G., et al. *Smart materials for smart production - A cross-disciplinary innovation network in the field of smart materials*. in *Procedia Manufacturing*. 2018.
7. Jiang, P., et al., *Recent advances in direct ink writing of electronic components and functional devices.* Progress in Additive Manufacturing, 2017. **3**(1-2): p. 65-86.
8. Ji, S. and M. Guvendiren, *Recent Advances in Bioink Design for 3D Bioprinting of Tissues and Organs.* Front Bioeng Biotechnol, 2017. **5**: p. 23.
9. *Printed Batteries: Materials, Technologies and Applications*. 2018, John Wiley & Sons, Ltd.
10. Zhang, A., et al., *3D printing hydrogels for actuators: A review.* Chinese Chemical Letters, 2021.
11. Guo, Z., et al., *High-precision resistance strain sensors of multilayer composite structure via direct ink writing: Optimized layer flatness and interfacial strength.* Composites Science and Technology, 2021. **201**: p. 108530.
12. Ching, T., et al., *Fabrication of integrated microfluidic devices by direct ink writing (DIW) 3D printing.* Sensors and Actuators B: Chemical, 2019. **297**.
13. Farahani, R.D., M. Dube, and D. Therriault, *Three-Dimensional Printing of Multifunctional Nanocomposites: Manufacturing Techniques and Applications.* Adv Mater, 2016. **28**(28): p. 5794-821.
14. Grifa, R.A. and G. Pozzoli, *Electro-medical devices: Environmental regulation on hazardous substances.* Microchemical Journal, 2019. **148**: p. 568-572.
15. Ilankoon, I., et al., *E-waste in the international context - A review of trade flows, regulations, hazards, waste management strategies and technologies for value recovery.* Waste Manag, 2018. **82**: p. 258-275.
16. Kunnari, E., et al., *Environmental evaluation of new technology: printed electronics case study.* Journal of Cleaner Production, 2009. **17**(9): p. 791-799.
17. Chen, Y., *Properties and development of hydrogels*, in *Hydrogels Based on Natural Polymers*, Y. Chen, Editor. 2020, Elsevier. p. 3-16.
18. George, A., P.A. Shah, and P.S. Shrivastav, *Natural biodegradable polymers based nano-formulations for drug delivery: A review.* Int J Pharm, 2019. **561**: p. 244-264.
19. Wu, W., *Inorganic nanomaterials for printed electronics: a review.* Nanoscale, 2017. **9**(22): p. 7342-7372.
20. Li, R., et al., *Recent progress on biodegradable materials and transient electronics.* Bioact Mater, 2018. **3**(3): p. 322-333.
21. Sreenilayam, S.P., et al., *Advanced materials of printed wearables for physiological parameter monitoring.* Materials Today, 2020. **32**: p. 147-177.
22. Wang, Q., et al., *Facile production of natural silk nanofibers for electronic device applications.* Composites Science and Technology, 2020. **187**: p. 107950.

23. Soares, R.M.D., et al., *Electrospinning and electrospray of bio-based and natural polymers for biomaterials development.* Mater Sci Eng C Mater Biol Appl, 2018. **92**: p. 969-982.
24. Kravchenko, A.O., et al., *Structural characteristics of carrageenans of red alga Mastocarpus pacificus from sea of Japan.* Carbohydr Polym, 2020. **229**: p. 115518.
25. Karbowiak, T., et al., *Effect of plasticizers (water and glycerol) on the diffusion of a small molecule in iota-carrageenan biopolymer films for edible coating application.* Biomacromolecules, 2006. **7**(6): p. 2011-9.
26. Kim, M.H., et al., *Enhanced rheological behaviors of alginate hydrogels with carrageenan for extrusion-based bioprinting.* J Mech Behav Biomed Mater, 2019. **98**: p. 187-194.
27. Li, L., et al., *Advanced Polymer Designs for Direct-Ink-Write 3D Printing.* Chemistry – A European Journal, 2019. **25**(46): p. 10768-10781.
28. Li, L., et al., *Advanced Polymer Designs for Direct-Ink-Write 3D Printing.* Chemistry - A European Journal, 2019. **25**(46): p. 10768-10781.
29. Henderson, R.K., et al., *Expanding GSK's solvent selection guide – embedding sustainability into solvent selection starting at medicinal chemistry.* Green Chemistry, 2011. **13**(4): p. 854.
30. Prat, D., et al., *Correction: CHEM21 selection guide of classical- and less classical-solvents.* Green Chemistry, 2015. **17**(10): p. 4848-4848.
31. Mouret, A., et al., *Eco-friendly solvents and amphiphilic catalytic polyoxometalate nanoparticles: a winning combination for olefin epoxidation.* Green Chem., 2014. **16**(1): p. 269-278.
32. Carlos, L., et al., *Applications of magnetite nanoparticles for heavy metal removal from wastewater.* Waste Water - Treatment Technologies and Recent Analytical Developments, 2013: p. 63-78.
33. Cai, Y., et al., *Green synthesis of soya bean sprouts-mediated superparamagnetic Fe3O4 nanoparticles.* Journal of Magnetism and Magnetic Materials, 2010. **322**(19): p. 2938-2943.
34. Perales-Pérez, O. and Y. Cedeño-Mattei, *Optimizing processing conditions to produce cobalt ferrite nanoparticles of desired size and magnetic properties*, in *Magnetic Spinels—Synthesis, Properties and Applications*. 2017, InTech.
35. Sharifianjazi, F., et al., *Magnetic CoFe2O4 nanoparticles doped with metal ions: A review.* Ceramics International, 2020. **46**(11): p. 18391-18412.
36. Phuyal, S., D. Bista, and R. Bista, *Challenges, Opportunities and Future Directions of Smart Manufacturing: A State of Art Review.* Sustainable Futures, 2020. **2**: p. 100023.
37. *Environmental Guidelines* in *Environmental Guidelines for Electronics Manufacturing* 2012, Multilateral Investment Guarantees Agency.
38. Briseño, R., A.P. Arceo, and P.I. Alcántara Llanas, *Silicon as a MEMS material*. 2015.
39. Biligiri, S., *Fundamentals of IC manufacturing*. 2010.
40. *MEMS Technology*. Available from: https://mems-iss.com/mems-technologies/.
41. *About MEMS: What is MEMS Technology?* ; Available from: https://www.mems-exchange.org/MEMS/what-is.html.
42. Fischer, A.C., et al., *Integrating MEMS and ICs.* Microsystems & Nanoengineering, 2015. **1**(1): p. 15005.
43. P.S, S., *Fabrication of IC*. 2009.
44. Mamilla, V.R. and K.S. Chakradhar, *Micro Machining for Micro Electro Mechanical Systems (MEMS).* Procedia Materials Science, 2014. **6**: p. 1170-1177.
45. Walraven, J., *Introduction to Microelectricalmechanical Systems (MEMS) Materials, Fabrication, Processes and Failure Analysis*. 2012.
46. Ortiz-Acosta, D. and T. Moore, *Functional 3D Printed Polymeric Materials*, in *Functional Materials*. 2019, IntechOpen.
47. Bikas, H., P. Stavropoulos, and G. Chryssolouris, *Additive manufacturing methods and modelling approaches: a critical review.* The International Journal of Advanced Manufacturing Technology, 2015. **83**(1-4): p. 389-405.

48. *3D Printing / Additive Manufacturing Using Polymers - Complete Guide*. Available from: https://omnexus.specialchem.com/selection-guide/3d-printing-and-additive-manufacturing-polymers-and-processes#Applications.
49. Pérez, M., et al., *Current advances in additive manufacturing.* Procedia CIRP, 2020. **88**: p. 439-444.
50. Acosta, D.O. and T. Moore, *In book: Functional Materials.* Intech Open Chapter Functional 3D Printed Polymeric Materials, 2018. **1**: p. 15.
51. Cano-Raya, C., et al., *Chemistry of solid metal-based inks and pastes for printed electronics – A review.* Applied Materials Today, 2019. **15**: p. 416-430.
52. Keskinen, M., *End-of-life options for printed electronics*, in *Waste Electrical and Electronic Equipment (WEEE) Handbook*. 2012, Elsevier. p. 352-364.
53. Dahiya, A.S., et al., *High-performance printed electronics based on inorganic semiconducting nano to chip scale structures.* Nano Converg, 2020. **7**(1): p. 33.
54. Magliulo, M., et al., *Printable and flexible electronics: from TFTs to bioelectronic devices.* Journal of Materials Chemistry C, 2015. **3**(48): p. 12347-12363.
55. *Manufacturing Processes and Machinery Lab*. Available from: https://labs.wsu.edu/mpml/projects/.
56. Poudelet, L., A. Castellví, and L. Calvo, *An Innovative (DIW-Based) Additive Manufacturing Process*, in *New Business Models for the Reuse of Secondary Resources from WEEEs*, P. Rosa and S. Terzi, Editors. 2021, Springer International Publishing: Cham. p. 65-80.
57. Zeng, X.L., et al., *Solving e-waste problem using an integrated mobile recycling plant.* Journal of Cleaner Production, 2015. **90**: p. 55-59.
58. Heacock, M., et al., *E-Waste and Harm to Vulnerable Populations: A Growing Global Problem.* Environ Health Perspect, 2016. **124**(5): p. 550-5.
59. Perkins, D.N., et al., *E-waste: a global hazard.* Ann Glob Health, 2014. **80**(4): p. 286-95.
60. Lepawsky, J., *The changing geography of global trade in electronic discards: time to rethink the e-waste problem.* The Geographical Journal, 2014. **181**(2): p. 147-159.
61. Nigam, S., R. Jha, and R.P. Singh, *A different approach to the electronic waste handling – A review.* Materials Today: Proceedings, 2021. **46**: p. 1519-1525.
62. Rene, E.R., et al., *Electronic waste generation, recycling and resource recovery: Technological perspectives and trends.* J Hazard Mater, 2021. **416**: p. 125664.
63. Niu, X. and Y. Li, *Treatment of waste printed wire boards in electronic waste for safe disposal.* J Hazard Mater, 2007. **145**(3): p. 410-6.
64. Yang, Y., et al., *Overview on the applications of three-dimensional printing for rechargeable lithium-ion batteries.* Applied Energy, 2020. **257**: p. 114002.
65. Ruys, A.J., *Introduction*, in *Biomimetic Biomaterials*, A.J. Ruys, Editor. 2013, Woodhead Publishing. p. xix-xxvi.
66. Saravana, P.S. and B.S. Chun, *Chapter 4 - Seaweed Polysaccharide Isolation Using Subcritical Water Hydrolysis*, in *Seaweed Polysaccharides*, J. Venkatesan, S. Anil, and S.-K. Kim, Editors. 2017, Elsevier. p. 47-73.
67. Ghani, N.A.A., et al., *Impact of purification on iota carrageenan as solid polymer electrolyte.* Arabian Journal of Chemistry, 2019. **12**(3): p. 370-376.
68. Prado-Fernández, J., et al., *Quantitation of κ-, ι- and λ-carrageenans by mid-infrared spectroscopy and PLS regression.* Analytica Chimica Acta, 2003. **480**(1): p. 23-37.
69. Pereira, L., *EXTRACÇÃO, CARACTERIZAÇÃO E UTILIZAÇÃO DAS CARRAGENANAS.* 2010.
70. Moniha, V., et al., *Conductive bio-polymer electrolyte iota-carrageenan with ammonium nitrate for application in electrochemical devices.* Journal of Non-Crystalline Solids, 2018. **481**: p. 424-434.
71. Zia, K.M., et al., *A review on synthesis, properties and applications of natural polymer based carrageenan blends and composites.* Int J Biol Macromol, 2017. **96**: p. 282-301.
72. Saravana, P.S. and B.S. Chun, *Seaweed Polysaccharide Isolation Using Subcritical Water Hydrolysis*, in *Seaweed Polysaccharides*. 2017, Elsevier. p. 47-73.

73. Moniha, V., et al., *Development and Characterization of Bio-Polymer Electrolyte iota-carrageenan with Ammonium Salt for Electrochemical Application.* Materials Today-Proceedings, 2019. **8**: p. 449-455.
74. Tanusorn, N., et al., *Influence of carrageenan molecular structures on electromechanical behaviours of poly(3-hexylthiophene)/carrageenan conductive hydrogels.* Int J Biol Macromol, 2018. **118**(Pt B): p. 2098-2107.
75. Popescu, E., M. Iordan, and C. Boscornea, *Structure and properties of carragenan.* 2007.
76. Takemasa, M., A. Chiba, and M. Date, *Counterion Dynamics of κ- and ι-Carrageenan Aqueous Solutions Investigated by the Dielectric Properties.* Macromolecules, 2002. **35**(14): p. 5595-5600.
77. de Oliveira, V.A.V., et al., *Testing carrageenans with different chemical structures for water-based drilling fluid application.* Journal of Molecular Liquids, 2020. **299**: p. 112139.
78. Aillon, K.L., et al., *Effects of nanomaterial physicochemical properties on in vivo toxicity.* Adv Drug Deliv Rev, 2009. **61**(6): p. 457-66.
79. Kume, G., M. Gallotti, and G. Nunes, *Review on anionic/cationic surfactant mixtures.* Journal of Surfactants and Detergents, 2008. **11**(1): p. 1-11.
80. Hassan, P.A., G. Verma, and R. Ganguly, *Soft Materials — Properties and Applications*, in *Functional Materials*. 2012, Elsevier. p. 1-59.
81. Vaisman, L., H.D. Wagner, and G. Marom, *The role of surfactants in dispersion of carbon nanotubes.* Adv Colloid Interface Sci, 2006. **128-130**: p. 37-46.
82. Rausch, J., R.C. Zhuang, and E. Mader, *Surfactant assisted dispersion of functionalized multi-walled carbon nanotubes in aqueous media.* Composites Part a-Applied Science and Manufacturing, 2010. **41**(9): p. 1038-1046.
83. *Triton™ X-100 laboratory grade*. [cited 2021 June]; Available from: https://www.sigmaaldrich.com/PT/en/product/sial/x100.
84. Cortes, H., et al., *Non-Ionic Surfactants for Stabilization of Polymeric Nanoparticles for Biomedical Uses.* Materials (Basel), 2021. **14**(12): p. 3197.
85. Supriya, S., S. Kumar, and M. Kar, *Structural and Electrical Properties of CFO Nanoparticle-Filled PVA.* Journal of Electronic Materials, 2019. **48**(6): p. 3612-3623.
86. Munjal, S. and N. Khare, *Transforming single domain magnetic CoFe2O4 nanoparticles from hydrophobic to hydrophilic by novel mechanochemical ligand exchange.* Journal of Nanoparticle Research, 2017. **19**(1): p. 18.
87. Munjal, S., et al., *Water dispersible CoFe2O4 nanoparticles with improved colloidal stability for biomedical applications.* Journal of Magnetism and Magnetic Materials, 2016. **404**: p. 166-169.
88. Raza, S.A., et al., *Structural, ferromagnetic, electrical, and dielectric relaxor properties of BaTiO3 and CoFe2O4 bulk, nanoparticles, and nanocomposites materials for electronic devices.* Journal of Applied Physics, 2020. **128**(12): p. 124101.
89. Czichos, H., T. Saito, and L. Smith, *Springer Handbook of Materials Measurement Methods*. 2006: Springer Berlin Heidelberg.
90. Mund, H.S., et al., *Investigation of orbital magnetization in inverse spinel cobalt ferrite using magnetic Compton scattering.* Journal of Applied Physics, 2011. **110**(7): p. 073914.
91. Caraballo-Vivas, R., *Magnetism from intermetallics and perovskite oxides*. 2017.
92. Muljadi, P. Sardjono, and Suprapedi, *Preparation and Characterization of 5wt.% Epoxy Resin Bonded Magnet NdFeB for Micro Generator Application.* Energy Procedia, 2015. **68**: p. 282-287.
93. Cheng, C., et al., *Preparation and Magnetic Properties of CoFe2O4 Oriented Fiber Arrays by Electrospinning.* Materials (Basel), 2020. **13**(17): p. 3860.
94. Ansari, S.M., et al., *Particle Size, Morphology, and Chemical Composition Controlled CoFe2O4 Nanoparticles with Tunable Magnetic Properties via Oleic Acid Based Solvothermal Synthesis for Application in Electronic Devices.* Acs Applied Nano Materials, 2019. **2**(4): p. 1828-1843.

95. Li, X.H., et al., *Synthesis and Magnetic Properties of Nearly Monodisperse CoFe2O4Nanoparticles Through a Simple Hydrothermal Condition.* Nanoscale Res Lett, 2010. **5**(6): p. 1039-44.
96. Kaufmann Junior, C.G., et al., *Synthesis of cobalt ferrite (CoFe2O4) by combustion with different concentrations of glycine.* IOP Conference Series: Materials Science and Engineering, 2019. **659**: p. 012079.
97. Vieira Segundo, J.E.D. and E.O. Vilar, *Grafeno: Uma revisão sobre propriedades, mecanismos de produção e potenciais aplicações em sistemas energéticos.* Revista Eletrônica De Materiais E Processos, 2015. **11**(2): p. 54-57.
98. Arun, H., *Advancements in the use of carbon nanotubes for antenna realization.* Aeu-International Journal of Electronics and Communications, 2021. **136**: p. 153753.
99. Abdallah, B., et al., *Carbon nanotubes drug delivery system for cancer treatment*, in *Advances in Medical and Surgical Engineering*. 2020, Elsevier. p. 313-332.
100. Evingür, G.A. and Ö. Pekcan, *Optical, Mechanical, and Electrical Properties of Polymer Composites Doped by Multiwalled Carbon Nanotubes*, in *Carbon Nanotubes - Current Progress of their Polymer Composites*. 2016, InTech.
101. Nag, A., et al., *Multi-Walled Carbon Nanotubes-Based Sensors for Strain Sensing Applications.* Sensors (Basel), 2021. **21**(4).
102. Soni, S.K., B. Thomas, and V.R. Kar, *A Comprehensive Review on CNTs and CNT-Reinforced Composites: Syntheses, Characteristics and Applications.* Materials Today Communications, 2020. **25**: p. 101546.
103. Popov, V.N., *Carbon nanotubes: properties and application.* Materials Science & Engineering R-Reports, 2004. **43**(3): p. 61-102.
104. Ferreira, T., M.C. Paiva, and A.J. Pontes, *Dispersion of carbon nanotubes in polyamide 6 for microinjection moulding.* Journal of Polymer Research, 2013. **20**(11).
105. Damian, C.M., et al., *Covalent and non-covalent functionalized MWCNTs for improved thermo-mechanical properties of epoxy composites.* Composites Part B-Engineering, 2012. **43**(8): p. 3507-3515.
106. Ramasamy, G., *Development of Nanoprobe for the Determination of Blood Cholesterol.* 2012.
107. Bhatia, R., et al., *A critical review of experimental results on low temperature charge transport in carbon nanotubes based composites.* Reviews in Physics, 2018. **3**: p. 15-25.
108. Chen, M., et al., *Understanding the influence of carbon nanomaterials on microbial communities.* Environ Int, 2019. **126**: p. 690-698.
109. Ribeiro, D.d.F., *Estudo da influência de nanotubos de carbono funcionalizados nas propriedades de revestimentos de poliuretano*, in *Polymer Engennering*. 2015, University of Minho.
110. Kingston, C., et al., *Release characteristics of selected carbon nanotube polymer composites.* Carbon, 2014. **68**: p. 33-57.
111. Zhang, Q., et al., *The Road for Nanomaterials Industry: A Review of Carbon Nanotube Production, Post-Treatment, and Bulk Applications for Composites and Energy Storage.* Small, 2013. **9**(8): p. 1237-1265.
112. Mohanta, D., et al., *Carbon nanotubes: Evaluation of toxicity at biointerfaces.* J Pharm Anal, 2019. **9**(5): p. 293-300.
113. Nasibulina, L.I., et al., *Effect of Carbon Nanotube Aqueous Dispersion Quality on Mechanical Properties of Cement Composite.* Journal of Nanomaterials, 2012. **2012**: p. 1-6.
114. Lehman, J.H., et al., *Evaluating the characteristics of multiwall carbon nanotubes.* Carbon, 2011. **49**(8): p. 2581-2602.
115. Cerconi, C. and P.P. González-Borrero, *Preparação e caracterização de pós e filmes finos de BaTiO3 sintetizados via método Pechini.* Matéria (Rio de Janeiro), 2013. **18**(4): p. 1510-1524.
116. Mesquita, A., *Síntese e caracterização estrutural e dielétrica de compostos ferroelétricos 'PB IND.1-X''R IND.X''ZR IND.0,40''TI IND.0,60''O IND.3' (R = La, Ba)*. Universidade de Sao Paulo, Agencia USP de Gestao da Informacao Academica (AGUIA).

117. Shah, M.N., et al., *FTIR: Important tool to investigate the chemical bond formation in the polycrystalline xBaTiO3 – (1-x)BiFeO3.* Materials Today: Proceedings, 2021.
118. Jarabana, K.M., A. Mishra, and S. Bisen, *Structural and Optical properties of poly-crystalline BaTiO3and SrTiO3prepared via solid state route.* Journal of Physics: Conference Series, 2016. **755**: p. 012020.
119. Ashiri, R., *Detailed FT-IR spectroscopy characterization and thermal analysis of synthesis of barium titanate nanoscale particles through a newly developed process.* Vibrational Spectroscopy, 2013. **66**: p. 24-29.
120. Baraskar, B.G., et al., *BaTiO3-Based Lead-Free Electroceramics with Their Ferroelectric and Piezoelectric Properties Tuned by Ca2+, Sn4+ and Zr4+ Substitution Useful for Electrostrictive Device Application*, in *Ferroelectrics and Their Applications*. 2018, InTech.
121. Ahmadu, U., A. Muazu, and S. Umar, *Physical Properties of Porous Pure and Zr/Sn-Doped Nanocrystalline BaTiO3 Ceramics*, in *Recent Advances in Porous Ceramics*. 2018, InTech.
122. Corral-Flores, V. and D. Bueno-Baques, *Flexible Ferroelectric BaTiO3 – PVDF Nanocomposites*, in *Ferroelectrics - Material Aspects*. 2011, InTech.
123. Ehterami, A., et al., *Fabrication and characterization of highly porous barium titanate based scaffold coated by Gel/HA nanocomposite with high piezoelectric coefficient for bone tissue engineering applications.* J Mech Behav Biomed Mater, 2018. **79**: p. 195-202.
124. Gao, J., et al., *Influencing Factor Investigation on Dynamic Hydrothermal Growth of Gapped Hollow BaTiO3 Nanospheres.* Nanoscale Res Lett, 2015. **10**(1): p. 1033.
125. Fuentes, S., et al., *Synthesis and characterization of BaTiO3 nanoparticles in oxygen atmosphere.* Journal of Alloys and Compounds, 2010. **505**(2): p. 568-572.
126. Cho, W.S., *Structural evolution and characterization of BaTiO3 nanoparticles synthesized from polymeric precursor.* Journal of Physics and Chemistry of Solids, 1998. **59**(5): p. 659-666.
127. Wada, S., et al., *Preparation of nm-sized barium titanate fine particles and their powder dielectric properties.* Japanese Journal of Applied Physics Part 1-Regular Papers Brief Communications & Review Papers, 2003. **42**(9b): p. 6188-6195.
128. Li, W., et al., *Green Electronics: Biodegradable Materials and Green Processing for Green Electronics (Adv. Mater. 33/2020).* Advanced Materials, 2020. **32**(33): p. 2070245.
129. Sun, Q., et al., *Functional biomaterials towards flexible electronics and sensors.* Biosens Bioelectron, 2018. **119**: p. 237-251.
130. Irimia-Vladu, M., et al., *Green and biodegradable electronics.* Materials Today, 2012. **15**(7-8): p. 340-346.
131. Zhu, M., et al., *Isotropic Paper Directly from Anisotropic Wood: Top-Down Green Transparent Substrate Toward Biodegradable Electronics.* ACS Appl Mater Interfaces, 2018. **10**(34): p. 28566-28571.
132. *Construction of Transparent Cellulose-Based Nanocomposite Papers and Potential Application in Flexible Solar Cells*. American Chemical Society (ACS).
133. Ma, X.J., et al., *Cellulose transparent conductive film and its feasible use in perovskite solar cells.* Rsc Advances, 2019. **9**(17): p. 9348-9353.
134. Jin, J., et al., *Chitin Nanofiber Transparent Paper for Flexible Green Electronics.* Adv Mater, 2016. **28**(26): p. 5169-75.
135. Rincon-Iglesias, M., et al., *Water-based 2D printing of magnetically active cellulose derivative nanocomposites.* Carbohydr Polym, 2020. **233**: p. 115855.
136. Lei, T., et al., *Biocompatible and totally disintegrable semiconducting polymer for ultrathin and ultralightweight transient electronics.* Proc Natl Acad Sci U S A, 2017. **114**(20): p. 5107-5112.
137. Jia, C., et al., *Scalable, anisotropic transparent paper directly from wood for light management in solar cells.* Nano Energy, 2017. **36**: p. 366-373.
138. Ji, X.L., et al., *Biodegradable and Flexible Resistive Memory for Transient Electronics.* Journal of Physical Chemistry C, 2018. **122**(29): p. 16909-16915.

139. Irimia-Vladu, M., et al., *Edible Electronics: Biocompatible and Biodegradable Materials for Organic Field-Effect Transistors (Adv. Funct. Mater. 23/2010).* Advanced Functional Materials, 2010. **20**(23): p. 4017-4017.
140. Jin, Y.X., et al., *Long-term stable silver nanowire transparent composite as bottom electrode for perovskite solar cells.* Nano Research, 2018. **11**(4): p. 1998-2011.
141. Seck, M., et al., *Organic FETs using biodegradable almond gum as gate dielectric: A promising way towards green electronics.* Organic Electronics, 2020. **83**: p. 105735.
142. Lin, D.X., et al., *Stable and scalable 3D-2D planar heterojunction perovskite solar cells via vapor deposition.* Nano Energy, 2019. **59**: p. 619-625.
143. Chen, H., et al., *A solvent- and vacuum-free route to large-area perovskite films for efficient solar modules.* Nature, 2017. **550**(7674): p. 92-95.
144. Huang, X., et al., *A Fully Biodegradable Battery for Self-Powered Transient Implants.* Small, 2018. **14**(28): p. e1800994.
145. Fu, K., et al., *All-Component Transient Lithium-Ion Batteries.* Advanced Energy Materials, 2016. **6**(10): p. 1502496.
146. Chen, Y.L., et al., *Chitosan as a functional additive for high-performance lithium-sulfur batteries.* Journal of Materials Chemistry A, 2015. **3**(29): p. 15235-15240.
147. Edupuganti, V. and R. Solanki, *Fabrication, characterization, and modeling of a biodegradable battery for transient electronics.* Journal of Power Sources, 2016. **336**: p. 447-454.
148. Mashkour, M., et al., *MWCNT-coated cellulose nanopapers: Droplet-coating, process factors, and electrical conductivity performance.* Carbohydr Polym, 2018. **202**: p. 504-512.
149. Babayigit, A., et al., *Toxicity of organometal halide perovskite solar cells.* Nat Mater, 2016. **15**(3): p. 247-51.
150. Mizutani, W., et al., *Influences of submonolayer proteins on organic light-emitting diodes.* Applied Physics Letters, 2007. **91**(2): p. 024101.
151. Hu, T., et al., *3D-printable supramolecular hydrogels with shear-thinning property: fabricating strength tunable bioink via dual crosslinking.* Bioact Mater, 2020. **5**(4): p. 808-818.
152. Diañez, I., et al., *3D printing in situ gelification of κ-carrageenan solutions: Effect of printing variables on the rheological response.* Food Hydrocolloids, 2019. **87**: p. 321-330.
153. Moniha, V., et al., *Synthesis and characterization of bio-polymer electrolyte based on iota-carrageenan with ammonium thiocyanate and its applications.* Journal of Solid State Electrochemistry, 2018. **22**(10): p. 3209-3223.
154. Sugumaran, T., et al., *The conductivity and dielectric studies of polymer electrolytes based on iota-carrageenan with sodium iodide and 1-butyl-3-methylimidazolium iodide for the dye-sensitized solar cells.* Ionics, 2019. **25**(2): p. 763-771.
155. Arof, A.K., et al., *Application of chitosan/iota-carrageenan polymer electrolytes in electrical double layer capacitor (EDLC).* Journal of Solid State Electrochemistry, 2010. **14**(12): p. 2145-2152.
156. Bener, M., et al., *Carrageenan-based colorimetric sensor for total antioxidant capacity measurement.* Sensors and Actuators B-Chemical, 2018. **273**: p. 439-447.
157. Zhu, C., et al., *Highly compressible 3D periodic graphene aerogel microlattices.* Nat Commun, 2015. **6**: p. 6962.
158. Lacey, S.D., et al., *Extrusion-Based 3D Printing of Hierarchically Porous Advanced Battery Electrodes.* Adv Mater, 2018. **30**(12): p. e1705651.
159. Sun, G.Z., et al., *Layer-by-layer printing of laminated graphene-based interdigitated microelectrodes for flexible planar micro-supercapacitors.* Electrochemistry Communications, 2015. **51**: p. 33-36.
160. Zhang, D., et al., *Fabrication of highly conductive graphene flexible circuits by 3D printing.* Synthetic Metals, 2016. **217**: p. 79-86.
161. Hu, M., et al., *Direct Pen Writing of Adhesive Particle-Free Ultrahigh Silver Salt-Loaded Composite Ink for Stretchable Circuits.* ACS Nano, 2016. **10**(1): p. 396-404.

162. Vatani, M., E.D. Engeberg, and J.W. Choi, *Conformal direct-print of piezoresistive polymer/nanocomposites for compliant multi-layer tactile sensors.* Additive Manufacturing, 2015. **7**: p. 73-82.
163. Abas, M. and K. Rahman, *Fabrication of flex sensors through direct ink write technique and its electrical characterization.* Applied Physics a-Materials Science & Processing, 2016. **122**(11).
164. Correia, D.M., et al., *Development of bio-hybrid piezoresistive nanocomposites using silk-elastin protein copolymers.* Composites Science and Technology, 2019. **172**: p. 134-142.
165. Reizabal, A., et al., *Optimized silk fibroin piezoresistive nanocomposites for pressure sensing applications based on natural polymers.* Nanoscale Advances, 2019. **1**(6): p. 2284-2292.
166. Nunes-Pereira, J., et al., *Energy harvesting performance of BaTiO3/poly(vinylidene fluoride–trifluoroethylene) spin coated nanocomposites.* Composites Part B: Engineering, 2015. **72**: p. 130-136.
167. Reizabal, A., et al., *Silk Fibroin Based Magnetic Nanocomposites for Actuator Applications.* Advanced Engineering Materials, 2020. **22**(6): p. 2000111.
168. Hermenegildo, B.F.d.C., *Development of active and biodegradable hydrogels for bone tissue engineering applications*, in *Science* 2018, University of Minho. p. 125.
169. Zhu, F.Y., et al., *3D nanostructure reconstruction based on the SEM imaging principle, and applications.* Nanotechnology, 2014. **25**(18): p. 185705.
170. Gniadek, M. and A. Dabrowska, *The marine nano- and microplastics characterisation by SEM-EDX: The potential of the method in comparison with various physical and chemical approaches.* Mar Pollut Bull, 2019. **148**: p. 210-216.
171. Rades, S., et al., *High-resolution imaging with SEM/T-SEM, EDX and SAM as a combined methodical approach for morphological and elemental analyses of single engineered nanoparticles.* Rsc Advances, 2014. **4**(91): p. 49577-49587.
172. Pereira, F.J., et al., *Synergism between SEM/EDX microanalysis and multivariate analysis for a suitable classification of Roman and Byzantine papyri.* Microchemical Journal, 2021. **160**: p. 105688.
173. Prime, R.B. *Thermoset Characterization Part 12: Introduction to Thermogravimetric Analysis (TGA)*. 2014; Available from: https://polymerinnovationblog.com/thermoset-characterization-part-12-introduction-thermogravimetric-analysis-tga/.
174. Mourad, A.H.I., et al., *Characterisation of thermally treated and untreated polyethylene–polypropylene blends using DSC, TGA and IR techniques.* Plastics, Rubber and Composites, 2013. **38**(7): p. 265-278.
175. A, A., R. T, and B. W, *Determination of Folding Reversibility of Lysozyme Crystals Using Microcalorimetry*, in *Applications of Calorimetry in a Wide Context - Differential Scanning Calorimetry, Isothermal Titration Calorimetry and Microcalorimetry*. 2013, InTech.
176. *Principles and Applications of Thermal Analysis*. 2008, Blackwell Publishing Ltd.
177. *Differential Scanning Calorimetry (DSC) Analysis*. Available from: https://www.intertek.com/analysis/dsc/.
178. Montenegro, R.V.D., *Crystallization, biomimetics and semiconducting polymers in confined systems*

Kristallisation, Biomimetik und halbleitende Polymere in räumlich begrenzten Systemen. 2003.
179. Steinmann, W., et al., *Thermal Analysis of Phase Transitions and Crystallization in Polymeric Fibers*, in *Applications of Calorimetry in a Wide Context - Differential Scanning Calorimetry, Isothermal Titration Calorimetry and Microcalorimetry*. 2013, InTech.
180. Nasrollahzadeh, M., et al., *Plant-Mediated Green Synthesis of Nanostructures: Mechanisms, Characterization, and Applications*, in *Interface Science and Technology*. 2019, Elsevier. p. 199-322.
181. *Understanding Remanence*. Available from: https://idealmagnetsolutions.com/knowledge-base/remanence-meaning/.

182. Adeyeye, A.O. and G. Shimon, *Growth and Characterization of Magnetic Thin Film and Nanostructures*, in *Magnetism of Surfaces, Interfaces, and Nanoscale Materials*. 2015, Elsevier. p. 1-41.
183. *Fourier Transform Infrared Spectroscopy (FTIR) Analysis*. Available from: https://www.intertek.com/analysis/ftir/.
184. Gopanna, A., et al., *Fourier transform infrared spectroscopy (FTIR), Raman spectroscopy and wide-angle X-ray scattering (WAXS) of polypropylene (PP)/cyclic olefin copolymer (COC) blends for qualitative and quantitative analysis.* Polymer Bulletin, 2018. **76**(8): p. 4259-4274.
185. Ismail, A.A., F.R. van de Voort, and J. Sedman, *Chapter 4 Fourier transform infrared spectroscopy: Principles and applications*, in *Techniques and Instrumentation in Analytical Chemistry*. 1997, Elsevier. p. 93-139.
186. Gaffney, J.S., N.A. Marley, and D.E. Jones, *Fourier Transform Infrared (FTIR) Spectroscopy*, in *Characterization of Materials*. 2012, John Wiley & Sons, Inc.
187. Berthomieu, C. and R. Hienerwadel, *Fourier transform infrared (FTIR) spectroscopy.* Photosynth Res, 2009. **101**(2-3): p. 157-70.
188. Elias, S.A., *Geoarchaeology*, in *Encyclopedia of Geology*. 2021, Elsevier. p. 538-553.
189. Pütz, J., S. Heusing, and M.A. Aegerter, *Characterization of Electrical Properties*, in *Handbook of Sol-Gel Science and Technology*. 2016. p. 1-30.
190. *Fourier Transform Infrared Spectroscopy (FTIR)**, in *Characterization of Integrated Circuit Packaging Materials*. 1993, Elsevier. p. 235.
191. Heaney, M., *Electrical Conductivity and Resistivity*. 2003. p. 7-1 to 7.
192. James, J., K.P. Pramoda, and S. Thomas, *Polymers and Multicomponent Polymeric Systems*. 2019: CRC Press.
193. Dizon, J.R.C., et al., *O Mechanical characterization of 3D-printed polymers.* Additive Manufacturing, 2018. **20**: p. 44-67.
194. *Mechanical Properties of Materials*. Available from: https://mechanicalc.com/reference/mechanical-properties-of-materials.
195. Tu, S., et al., *Stress–strain curves of metallic materials and post-necking strain hardening characterization: A review.* Fatigue & Fracture of Engineering Materials & Structures, 2019. **43**(1): p. 3-19.
196. Singh, J.P. and S. Verma, *Raw materials for terry fabrics*, in *Woven Terry Fabrics*. 2017, Elsevier. p. 19-28.
197. Goncalves, R., et al., *Development of magnetoelectric CoFe2O4/poly(vinylidene fluoride) microspheres.* Rsc Advances, 2015. **5**(45): p. 35852-35857.
198. Jumaah, F.N., et al., *Derivative of iota-carrageenan as solid polymer electrolyte.* Ionics, 2014. **21**(5): p. 1311-1320.
199. Mitsuda, K., H. Kimura, and T. Murahashi, *Evaporation and Decomposition of Triton-X-100 under Various Gases and Temperatures.* Journal of Materials Science, 1989. **24**(2): p. 413-419.
200. Hossain, K.S., et al., *Sol-Gel transition behavior of pure iota-carrageenan in both salt-free and added salt states.* Biomacromolecules, 2001. **2**(2): p. 442-9.
201. Kamranifar, M., A. Allahresani, and A. Naghizadeh, *Synthesis and characterizations of a novel CoFe2O4@CuS magnetic nanocomposite and investigation of its efficiency for photocatalytic degradation of penicillin G antibiotic in simulated wastewater.* J Hazard Mater, 2019. **366**: p. 545-555.
202. Margabandhu, M., et al., *Investigation of Structural, Morphological, Magnetic Properties and Biomedical applications of Cu2+ Substituted Uncoated Cobalt Ferrite Nanoparticles.* Brazilian Archives of Biology and Technology, 2016. **59**(spe2).
203. Tabit, R., et al., *Magnetic CoFe2O4 nanoparticles supported on graphene oxide (CoFe2O4/GO) with high catalytic activity for peroxymonosulfate activation and degradation of rhodamine B.* Rsc Advances, 2018. **8**(3): p. 1351-1360.
204. Her, S.C. and C.Y. Lai, *Dynamic Behavior of Nanocomposites Reinforced with Multi-Walled Carbon Nanotubes (MWCNTs).* Materials (Basel), 2013. **6**(6): p. 2274-2284.

205. Alex, K.V., et al., *Charge Coupling Enhanced Photocatalytic Activity of BaTiO3/MoO3 Heterostructures.* ACS Appl Mater Interfaces, 2019. **11**(43): p. 40114-40124.
206. Chitra, R., et al., *Synthesis and characterization of iota-carrageenan solid biopolymer electrolytes for electrochemical applications.* Ionics, 2018. **25**(5): p. 2147-2157.
207. Farhana, N.K., et al., *Iota-carrageenan-based polymer electrolyte: impact on ionic conductivity with incorporation of AmNTFSI ionic liquid for supercapacitor.* Ionics, 2019. **25**(7): p. 3321-3329.
208. Chitra, R., et al., *Investigation of seaweed derivative iota-carrageenan based biopolymer electrolytes with lithium trifluoromethanesulfonate.* Materials Research Express, 2019. **7**(1): p. 015309.
209. Vega-Rios, A., et al., *Synthesis and electrical properties of polyaniline/iota-carrageenan biocomposites.* Carbohydr Polym, 2014. **110**: p. 78-86.
210. Yang, D.Y., S. Gao, and H.S. Yang, *Effects of sucrose addition on the rheology and structure of iota-carrageenan.* Food Hydrocolloids, 2020. **99**: p. 105317.
211. Mendes-Felipe, C., et al., *High dielectric constant UV curable polyurethane acrylate/indium tin oxide composites for capacitive sensing.* Composites Science and Technology, 2020. **199**: p. 108363.
212. Smith, J. and J. Mader, *Ohm's Law*. 2015.
213. Guillot-Ferriols, M., et al., *Poly(vinylidene) fluoride membranes coated by heparin/collagen layer-by-layer, smart biomimetic approaches for mesenchymal stem cell culture.* Mater Sci Eng C Mater Biol Appl, 2020. **117**: p. 111281.
214. Gonçalves, S., et al., *Environmentally Friendly Printable Piezoelectric Inks and Their Application in the Development of All-Printed Touch Screens.* ACS Applied Electronic Materials, 2019. **1**(8): p. 1678-1687.